

Electrical Grid interface for an Induction Motor

by

A R N M REAZ UL HAQUE

A thesis submitted in partial fulfillment of the requirements for the degree of

Doctor of Philosophy

in

Energy Systems

Electrical and Computer Engineering
University of Alberta

© A R N M REAZ UL HAQUE, 2017

Abstract

The 3-phase induction motor is the workhorse of modern industry and is widely regarded as a highly reliable electromechanical device. Two motor operational modes were of interest in this thesis work, motor starting and steady state operation when connected directly to the electrical grid and operating at the same grid frequency. Typical industrial applications include pumps, compressors and fan loads. Motor starting on isolated or weak grid systems is a highly dynamic process that can cause damage to the motor and load as well as grid voltage fluctuations. During steady-state operation, the induction motor draws reactive lagging currents and is exposed to variable grid voltages that reduce the motor operating efficiency and lifetime expectancy. Hence, the prime purpose of the thesis is to present power electronics that connect the induction motor to the grid and that can control the motor voltage above and below the grid voltage. As a result, the power electronics can provide a range of operational features such as: motor soft start, VAR compensation, improved power conversion efficiency, increased operational lifetime expectancy.

The power electronics presented consists of a 3-phase floating H-bridge that is connected in series with the utility grid and a cage induction motor to provide series voltage compensation. By injecting a series voltage in each phase, the proposed system can be used to control the motor voltage during starting and hence limit the motor starting current. The voltage injection can provide a voltage sag ride through capability and operate with a leading grid power factor under steady state, hence generates VARs into the grid. The 3-phase H-bridges produce 5-level pwm motor line voltages with a pwm frequency up-to four times the switching. This compares with the 3-level line voltages produce in a standard VFD at twice the switching frequency, using

larger voltage step sizes. The 3-phase H-bridge system therefore results in lower high frequency pwm induced iron losses and Cu losses in the motor.

Besides soft start and reactive power generation capability, the proposed system has many other desirable operating features, such as; improved motor operating efficiencies, reduced motor losses. Floating capacitor converters can set the motor voltage at a fixed desired value, above or below the grid voltage, under transient or continuous steady-state conditions, and over the entire range of the motor load. This is useful when the motor is connected to a grid whose nominal voltage differs from the machine's rated value or that may fluctuate over time (sag or swell). A variety of control options exist to lower the losses of an induction motor, the approach presented is based upon measuring the motor electrical input power and using readily available motor nameplate data to control the motor voltage. The conversion efficiencies of both the motor and the power electronics power can be improved over the entire motor load range. This results in lowering the motor's operating temperature to improve lifetime expectancy, and avoids derating the motor power rating. The cooling requirements of the power electronics can be reduced, lowering their size, cost and weight.

Motor voltage control with bridge voltage control is explained. Simulation and theoretical analysis is presented to predict operation of system as well as theoretical performance curves for the 3-phase H-bridge is presented for motor control modes. Relationship between motor winding temperature rise and motor loss is also established.

A 5 HP experimental testbed is used to validate the concepts. Soft start, the grid voltage ride through capability feature and the reactive power generation characteristics are verified. Experimental results show that the proposed system can successfully soft start a standard squirrel cage induction machine under different modes and load conditions. Also the experimental

performance of the power electronics, motor and total system is presented with respect to power losses, system efficiency and the motor output power. For applications where frequency control is not required, the proposed 3-phase H-bridge system is a viable cost effective solution.

Acknowledgements

I would like to thank my supervisor Professor John Salmon for his support, professional guidance and continuous encouragement throughout my time at the University of Alberta. His deep knowledge and sparking ideas made every discussion inspirational. I truly appreciate the freedom and opportunities he provided to work on different projects which elevated my interest and experience.

Additionally, I would also like to thank my supervisory committee, for their time and effort in reviewing my thesis.

Special thanks to Albert Terheide, Siyu Leng for friendly support in developing and implementing test facilities in the lab. I also like to thank Nirmana, Ian, Jeff and everyone in the common power electronics laboratory for their help over the years.

My special gratitude to my family- my wife Zisha, son Rihan, parents, in laws, brothers and sister for being relatively patient and be considerate for the amount of time I spent in the lab. Without them I would not have had courage to start this long term journey.

Contents

List of Figures	x
List of Tables.....	xv
Nomenclature	xvi
Chapter 1.....	1
Introduction.....	1
1.1 Introduction	1
1.2 Motivation	3
1.2.1 Motor Voltage Control.....	3
1.2.2 Typical Motor Starting Transients	5
1.2.3 Motor Voltage Mismatch.....	7
1.2.4 Oversized Motor	8
1.2.5 Efficiency	8
1.2.6 Low Power Factor and Reactive Power Consumption:	9
1.3 Non Power Electronics Solution to reduce The Impact of The Start-up Process	10
1.3.1 Full Voltage Starting.....	10
1.3.2 Reduced Voltage Starting	11
1.4 Thesis Objective and Outline	14
1.5 Thesis Contributions	15
Chapter 2.....	17
2 Smart Electrical Grid Interface for an Induction Motor	17
2.1 Introduction	17
2.2 Reduced Voltage Starting-Solid State Starter	19
2.3 Standard VFD.....	20
2.4 Dual Inverter Drive	22
2.5 VAR Compensation	23
2.6 Floating H-Bridge Converter	24
2.7 Proposed 3-phase Floating H-bridge System.....	26
2.8 Basic Bridge Operating Principle.....	27
2.9 Voltage Vector Analysis	31
2.10 Conclusion.....	33

Chapter 3	34
3 Soft Start	34
3.1 Introduction	34
3.2 Motor Voltage Control	35
3.3 Controller	36
3.3.1 Control Block Diagram	38
3.4 Maximum Bridge DC Voltage Prediction	38
3.5 DC Capacitor Charging	41
3.6 Dc Capacitor Ripple Voltage Modeling	42
3.7 Simulation Results	44
3.8 Experimental Setup	46
3.9 Experimental Results	47
3.9.1 Current Limit Soft Start	48
3.9.2 Voltage Ramp Soft Start	49
3.9.3 Bridge DC Voltage Prediction	50
3.9.4 Peak Inrush Current for capacitor Charging	51
3.9.5 Leading Power Factor	52
3.9.6 Five Level Line to Line PWM Voltage Generation	52
3.9.7 Conclusions	53
Chapter 4	54
4 Series Voltage Compensation	54
4.1 Introduction	54
4.2 Grid Voltage Sag Tolerance	57
4.3 Motor Fundamental Current Angle Estimation	59
4.4 Reactive Power Generation	61
4.5 Experimental Validation	62
4.5.1 Voltage Sag Tolerance	62
4.5.2 Reactive Power Generation	66
4.6 Conclusions	66
Chapter 5	68
5 Performance Improvement of Induction Motors	68

5.1	Introduction	68
5.2	Experimental Setup	69
5.3	Induction Motor Performance	70
5.3.1	3-phase H-bridge vs Direct Grid: Motor Voltage = Rated	71
5.3.2	3-phase H-bridge vs Direct Grid: Motor Voltage < Rated	71
5.3.3	3-phase H-bridge vs VFD	74
5.3.4	Power Electronics	75
5.3.5	3-phase H- Bridge and a Variable Motor Voltage	77
5.3.6	Total System Performance	79
5.4	Conclusions	81
Chapter 6.....		82
6	Variable Motor Voltage Control.....	82
6.1	Introduction	82
6.2	Motor Voltage Control.....	84
6.3	3-phase H-bridge Control.....	87
6.4	Motor Voltage Controller.....	89
6.5	Experimental Results.....	90
6.5.1	General Motor Performance	91
6.5.2	Motor Reactive VARs and Rotor Speed.....	92
6.5.3	Grid: Power Factor and VARs.....	93
6.5.4	Temperature Dependence	94
6.5.5	DC Voltage Reduction.....	95
6.5.6	Power Electronics Performance	96
6.6	Conclusions	97
Chapter 7.....		99
7	Conclusion.....	99
7.1	Summary	99
7.2	Future work	101
7.3	Concluding remark.....	102
Bibliography		103
Appendices.....		113

Appendix A 113
 Triangle Intersection Implementation of SVPWM 113
Appendix B 116
 Modified PWM Scheme 116
Appendix C 118
 Conservative DC Voltage Prediction before Motor Start..... 118
Appendix D 119
 dSpace Implementation 119
Appendix E..... 123
 Control Interface..... 123

List of Figures

Fig.1-1. Simplified per-phase phasor analysis, (a) per phase equivalent circuit schematic (b) vector diagram with zero floating bridge voltage; (c) vector diagram at higher lagging power factor; (d) vector diagram at unity power factor; (e) vector diagram at leading power factor.	4
Fig.1-2. Starting characteristic of an induction motor a) motor current vs speed b) motor torque vs speed	5
Fig.1-3. Static terminal shunt capacitor connection	11
Fig.1-4. Reduced voltage starting of an induction motor; a) motor current vs speed, b) motor torque vs speed	12
Fig.2-1. Electric drive system	18
Fig.2-2. Thyristor based soft start	19
Fig.2-3. Variable frequency drive (VFD)	20
Fig. 2-4: Back to back (BTB) converter	21
Fig.2-5. Open winding induction motor configuration	22
Fig.2-6. VAR compensation; a) series compensation, b) shunt compensation	23
Fig.2-7. The cascaded H-bridge topology a); with b) phase-shifted transformers, c) batteries supplying cell isolated cell.	25
Fig. 2-8. Configuration of the MERS	26
Fig.2-9. Power electronic converters for series voltage compensation of a smart grid connected induction motor: (a) 3-phase H-bridge, (b) 3-phase inverter.	27
Fig. 2-10. Simplified system fundamental voltage single phase representation; (a) equivalent circuit, (b) vector diagram with angles labelled.	28

Fig.2-11. Voltage waveforms; (a) Phase A and (b) Phase B of H-bridge output voltage, (c) grid line voltage, (d) motor line voltage component due to the H-bridges, (e) 5-level PWM waveforms generated by H-bridge.	29
Fig. 2-12. Phasor diagram for floating capacitor H-bridge converter motor drive system	30
Fig. 2-13: Phasor voltage vectors: (a) $V_m = \text{rated}$, high load, (b) $V_m = \text{rated}$, light load, (c) $V_m = \text{rated} > V_g$, high load.	30
Fig. 2-14. System operations under 3-phase H-bridge configuration: a) control angle α , b) angles β and γ , c) power factor, d) capacitor dc voltage.	32
Fig.3-1. Vector diagrams for the proposed alpha angle control	35
Fig. 3-2. Reduced voltage starting; a) voltage limit, b) current limit soft start.	36
Fig.3-3. Schematic diagram for soft start	37
Fig.3-4. Control block diagram.	39
Fig.3-5. H-bridge ac voltage trend under various induction motor power factor angles	40
Fig. 3-6. Per-phase (a) equivalent circuit of the proposed system and (b) equivalent circuit during initial capacitor charging process	42
Fig. 3-7. Waveforms of different aspects of the H-bridge system	43
Fig. 3-8: Effect of capacitance on ripple voltage	44
Fig. 3-9. System operation-torque: (a) half load; (b) full load, motor current: (c) half load; (d) full load, speed: (e) half load; (f) full load; motor reference voltage: (g) half load; (h) full load, capacitor dc voltage: (i) half load; (j) full load.	45
Fig. 3-10. Experimental test facility (a) schematic for test platform (b) controller with power electronics (b) Induction motor-dc generator set	46
Fig. 3-11. Current limit soft-start: different conditions; (a) full-voltage; no load (b) 2.0 p.u. motor current limit; no load, (c) 2.5 p.u. current limit; half load, (d) 3.1 p.u. current limit;	48

full load, (e) 2.0 p.u. current limit; full load.

Fig. 3-12. Voltage ramp soft-start results: (a) 2 second ramp time, no load condition (b) 3 50
second ramp time, half load condition (c) 4 second ramp time, full load condition

Fig. 3-13. Comparison between predicted and actual maximum DC voltage with no 51
resistive load connected to DC generator (a) $V_{dc}=303.3$ (b) $V_{dc}=319.3$

Fig. 3-14. Inrush current for capacitor charging (a) H bridge system (b) VFD 51

Fig. 3-15. Relationship between grid phase voltage and motor current under rated motor 52
voltage (a) no load (b) full load

Fig. 3-16. Line to line PWM voltages generated by the proposed H-bridge system 52

Fig. 4-1. Phasor diagram illustrating the system response to a grid voltage sag: (a) during 57
voltage sag: V_{g1} goes to V_{g2} , (b) critical condition.

Fig. 4-2. Effect of the motor power factor angle ϕ_m on the critical condition for the 58
permissible maximum voltage sag compensation

Fig. 4-3. System vector diagram under nominal steady-state operating conditions to predict 60
the motor fundamental power factor angle.

Fig. 4-4. Voltage sag ride through performance: (a) full-load, voltage sag 85% of rated grid 63
voltage (b) half-load, voltage sag 66% of rated grid voltage (c) no load, voltage sag 16% of
rated grid voltage

Fig. 4-5. Reactive power generation of the proposed H-bridge induction motor drive system 64
under full load condition ($I=13.6A$, $PF_m =0.76$): (a) $V_g = 196V$ (c) $V_g = 184V$ (e) $V_g =$
 $176.5V$; under half load condition ($I=10.3A$, $PF_m =0.581$): (b) $V_g = 196V$ (d) $V_g = 159.2V$
(f) $V_g = 137.5V$

Fig. 4-6. Comparison between theoretical and experimental values of maximum voltage sag 65
whilst maintaining rated motor voltage

Fig. 4-7. Comparison of: (a) the motor power factor, (b) Reactive power generation trend as 66

a function of the motor load condition.

Fig. 5-1. Experimental setup: (a) block diagram, (b) 3-phase H-bridge system with a dSPACE controller, (c) Induction motor with dynamometer. 70

Fig. 5-2. Experimental motor performance comparison ($V_{Lg}=230V$, direct grid connection: $V_{Lm}=230V$, 3-phase H-bridge: $V_{Lm}=230V$): (a) voltage vectors for the motor at full-load and light load, (b) motor current, (c) power factor, (d) speed (e) efficiency (f) power losses (g) output power 72

Fig. 5-3. Experimental motor performance comparison ($V_{Lg}= 208V$, direct grid connection: $V_{Lm}=208V$, 3-phase H-bridge: $V_{Lm}=230V$); (a) vector diagram, ((b) motor current, (c) power factor, (d) speed (e) efficiency (f) power losses (g) output power 73

Fig. 5-4. Experimental motor performance comparison ($V_{Lg} = 230V$, VFD: $V_{Lm} = 225-214V$, 3-phase H-bridge: $V_{Lm}=230V$): (a) efficiency, (b) power losses, (c) output power 75

Fig. 5-5. Experimental power electronics performance comparison ($V_{Lg} = 230V$, VFD; $V_{Lm} = 225-214V$, 3-phase H-bridge; $V_{Lm}=230V$); (a) efficiency, (b) power losses, (c) dc voltage, (d) VFD rectifier & inverter losses. 76

Fig. 5-6. Experimental motor performance comparison for the motor performance using the 3-phase H-bridge ($V_{Lm}=208V$, $230V$, variable): (a) voltage vectors, (b) motor voltage, (c) efficiency, (d) power losses. 78

Fig. 5-7: System performance comparison; (a) motor, power electronic and total system losses, (b) system efficiency; 3-phase H-bridge vs VFD. 79

Fig. 6-1. Equivalent circuit of induction motor 85

Fig. 6-2: Motor operation under rated and variable voltage control: (a) motor voltage and power factor, (b) bridge voltage as a function of the motor power factor angle, (c) input current 86

Fig. 6-3. Motor operation under rated and variable voltage control with temperature variation; (a) motor efficiency, (b) motor losses. 87

Fig. 6-4. Phasor voltage vectors: (a) $V_m > \text{rated}$, high load, (b) $V_m < \text{rated}$, light load.	88
Fig. 6-5. Rated & variable voltage control;(a) control angle α (b) angles γ and β , (c) grid & motor displacement angles ϕ_g and ϕ_m , (d) capacitor dc voltage.	89
Fig. 6-6. Control block diagram for variable motor voltage control	90
Fig. 6-7. Motor performance as a function of the motor output load in %; (a) motor voltage, (b) current, (c) efficiency, (d) power losses	92
Fig. 6-8. . Motor reactive power and speed curves: (a) rotor speed, (b) torque-speed, (c) power factor, (d) reactive power	93
Fig. 6-9. Reactive VAR generation and grid Power Factor: (a) leading grid current, (b) grid power factor (PF_g), (c) grid VAR generation.	94
Fig. 6-10. Motor stator temperature rise dependence on losses; (a) stator temperature as a function of motor losses ($V_{Lm}=230$ V), (b) temperature rise comparison between rated and variable motor voltage.	95
Fig. 6-11. Comparison of dc capacitor voltage	96
Fig. 6-12. Transient operation of the system	96
Fig. 6-13. Experimental: (a) H bridge losses, (b) efficiency comparison.	97

List of Tables

Table 1	Induction motor-1 parameters	6
Table 2	Induction motor-2 parameters	47

Nomenclature

f_s	supply frequency
I	stator current
I_A	phase A current
I_{rms}	motor rms current
$I_{\text{rms}}^{\text{max}}$	motor maximum rms current
I_{rated}	rated motor current
m_a	modulation index
p	number of poles
P_A	phase A power
P_{in}	electrical input power
P_{mo}	rated input power
PF_g	grid power factor
PF_m	motor power factor
Q	reactive power
R_s	stator resistance
R_r	rotor resistance
s	slip of the motor
s_{min}	voltage sag limit
V_A	phase A voltage
V_b	per-phase component of injected bridge voltage
$V_{b,\text{pu}}$	per phase bridge voltage in per unit
V_{cap}	capacitor voltage
$v_{\text{dc}}^{\text{ave}}$	average dc capacitor voltage
V_g	per-phase component of the grid voltage
$V_{g,\text{min}}$	minimum grid voltage
V_{Lg}	line to line grid voltage
V_{Lm}	line to line motor voltage
V_m	per-phase component of motor voltage
$V_{m,\text{pu}}$	motor voltage in per unit

$V_{m, \text{rated}}$ rated motor voltage
 V_m^* reference signal for induction motor terminal voltage
 $V_{\text{peak}+}$ peak capacitor voltage
 $V_{\text{peak}-}$ lowest peak capacitor voltage
 ΔV capacitor voltage ripple
 V_{rated} rated voltage control
 $V_{\text{var.}}$ variable voltage control
 V_X voltage vector perpendicular to bridge voltage
 W_{charge} charged store by capacitor
 X_s stator inductance
 X_r rotor inductance
 X_m magnetizing inductance
 Z_{ph} motor input impedance
 φ_m motor current angle
 φ_g grid current angle
 α angle between the grid voltage and bridge voltage
 β angle between the grid voltage and motor voltage
 γ angle between the bridge voltage and motor voltage

Chapter 1

Introduction

Over the past few decades new switch-mode converter topologies and control methods have been studied to improve the performance of induction motors. This thesis describes power electronics that uses floating H-bridge converters to inject a voltage in series with the 3-phase electrical grid voltage to control the motor voltage and thus improve the motor performance over a wide range of motor operating conditions. The thesis work is placed in context here by highlighting the importance of the motor and describing various operating conditions associated with a grid connected induction machine. Various problems are described in relation to the continuous steady-state and transient starting conditions of the induction machine. The objectives of the work are described and then the most significant contributions are summarized.

1.1 Introduction

Induction motors (IMs) are complex electro-mechanical devices widely used in most industrial and commercial applications requiring the conversion of electrical power into mechanical form, such as pumps, compressors, fans etc.. The IM is regarded as a robust machine for many general industrial, but also a good choice for hazardous environments where the machine can be exposed to corrosive chemicals and explosive gaseous environments. Reasons for the popularity of induction motors include: simplicity, reliability, low cost, totally enclosed structure, combined with significant overload capacity, minimal service requirement, and high power conversion efficiency. Moreover, since the induction motor can be designed for a wide range of power ratings, it meets the power requirements of most industrial processes, ranging from hundreds of watts to megawatts [1-3].

Globally, 65-70% of total electrical power utilized in various industries is consumed by electric motors, and 85-90% of this power is consumed by three-phase ac induction motors alone, especially the squirrel-cage induction motor (SCIM) [4-11]. The relatively high power

conversion efficiency of the induction motor is convenient as even a small improvement in efficiency contributes towards significant saving of revenue, fuel consumption and other associated factors: a 1 % improvement in motor efficiency globally can lead to savings of over \$1 billion per annum in energy prices, 5.4-9.1 million tons less consumption per annum of combusted coal, and 13.6-18.1 million tons less greenhouse gas emission into the atmosphere [5]. In addition, recent government regulations and utility incentives make it imperative to improve the operational efficiency of induction motors.

Various methods that improve motor power conversion efficiencies have been known to motor manufacturers for years. In addition to advances in computer design optimization and modern manufacturing techniques, the application of higher quality materials have resulted in an increase in machine efficiency [12]. One technique is to use thinner laminations in the rotor stack; achieved with the consequence of using more laminations and increasing production costs. Efficiency can also be improved by using more copper in the motor, using high performance cooling fans and bearings, reducing air gaps between the stator and rotor etc. [13]. All these design techniques can add cost of the motor. Higher power conversion efficiencies can be also obtained from overall system improvements such as intensive deployment of demand side management, optimal selection of retrofit programs and the implementation of power electronic drives [14].

Due to their dramatic improvement of power conversion efficiencies, together with lowering costs and improving reliability, power electronics have increasingly been applied in more and more applications since the early 1970's [15]. One example of the importance of power electronics are their extensive use in renewable electrical power generation systems such as wind power generators and photovoltaics. As power electronics has matured over the years, innovations in topological configurations have resulted in the development of specialized converters and improvements in power conversion efficiencies in various applications. The continuous emphasis on improving overall power conversion efficiencies has resulted in the continuous innovations in semiconductor devices and power electronic topologies [16].

The starting and operation of motors and their associated loads have always presented a challenge in electrical equipment design [17]. The prime purpose of the power electronics presented in this thesis is the development of low voltage multi-level converter topologies based

on the application of the floating capacitor H-bridge. The series voltage injection function provided by the converter is utilized to soft start an induction motor, improve the grid power factor, and protect the motor against grid voltage fluctuations as well as operating the motor at its maximum efficiency. Motivating examples are given for development of floating capacitor H-bridge converter topology.

1.2 Motivation

In many applications, induction motors are operated continuously at full speed with no requirement for frequency control, e.g. fans, pumps, and conveyors, etc.. For these applications, motors can be equipped with power electronic soft-starters, in which the motor supply frequency is fixed: the motor voltage can be controlled to limit the motor starting current and also to lower energy losses under light load. This section details the power electronic requirements for the applications as a motivating example to develop 3-phase floating H-bridge converters.

1.2.1 Motor Voltage Control

AC machines are now used everywhere - large induction motors are used in industry facilities, smaller drives can be found at homes appliances. Controlling the voltage of the induction motor can improve steady state performance. Introducing floating bridge with the grid connected system can help to manipulate induction motor voltage, Fig. 1-1 If there is no real power transfer between the ac circuit and floating bridge, the voltage at the ac terminals of the floating bridge can be controlled to inject a voltage into the circuit that is perpendicular to the current phasor. As a result, machine voltage is phase shifted relative to the grid supply voltage. A desirable control approach is to keep the floating bridge modulation index at maximum. Based on angle α , angle between bridge voltage and grid voltage, with respect to grid, four modes of operation should be accomplished.

- Mode 1: Improved power factor: The utility power factor is made higher than the motor (Figure 1(b))
- Mode 2: Unity power factor: Current drawn from utility is made in phase with grid voltage (Figure 1(c))
- Mode 3: Constant Motor voltage: machine voltage is kept 1 p.u (Figure 1(d))

- Mode 4: Motor voltage control: Motor voltage is reduced for motor starting.

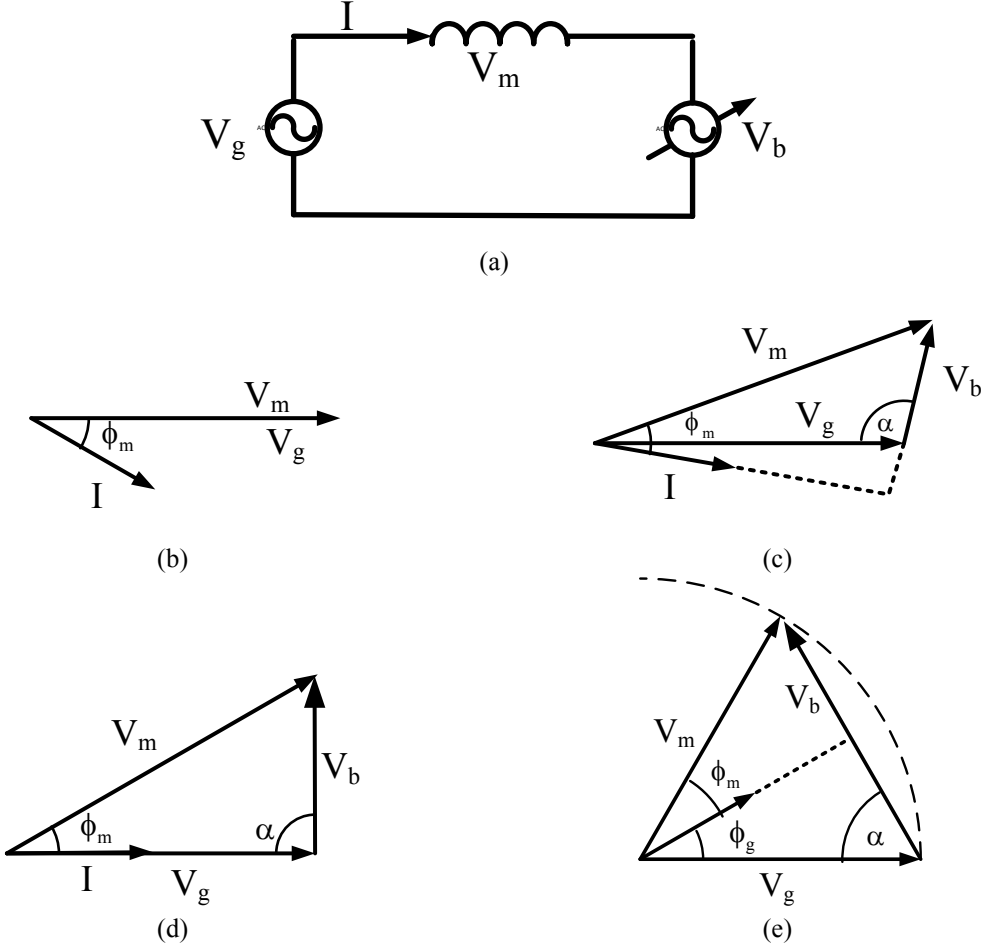


Fig. 1-1. Simplified per-phase phasor analysis, (a) per phase equivalent circuit schematic (b) vector diagram with zero floating bridge voltage; (c) vector diagram at higher lagging power factor; (d) vector diagram at unity power factor; (e) vector diagram at leading power factor

The operation is illustrated for one phase of a Y-equivalent motor, Fig. 1-1. Fig. 1-1(a) shows a simplified per phase schematic of the stator winding connections and Fig. 1-1(b) shows corresponding voltage and current phasors for the stator winding. If the per-phase voltage injected by the floating bridge, V_b , is zero the system work as standard Y connected machine. The grid voltage (V_g) and motor voltage (V_m) are equal and the stator current (I), lagging the stator voltage, will flow from the grid with a lagging power factor, ϕ_m . If a voltage is applied at the floating bridge, the machine voltage is changed and the grid power factor may be improved, as shown in Fig.1-1(b). Increasing the floating bridge voltage will result such a condition where the stator current is in phase with the applied grid voltage, shown in Fig. 1-1(c). This is the unity power factor operation of grid. The current drawn from the grid can be made to lead if

continuing to increase the floating bridge voltage. This case is illustrated in Fig. 1-1(d). The grid is at leading power factor at the same magnitude as the winding lagging power factor. Thus, injecting series voltage with the grid, the motor voltage can be controlled and can be utilized in steady state performance improvement.

1.2.2 Typical Motor Starting Transients

The simplest method for starting a poly-phase squirrel-cage induction motor is to connect it directly to an ac supply. Under this condition, the motor initially draws a large current (frequently referred to as inrush current) as it accelerates toward its operating speed, Fig. 1-2 (motor parameters are defined in Table 1). At the moment of energization, the current drawn by a squirrel-cage induction motor is a function of its locked-rotor impedance. Typically, the current is anywhere from four to ten times higher than the motor rated current at full speed [18-20]. When voltage is first applied to the motor at starting, the stator produces a rotating magnetic field at synchronous speed. The back EMF produced by the rotor's rotation is not yet induced and behaves as a transformer with the secondary short circuited. As the rotor reaches close to synchronous speed, motor back EMF is produced and the motor current reduces. In reality, the first half-cycle current is considerably higher in magnitude due to dc offset transients, but is short in duration. This large inrush current can cause problems for the electrical grid. Power companies may apply restrictions as to how much over-current is allowed. These restrictions can result in specifying the maximum allowable voltage droop at grid point of common coupling or the maximum allowable current that may be drawn by the plant. These restrictions may limit when and how many times a particular motor can be started.

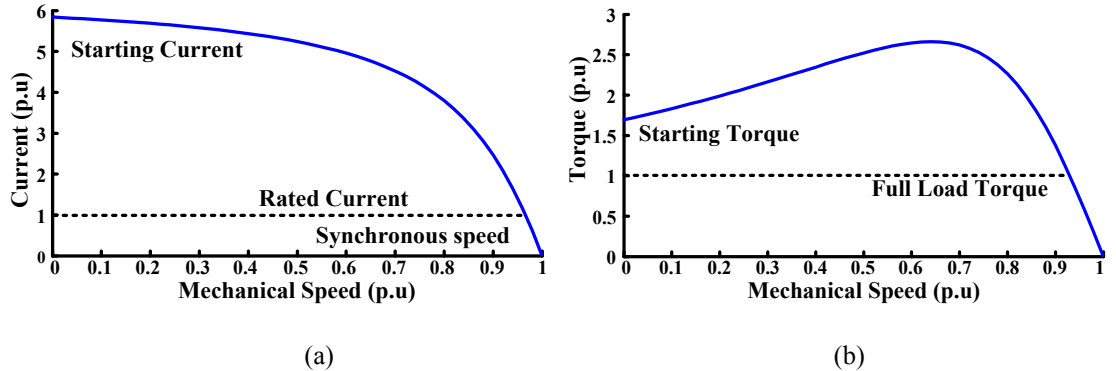


Fig. 1-2. Starting characteristic of an induction motor; a) motor current vs speed, b) motor torque vs speed

TABLE I. INDUCTION MOTOR-1 PARAMETERS

P_{rated}	=	3.7	kW	R_s	=	0.65	Ω
$I_{s,\text{rated}}$	=	12.6	A	R_R	=	0.26	Ω
$V_{s,\text{rated}}$	=	230	V	X_s	=	0.74	Ω
f_s	=	60	Hz	X_R	=	0.9	Ω
p	=	4		X_M	=	23	Ω

Another problem is associated with in-plant bus capacity where the electrical grid simply cannot handle a temporary over-current. Brownout or other associated problems may be experienced. A large inrush current also induces large magnetic forces in the stator windings, which try to force the windings to move and distort. Power dissipation associated with the high levels of inrush current can produce a rapid temperature rise and damage winding insulation [21-23, 29, 30, and 31]. In addition to the inrush current, there are often various degrees of transient torques present during the start-up period. The starting motor torque must be capable of starting the motor from standstill and exceed the load torque by a magnitude that allows acceleration to full speed while staying within the thermal limits of the motor and starting device. Full-voltage starting produces the greatest amount of starting torque, Fig. 1-2 (b). High starting torque is generally desired when trying to start a high-inertia load in order to limit the acceleration time. However, in certain cases, a high starting torque may damage the mechanical system [22, 23]. A consideration of such torques is particularly advisable for cases where induction motors are started and stopped frequently or continuously. An induction motor may produce severe pulsations in electromechanical torque [24-27] depending upon the initial switching instants of all three-phases to the supply, regardless of the starting method: direct-online or soft starting. The amount of electromagnetic torque pulsations reflected to the shaft depends on the parameters of the mechanical subsystem [6]. Moreover, if the closing of the switch contacts of the several phases is not simultaneous, 40% higher torque can be produced compare to starting torque [25].

Probably the most widely recognized and studied effect of motor starting is the voltage dip that is experienced throughout an industrial power system as the direct result of starting large motors. At start, the rapid increase in current flowing to the motor causes a momentary increase in the voltage drop along with the distribution system and a reduction in the voltage supplied to the motor and other loads on the same distribution system. The available accelerating torque

drops appreciably as the voltage at the motor bus dips to a lower value, thus extending the starting interval and affecting (sometimes adversely) overall motor starting performance [28].

If the voltage sag associated with motor starting is too large, ill effects such as flickering lights, excessive motor currents, and nuisance tripping of relays or main contactor dropout can occur. The voltage sag that occurs on the utility system due to motor starting will normally need to be limited to a maximum of approximately 6%. 3% voltage sag represents the point at which light flicker starts to become visibly noticeable, and 6% is the point at which light flicker becomes irritating [17]. The magnitude of the voltage flicker during starting is a function of the motor inrush current; the available short-circuit fault capacity of the utility system, and the impedance of the circuit between the utility power system and the motor [29].

In conclusion, induction motor starting poses many challenging problems to the machine a maintaining a stable electrical grid voltage. The dynamic characteristics desired during the starting process are often conflicting, and trade-offs must be made based on system characteristics.

1.2.3 Motor Voltage Mismatch

Many motors are located in environments in which their supply voltage are continually at or near the voltage limit specified by National Electric Manufacturing Association (NEMA) (-10 percent condition so that the motor has enough winding conductivity to carry the current and +10 percent condition so that motor has enough magnetic material as not to saturate too severely). For example, most of the three phases IM in low voltage distribution sites are rated for 230V. However, in North America most common residential service is single-phase 3 wire system also known as the Edison system [30]. Since the phase voltage for the Edison system is 120V, the line voltage is 208V which is lower than the rated IM line voltage (230V). Therefore, when these motors are used in commercial or resident buildings, their performance is compromised.

Another example occurs when the motor is located at the beginning of long feeder lines or in the evening hours on capacitor compensated lines, during which time the entire system is lightly loaded. Under these conditions, the voltage supplied to stator terminal voltage is higher than its rated value and motor efficiency is compromised as a result [31].

1.2.4 Oversized Motor

Due to over conservatism, erroneous information, or misapplication, the motor selected is oversized for its application. In fact, it has been pointed out that motor oversizing is a widespread practice [31-32]. Partial loading for an extended time in many applications, are the major contributor of higher electricity consumption as compared to other such factors like idling, cyclic loading, overloading etc., [33]. In such situations the motor is operated continuously at a load condition far from its maximum efficiency point. For example, in the European Union, the average load factor for motors, in both industrial and tertiary sectors, is 0.57. In another survey [32] in the USA, it is found 29% of the motors operating in the facilities were carrying less than 50% load. That is, 35-40% of the motors are wasting the power due to reduced efficiency at partial loading. Therefore, energy has to be consumed in the best possible way to increase the efficiency in operating condition and induction motors must be operated by an energy optimized control strategy [8].

1.2.5 Efficiency

New and increasingly stringent efficiency standards have made motor efficiency a priority among motor manufacturers and designers of motor-driven systems. While the energy independence and security act of 2010 mandated upgrades to full-load efficiencies in the U.S., future legislation is under consideration to require higher efficiencies even at partial loads and speeds. As a result, motor technology must continue improving to meet the efficiency standards proposed by energy-governing agencies [34]. In the existing economic climate, however, end users are also seeking more immediate solutions to boost motor system efficiency and decrease power costs. A number of strategies exist to boost motor efficiency [35].

One method to improve the part load efficiency is redesigning the machine with suitable optimization algorithms. This method requires good knowledge for the designer of machine and once the machine is designed for special purpose it cannot be used for other applications since the operating points of machine are fixed.

All induction motors carry an efficiency rating on their nameplates. The “nameplate efficiency” is defined for the motor’s rated point and varies by design and power output. Most NEMA premium efficient induction motors provide nameplate efficiencies close to the levels

defined under the NEMA standard. Motor efficiency does not peak at the motor's rated point, but peak efficiency decreases as operating speed or load diverges from that (maximum efficiency) point. A survey in centrifugal pumping system reveals that operated off the best-efficiency point (BEP) by only 20% resulted in an mean time between failure (MTBF) reduction of 50%. Plant systems and other mechanical systems operating off their design point will effectively turn inefficiency into heat or vibration, leading to ultimate failure. From the study results, many industries spend millions of dollars on vibration detection and analysis. Ironically, these sites could improve both motor energy efficiency and reliability by approving changes to guarantee that systems operate at their designed efficiency point [36].

1.2.6 Low Power Factor and Reactive Power Consumption:

One inherent drawback of induction machines is that it draws reactive power from the grid and the power factor can be poor. They require both real and reactive power to operate. The real power produces work and heat and the reactive power establishes the magnetic field in the motor that enables it to operate. The reactive component of the current, magnetizing current, established flux in the iron and is independent of the motor load current. Though, it is typically 20% to 60% of the rated full load current, it does not actually contribute to the actual work output of the motor. It is the catalyst that allows the motor to work properly. The magnetizing current can be considered passenger components of current that will not affect the power drawn by the motor, but will contribute to the power dissipated in the supply and distribution system. It has been reported [29] the power factor of large induction motors during across the line starting at zero speed is smaller than that of small induction motors. Therefore, large motors usually have more influence on power distribution systems using across-the-line starting. During the acceleration, the power factor of the motors goes up and reaches the maximum value. After reaching the maximum power factor, the power factor drops rapidly with the motor speed. The power factors of small motors drops at a much faster rate. Therefore, larger motors show a higher power factor at their operation zone although their power factors during the motor-starting transient is lower than that of smaller motors. And also beyond rated speed power factor drop is more significant. The power factor (PF) of a motor is lower when the motor is under-loaded and is significantly reduced when the motor load is less than 70%. Closely matching the motor to the load is the best way to keep the PF close to the motor design rating.

1.3 Non Power Electronics Solution to reduce The Impact of The Start-up Process

A number of techniques have been developed to reduce the impact of the start-up process. Taking into consideration the equipment used, motor starting methods can be divided into two broad categories: electronic drives and those that are not, i.e. conventional electrical network equipment. Other categorizations focus on the voltage management as applied to the terminals. In this part non electronic solutions are discussed in two broad categories based on their physical characteristics and function:

- (a) full voltage starting
- (b) electromechanical reduced voltage starting

1.3.1 Full Voltage Starting

Across the line or direct online starting (DOL) is the traditional and simplest method of motor starting, and most other methods are baselined against it. This method is the direct connection of the terminal voltage to the motor stator with no additional electrical components, and also for this reason is most economical in terms of installation cost and ease of use. It is also one of most reliable and robust methods.

A) Across-the-line magnetic induction motor starter

A typical full-voltage or across the-line magnetic induction motor starter circuit operation is very simple. When the start button is pressed, the relay (or contactor) coil is energized, causing the normally open contacts to shut. When these contacts shut, power is applied to the induction motor, and the motor starts. When the stop button is pressed, the relay is de-energized, the contacts open and the motor stops. Though magnetic motor starter circuit has several built -in protective features, they are not suitable for large motors.

B) Shunt capacitors

Connecting a capacitor in parallel to the motor can help compensate the reactive demand from the motor during start up by supplying a leading current and thus improving the power factor while still achieving high starting torque because of the full voltage, Fig. 1-3. This provides some relief to the supply source. Shunt capacitor banks are generally used to improve the receiving end power factor and voltage, by neutralizing part of the lagging current in the

circuit. However, an unsuitable selection of capacitance may result in overvoltage due to self-excitation when the machine is disconnected from the supply, [36-39]. Satisfactory compensation over the entire load range requires switching capacitor banks in or out of the circuit at a relatively slow speed [40].

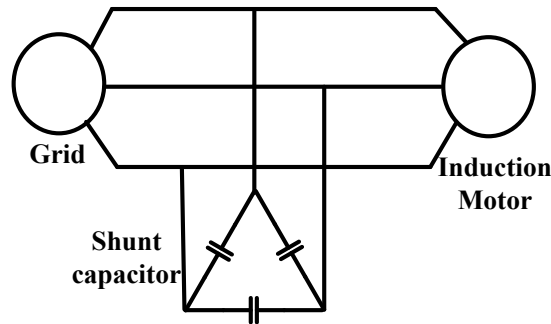


Fig. 1-3. Static terminal shunt capacitor connection

However, the improved power factor is realized only for the grid but not for the induction machine itself. The losses in the machine are not reduced thus the machine still suffers from poor power factor and high current stresses. In the 1980s, as an alternative to improve the mains power factor, the stator windings of a cage-rotor induction machine were rewound to achieve improved power factor [41-42]. The stator windings were divided into two groups with different number of turns. Different connections of two sets of identical stator windings are investigated in [42] and results show mechanical output capability of the rewound induction machine is reduced.

1.3.2 Reduced Voltage Starting

Another popular method that can be used to reduce the impact of the start-up transient on both the power system and the motor itself is to reduce the voltage supplied to the motor. This will, in turn, limit the inrush current drawn by the motor (for a given speed, motor current is proportional to the applied voltage), which will reduce the impact on the bus voltage and also the transient torques and forces seen by the motor [14, 22, 28]. The motor torque will also decrease at a rate roughly proportional to the square of the decrease in voltage (i.e., 80% reduced voltage results in $(0.8)^2 = 0.64$ or 64% of nominal motor torque). If the voltage is reduced too much, the torque may be reduced to the point where the motor may not start the load at all [20].

Reduced voltage starting can be accomplished in three different ways:

A) *Primary resistor/reactor*

Primary resistor/reactor starting is one of the least complicated ways to reduce the voltage to the motor during starting to reduce the impact of starting transients, Fig. 1-4. It is achieved by placing some form of impedance in series with each motor winding. The two most commonly used impedances are resistors and reactor assemblies. One of the main advantages of such starters is that they are usually supplied with adjustable impedance. The user can select the amount of voltage that will be applied to the motor while starting [22, 28].

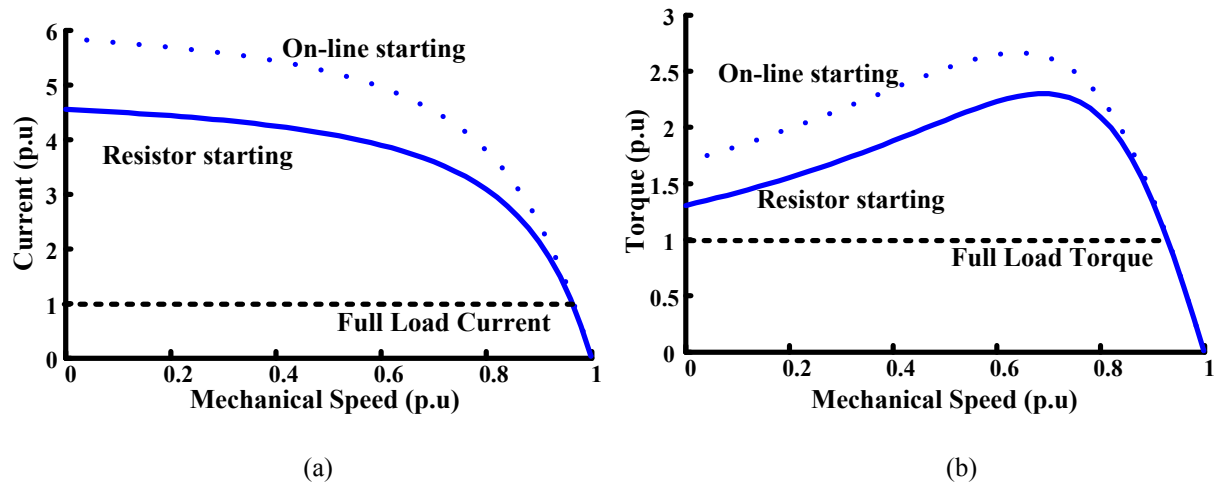


Fig. 1-4. Reduced voltage starting of an induction motor; a) motor current vs speed, b) motor torque vs speed

The use of a reactor during starting results in an exceptionally low starting power factor, but does not produce as much heat as that normally associated with a resistor. When using a series reactor bank, it will oppose the inrush current initially and reduce the terminal voltage proportionally. The most advantageous characteristic of the series reactor starting is that the voltage increases over time as a function of the rate of change of the current without additional control. But the added reactance will also further increase the starting reactive power.

B) *Star-delta.*

Another type of electromechanical reduced-voltage starting that is used extensively, motor voltage level below 1000V, is wye-delta starting. The effects of reduced-voltage starting are achieved by changing the way that the windings are connected to the line. During normal operation the windings are connected in a delta configuration, but for starting, the windings are connected in the wye configuration.

By connecting the motor in wye, the line voltage is applied across two of the windings, resulting in 58 percent ($1/\sqrt{3}$) of the line voltage across each winding. Both the starting current and torque are only 1/3 of the values that would be obtained by starting the motor in delta. There are no external resistors or transformers to reduce the voltage to the motor terminals.

A drawback of this method is that it requires the neutrals of the motor, in addition to the normal line leads, to be externally connected (six leads). Thus, this starter is not an option for use with a motor that was originally constructed with only three leads. Wye-delta starting requires additional contactors in the starter, which drives up the cost of the equipment. This system is relatively simple to operate, but adjusting the starting characteristics is not an option once the system is installed. Overload protection needs to be designed for both the wye and delta connections [22, 28].

C) *Auto transformer*

With autotransformer starting, a tapped transformer is used to supply reduced voltage to the motor. A three-coil autotransformer is used as wye configuration and connected to the motor in such a way as to supply reduced voltage to the motor when the line voltage is applied to the autotransformer. Several sets of taps are usually available to the user to provide different values of reduced voltage (NEMA standards are 80%, 65%, and 50% of the full line voltage) [22]. Additional taps can also be requested for supplementary reduced voltage ranges. With autotransformer starting, the line current is always less than the motor current during starting because the motor is on the secondary of a the transformer during acceleration, If a motor is connected to the 50 % tap of the autotransformer, the motor current would be reduced to 50 % of the normal starting value, but the line current would be only 25 % of the normal starting current. Since the motor starting current is greater than the line current with an autotransformer starter, the starter produces more torque per-ampere of line current than any other type of reduced voltage starter [43].

Its popularity is attributed to the fact that this type of starter can reduce the inrush current in the distribution system to the lowest level of all the different electromechanical types of starters. In addition, the taps on the autotransformer permit adjustment of voltage and motor torque. It is ideally suited for starting most industrial loads.

However, in all reduced voltage starting switching of voltage can result in a high spike of current during this transitory period of operation. The magnitude of this spike is dependent upon the motor speed and current when the switching occurs. There is a torque transient associated with this current peak which again may cause further problems [43].

1.4 Thesis Objective and Outline

This thesis describes the use of H-bridge converter with grid to control motor voltage. If the motor is directly connected with grid no control over the motor voltage, but with the proposed topology, termed as 3-phase H-bridge system can regulate the motor voltage during starting, or keep rated voltage under voltage sag and swells. Even the proposed system can maintain the motor operate at maximum efficiency through-out the load range.

This topology has two appealing aspects: from grid side performance- reactive power generation instead of consumption and sustain to voltage sag in utility. And from the motor point of view the proposed system can soft start the motor, reduce the motor loss by operating the motor at variable voltage under fixed efficiency point.

To clarify the operation, the motor voltage control is presented with existing power electronics solution to induction motor drive system. The necessary vector diagrams with mathematical equations under steady state condition are derived for the operation of the H-bridge converter. As the system response is slow in nature, steady state equations are sufficient to describe the system. Equivalent circuit model parameter of induction motor is used to derive the plots.

The application of bridge voltage control during soft start operation is explained. Controlling the bridge voltage during start reduce starting stress in the system. Transient conditions during starting are simulated in the Matlab environment with experimental validation.

During voltage sag or swells the proposed system can maintain the motor at its rated value. Theoretical maximum sag tolerance is explained. Experimental and theoretical sag tolerance with reactive power generation capability of the proposed system is presented.

Though the motors are rated for nameplate data but many motors are operated from the name plate rating (deviate from name plate data rating) and their performance is compromised.

Motors performances are evaluated. Different motor operating conditions are considered and compared. The proposed topology is compared with VFD and results are given. Also a control method with motor name plate data is proposed. Relationship between the motor winding temperature rise and motor losses are presented. The experimental results validate the theoretical predictions. The results show 3-phase H-bridge is suitable solution where frequency control is not required.

1.5 Thesis Contributions

The work presented in this thesis contributes to voltage control of induction motor. The 3-phase H-bridge can be inserted between the utility grid and an induction motor to inject a voltage in series with the grid voltage. The magnitude and phase of this voltage is used to control the motor voltage to improve the performance of the overall system.

The main contributions are as follows:

A) *Model development and implementation*

- The model of the proposed system has been developed in the Matlab–simulink environment and simulation is completed for different settings.
- The controller is developed in dSpace and control the motor voltage in real time.
- Define the relationships between the grid voltage sag compensation limits with the machine load and its operating power factor.
- Propose a controller using readily available machine parameter from the motor nameplate data

B) *Advantages of the proposed topology*

- A controllable motor voltage allows the power electronics to function as a motor soft-start.
- Maintain motor voltage at its rated level during grid voltage disturbances (sags and swells).
- Controlling motor voltage-increase or decrease the voltage relative to the grid voltage can improve the motor operating efficiency over the entire motor load range, from no-load to full-load.

- Lower system losses can lower energy bills, improve the power rating of the machine.
- Lower motor loss can reduce operating temperature and prolong its operating lifetime.
- Improve motor operating efficiencies under a mismatch condition between grid voltage and rated motor voltage.
- With a relatively higher operating efficiency, lower cooling requirements are required for the power electronics and machine.
- Optimize the machine power conversion efficiency as the load changes; hence saves energy cost, lowers the machine operating temperature and extends the life-time of the machine.

C) *Comparison of the proposed H-bridge with drive*

The most widely used drive in electrical motor is variable frequency drive or VFD which can control both motor's voltage and frequency. But the standard drive can only reduce the motor voltage relative to grid and only two level voltage output can be obtained. High dv/dt stresses on the motor winding is observed. Moreover, with input L-C filter a VFD cannot supply the motor with rated voltage if the grid and motor and grid are rated at same voltage. So, it's a common practice to supply a 460 v rated motor from a 480 v supply. But

- The proposed system can increase or decrease the motor voltage relative to the grid voltage and thus improve system operating condition.
- 5-level pwm motor line voltage with a pwm frequency up to four times the switching frequency is achieved. Capacitor voltage is reduced by half. For a 230 V system, using a VFD, the capacitor voltage is reached to 325 V but in the proposed system the voltage is only 165 V. Reduced voltage step sizes results lower higher frequency pwm induced iron losses and Cu losses.
- The system generates VARs, hence improves the overall system power factor rather than lowering it.

Chapter 2

2 Smart Electrical Grid Interface for an Induction Motor

To place the thesis work in context, several power electronics systems are described that are used with an induction motor to provide either a soft-start or to improve its steady-state operating performance. From the perspective of this thesis, the phase-controlled thyristor ac/ac converter and the VFD represent opposite contrasting technologies. The thyristor converter controls the motor voltage only (frequency fixed), while the VFD provides both voltage and frequency control. The thyristor converter is often used as a soft-start and is more economic and energy efficient. Alternatively, the VFD provides a more superior motor control that includes a soft-start with lower supply rms currents, and also variable frequency motor control. However, the VFD has several disadvantages, including: higher energy losses; a higher cost; a larger product that often includes input and output ac reactors; sensitivity to grid voltage sags. The proposed 3-phase H-bridge converter described in this thesis provides an alternative solution to both these technologies, but also noting that it is not capable of motor frequency control. In short, the proposed system provides a series voltage injection with the utility voltage and can be used to control the motor voltage either above or below the grid voltage. This can be used to improve the operating efficiency of the motor and also to compensate for grid voltage sags and swells. The proposed system naturally generates VARs and can work as a series VAR compensator. The basic operation of the proposed system is described as an alternative to existing power electronic motor controllers.

2.1 Introduction

Starting large ac motors, with their associated loads, has always been a challenge from an electrical perspective. Motor starting systems using power electronics have increasingly been used over the years, replacing electromagnetic line starters and conventional voltage reduction starters, because of their higher performance, lower cost, size and weight, and more accurate

starting current control. Initially, 1970-1990, the thyristor phase controlled converter was the most popular semiconductor soft-start as it was the only device that could handle the large power required in many industrial applications. After 1990, the introduction of the IGBT made VFDs more feasible at industrial power levels and has been increasingly been used both as a soft-start and a variable frequency motor controller. Power electronic converters in general allows the induction motor to be more accurately controlled, together with its load, with higher power conversion efficiencies and associated lower energy consumption.

The main function of a VFD is to draw electrical energy from the electrical grid and supply electrical energy to the motor at whatever voltage, current and frequency necessary to achieve the desired mechanical output. Despite the wide range of specific applications, the generalized motor drive configuration can be viewed as five separate parts: the power supply, the power electronic converter, the electric motor, the controller, and the mechanical load, see Fig. 2-1. Electrical power applied to the motor flows through the power electronic converter where it is regulated by the controller using feedback information from the available sensors.

The power electronic converter essentially provides the interface between the power supply and the motor. A number of techniques using power electronics have been developed either to start an induction motor or to control its steady-state operation using variable frequency control. Hence, power electronic converters for supplying power to an induction motor can be classified into two broad categories: a) solid-state reduced voltage starting-control only voltage; b) VFD starting-control both voltage and frequency.

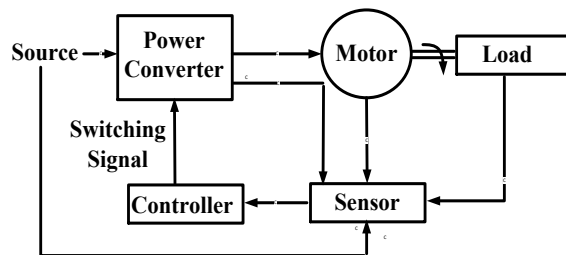


Fig. 2-1. Electric drive system

A traditional soft start system using voltage control is also associated with low lagging factor and high harmonic currents. Some attempts have been made to operate a grid connected induction motor with a leading power factor by modifying the motor structure or using a dual converter topology with an open winding motor. The majority of reactive power correction

techniques take the form of reactive current injection, such as using a capacitor bank, but these do not provide a motor soft start function. The prime purpose of the power electronics presented in this thesis is to bridge the functionality gap between soft start and VAR correction, whilst providing a range of useful features associated with the voltage control of a standard squirrel cage induction motor.

2.2 Reduced Voltage Starting-Solid State Starter

A solid-state reduced-voltage starter introduces power semiconductors between the power source and motor during the starting of a motor, just like a primary-impedance type starter [44-46], Fig. 2-2.

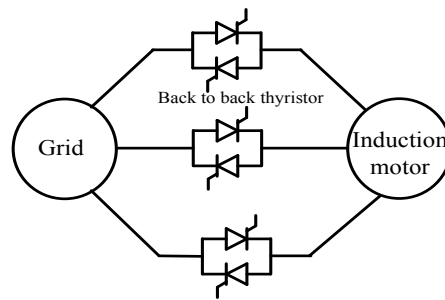


Fig. 2-2. Thyristor based soft start

The six thyristors (SCRs), two per phase, in a back-to-back or reverse parallel configuration control the power to the motor. The power to the motor is reduced by phase angle control the on times of the SCRs in a precise sequence. The SCRs only allow a portion of the three-phase supply voltage to be supplied to the motor on starting, thus reducing the current to the motor. The motor receives enough current to start rotation and accelerates to full load speed as the SCR's allow more voltage to reach the motor. When the motor has reached full speed, the SCR's may be "turned on" fully. However, the current should not be reduced beyond the level that is needed for the motor to accelerate. The current threshold level is often adjusted on an application basis to achieve acceptable acceleration [43].

The soft-starter has to have significant flexibility in operation (e.g. acceleration time and stator winding heat) due to the variability of the mechanical load characteristics. This can result in lower maintenance cost, increased operational lifetime and can result in improved energy efficiency. Solid-state starters are typically more expensive than electromechanical starting

techniques, but may provide a lower total cost of ownership over the life of the motor [43]. There are limitations to solid-state starters, primarily due to low lagging factors and low-order harmonic currents caused by the switching patterns of the thyristors. This may put the solid-state starters in conflict with more stringent standards of power quality [47]. Moreover, with high loads, mostly as a result of the harmonic currents, the efficiency of the system with a solid-state starter tends to get somewhat less than that of the motor alone [43, 46].

2.3 Standard VFD

Variable-speed motor drives have existed for more than a century. Enormous improvements have been made since the use of the Ward-Leonhard dc drive, first using mercury arc rectifier controlled drives then to silicon-based controlled drives. Since the 1980's microprocessors have enabled the development of cost effective digital drives. The widespread availability of the DSP and FPGA technologies has enabled the development of a large capacity of drives with advanced features [48-50]. For conventional VFDs, the uncontrolled front-end passive ac to dc rectifier is used with load side standard voltage source inverter (VSI), Fig. 2-3.

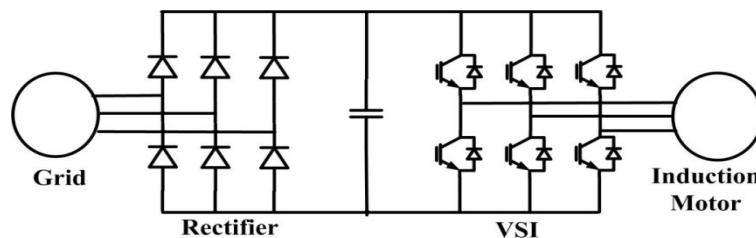


Fig. 2-3. Variable frequency drive (VFD)

The VSI has been one of the most influential power converter widely used in VFDs. Variable voltage and frequency control can be achieved by using the pulse width modulation (PWM) techniques [51, 53]. Control of the IM can be either scalar or vector control. Scalar control (V/F Control) is one common speed control technique. Generally, drives using this control do not use feedback signals (open loop control). Hence, a control of this type offers low cost and is an easy-to implement solution [49], with very little knowledge of the motor being required. A disadvantage of scalar control is that torque is not controlled directly, so any change in torque may result in electromagnetic torque and speed oscillations; the transient response is also slow in nature [54]. Contrarily, in vector control, not only magnitude and frequency but also instantaneous positions of voltage, current, and flux space vectors are controlled. A more stable

motor control is obtained [55-56]. The major drawback of this control is that it requires coordinate signal transformations and the control is dependent on the machine parameters.

Reliability of the VSI drive is of utmost importance in industries. Drives used in critical industrial processes often require the drive to run smoothly in spite of voltage dips or momentary power interruptions on the grid. But, these drives can be very sensitive to voltage sags. An improved sag ride through capability requires the use of energy storage elements using series voltage injection, or rotating shafts, and can be limited to a few ac supply voltage cycles [57].

VSIs can lead to a significant increase of the IMs operating temperature due to the additional losses associated with the harmonic distortion inherent to output PWM voltages (even when output filters are used). The operating temperature increase in VSI fed IMs, associated with the voltage transients at the motor terminals, due to the voltage reflection effects in the power cables, can also lead to a significant reduction in the motor stator winding insulation system lifetime [58]. Also, the commonly used uncontrolled input diode rectifier impresses low order harmonic currents on the utility grid system, which may cause power quality problems, especially for weak ac power systems [59, 60].

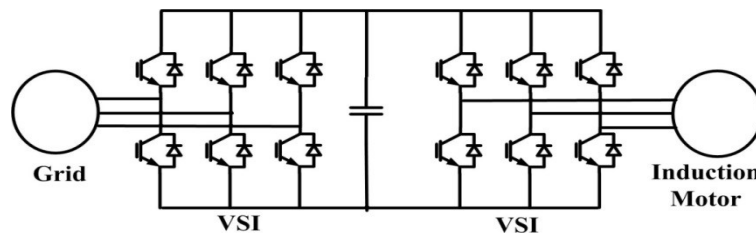


Fig. 2-4. Back to back (BTB) converter

To cope with more stringent power quality standards, some VFDs are equipped with active rectification or back-to-back (BTB) topology, in which a total of 12 switches are required, Fig. 2-4. The most common approach for active rectification is a voltage boosting ‘active’ voltage source rectifier (VSR) combined with LCL filters to synthesize sinusoidal input currents [61-63]. This topology has potential for full control of both dc-link voltage and input power factor, and it can work in both rectifying and regenerating modes. Appropriate filters (either L or LCL) may have to be inserted between the utility grid and the drive input terminals to reduce high frequency current harmonics. The use of these filters, along with heat sink requirements increases the drive overall cost and has been identified as a major barrier to increased power

density [63]. Back-to-back converters can also suffer from lower efficiency if the rated motor voltage is lower than the grid input voltage: the input voltage has to be boosted and then bucked [61]. Finally, with two-level BTB topology (12 switches), the motor line voltage waveform has only three levels, which introduces high dV/dt stresses on the insulation of the motor windings. If these voltage levels exceed the machine's insulation corona inception voltage, motor winding insulation life will be shortened.

2.4 Dual Inverter Drive

An inverter fed motor drive using two inverters is an attractive option for high power, high performance applications. In 1993, Stemmler and Guggenbach introduced the concept of the dual multilevel inverter for IMs with open-end stator windings: multilevel motor voltages are achieved by feeding both ends of the windings from the inverters [64], Fig. 2-5. The inverter increases the motor voltage which can be used to use a lower dc supply voltage, lower the motor current ratings or to extend the motor speed operating range [65-66]. When motor-drive systems are operated from a constant voltage battery source, the basic restraining factor on the motor operation is the need for flux weakening in the high speed range, hence lowering the motor torque and efficiency [67, 68]. Dual inverter topologies where the two inverters use the same dc voltage source has limited voltage boost capability and introduce circulating current in the system [66]. But the second inverter bridge can use a separate dc power source [68] or can be disconnected from any power source and thus make the dc side of the inverter floating [69]. The floating capacitor inverter can be allowed to fluctuate naturally depending on load [69]. This inverter provides reactive support to the electric machine and the motor voltage can be increased 70% or the supply voltage can be dropped to 30% by using this configuration when compared to using a single inverter and a wye connected machine [67, 69].

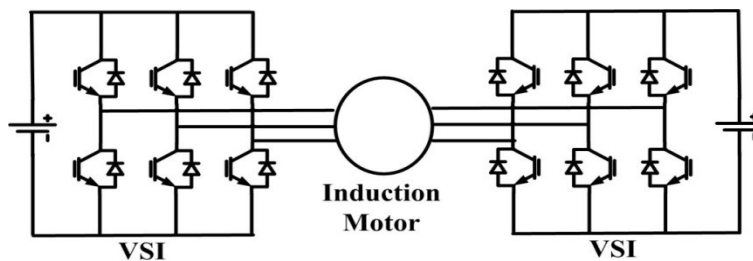


Fig. 2-5. Open winding induction motor configuration

2.5 VAR Compensation

As already mentioned the current drawn by induction motors are lagging in nature. To compensate the resultant reactive power many power electronic converters can be connected to the utility grid. FACTS (an abbreviation for flexible ac transmission systems) refer to a group of power electronic topologies used to overcome certain limitations in the static and dynamic transmission capacity of electrical networks. While FACTS has been available for many years, new communication and control technologies can improve power system reliability, reduce transmission costs and facilitate higher levels of renewable energy use [71].

Among the different types of FACTS devices, these are divided into two categories, determined by the way in which they are connected to the power system: parallel or shunt compensation (which continues to be the most common) and series compensation (Fig. 2-6).

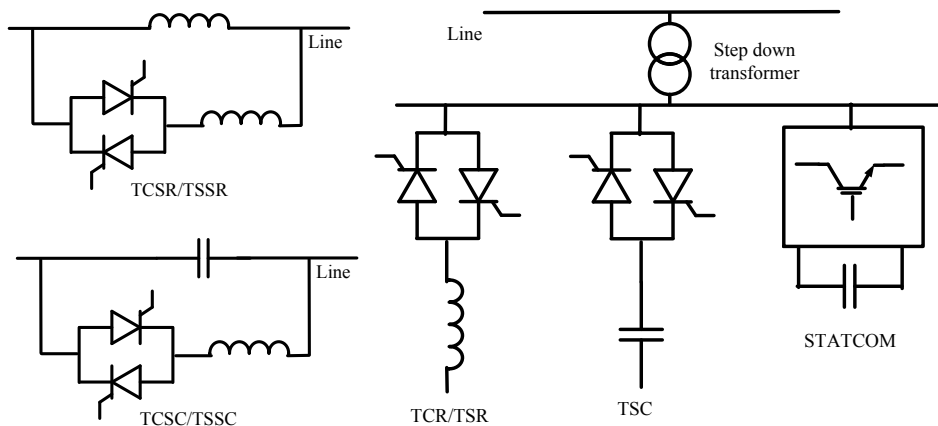


Fig. 2-6. VAR compensation; a) series compensation, b) shunt compensation

The thyristor switched capacitor (TSC) and the thyristor controlled reactor (TCR) are two thyristor based static VAR compensators (SVCs). The static synchronous compensator (STATCOM) or static synchronous condenser (STATCON) is a voltage source converter based shunt compensation device. By controlling injected current in quadrature with voltage at the point of coupling, the amount of reactive compensation can be adjusted. [72].

Thyristor controlled series compensator (TCSC) is a line impedance control device. Topologically, it is the same as TCR in parallel with fixed capacitor type SVC. It includes a back-to-back pair of thyristors, an inductor in series with the thyristors and a capacitor in parallel

with the inductor and thyristors, shown in Fig.2-6. By controlling the firing angle of the thyristor pair, the average reactive compensation can be continuously varied [73].

A more advanced series compensation FACTS system is the static synchronous series compensator (SSSC). As a dual of the STATCOM, the SSSC is a VSC based device. It can provide the same range of capacitive and inductive compensation. Power flow is controlled by varying the equivalent impedance between two buses in power grid. The dynamic voltage restorer (DVR) is a means of mitigating voltage sag in power systems and is a series compensation device using VSC with coupling transformer similar to the SSSC [74].

The unified power flow controller (UPFC) is a combination of series and shunt compensation and is able to control, simultaneously or selectively, all the parameters affecting power flow in the transmission line (i.e., voltage magnitude, impedance, and phase angle). But a transformer must be used as an interface between the transmission line and each inverter. Moreover, the transformer based UPFCs are still too slow in dynamic response due to large time constant of magnetizing inductance over resistance and pose control challenges because of transformer saturation, magnetizing current, and voltage surge [75].

2.6 Floating H-Bridge Converter

Single phase bridge topologies using phase floating capacitors are a viable multilevel power converter system. Compared to the traditional two-level converters, the multilevel converters have significant advantages such as the enhanced quality of the output voltage at low switching frequencies, low electromagnetic interference, low-voltage stress on semiconductor switches, reduced voltage derivative, higher efficiency, etc.. At higher number of voltage levels, the pulse width modulated staircase waveform is an approximation of a sinusoidal waveform, and hence, expensive and bulky filters can be avoided. Also, the massive transformer for stepping up the voltage in high voltage application can be eliminated, as the multilevel inverters can generate high-voltage waveforms using low voltage rated switching devices [76-77].

A number of multilevel converter topologies most commonly the neutral-point-clamped (NPC) inverter [78], the flying capacitor (FC) inverter [79], and the cascaded H-bridge (CHB) inverter [80] have been proposed since the introduction of the concept of multilevel power conversion in the late 1980s. The CHB multilevel converter is a widely accepted topology in the

industry. The series connected H-bridge cells are fed directly from isolated dc voltage sources, Fig. 2-7. This topology is chosen in many high-voltage applications due to its modular structure and simple control schemes [81]. A major limitation of this topology is the requirement of multiple dc voltage sources [82-83]. When conversion of real power is essential, the difficulty of supplying power to so many dc sources may preclude the use of the CHB inverters. In addition to the conventional multilevel converters, a number of new multilevel topologies for different applications have been proposed in the literature. A hybrid inverter topology comprising of a multi-level inverter in series with H-bridge cells is presented in [83]. This topology can provide five-level voltage output with effective capacitor-voltage balancing. Higher number of output voltage levels is always preferred in the multilevel inverter-fed ac drives as it reduces the harmonic distortion and also reduces torque ripple in the motor significantly. So, a hybrid converter formed by the series connection of a main three-level NPC converter and auxiliary floating H-bridges (NPC-HBs) has been presented in [84-86]. The NPC is used to supply the active power while the H-bridges (HBs) operate as series active filters, improving the voltage waveform quality by only handling the reactive power and thus reduces the need for bulky and expensive LCL passive filters; making it an attractive alternative for large power applications [85, 84]

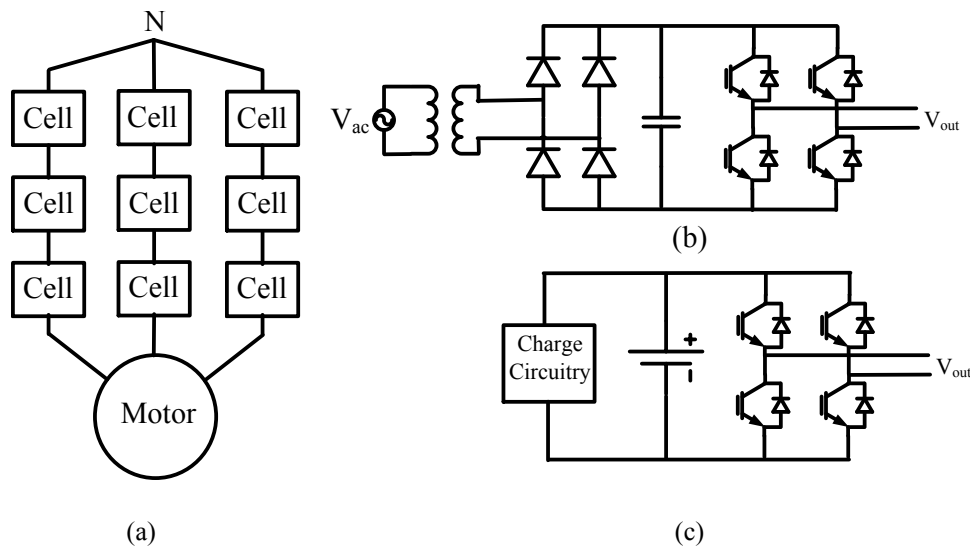


Fig. 2-7. The cascaded H-bridge topology a); with b) phase-shifted transformers, c) batteries supplying isolated cells

The magnetic energy recovery switch (MERS) was developed for high power application for reactive compensation and voltage control of loads or generators [87]. The configuration was

suggested for series compensation of transmission systems, Fig. 2-8. Recently, starting an induction motor using serial voltage injection has been proposed [87-89], in which magnetic energy recovery switches (MERS) are inserted between the utility grid and induction motor. However, this configuration uses line-frequency switching and harmonic currents are generated, which cause mechanical oscillations. It has been experimentally confirmed that open loop control of MERS cannot increase the motor voltage over a certain value because of oscillation and ‘runaway situation’. Close loop control was found to be useful to damp the oscillation, but the oscillation cannot be completely avoided [89].

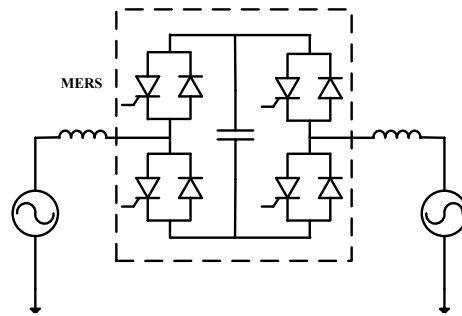


Fig. 2-8. Configuration of the MERS

In general, at higher number of voltage levels, the cost and the complexity of multilevel inverter circuits increase, and reliability decreases due to the presence of a large number of components and the associated control circuits. Hence, one of the main areas of research in this field is the development of multilevel inverter topologies for low voltage systems that use fewer components, with higher reliability and higher efficiency.

2.7 Proposed 3-phase Floating H-bridge System

The prime purpose of the power electronics system presented in this thesis is to provide: voltage control of an induction motor to mitigate inrush current during starting; voltage boosting during operation to compensate for low supply voltages; variable voltage to improve the motor efficiency, as well as to provide good ride-through capabilities for critical loads driven by induction motors. The implementation of the proposed topology reported in this thesis utilizes three single-phase floating capacitor voltage source H-bridge inverters to inject a voltage in each phase being supplied to the motor, see Fig. 2-9. The 3-phase H-bridge uses a standard 3-wire induction machine, Fig. 2-9(a); and uses 12 switches. The 3-phase inverter version, Fig. 2-9(b),

requires an open winding machine, using a 6-switch standard 3-phase inverter module, and operating with a dc voltage double that experienced in the 3-phase H-bridge version. Due to the potential benefits, the analysis and experimental results reported in this thesis were obtained using the 3-phase H-bridge; however the series voltage injection controller used is identical for both implementations.

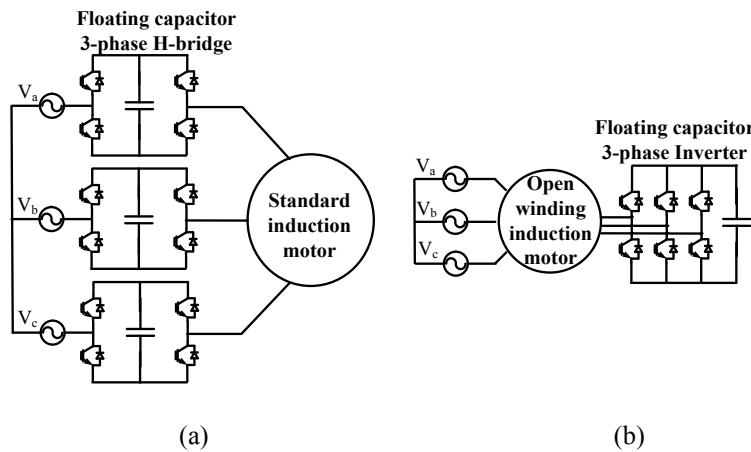


Fig. 2-9. Power electronic converters for series voltage compensation of a smart grid connected induction motor (a) 3-phase H-bridge, (b) 3-phase inverter

The principle of operation of an induction machine with series voltage injection is described and possible range of operation is investigated assuming an idealized system. Key assumptions for this discussion are: (1) that there is no real power transfer to the floating bridge, only reactive power flow; (2) that the power factor of the motor remains constant. These assumptions are suitable to enable a simple understanding of the system operation. The realities of operating with a non-ideal bridge, variable motor power factor and transient requirements are also discussed. As there is no real power transfer between the ac circuit and bridge, the voltage at the ac terminals of the floating bridge must be controlled to inject a voltage into the circuit that is perpendicular to the current phasor. As a result, the voltage across the terminals of the motor is phase shifted relative to the grid supply voltage.

2.8 Basic Bridge Operating Principle

The steady-state operating principle of the proposed system can be illustrated using a single phase equivalent circuit, Fig. 2-10 (a), and a voltage vector diagram representing one

phase of the system, Fig. 2-10 (b). Various angles are identified in Fig. 2-10 (b) for analysis purposes.

A single phase floating capacitor H-bridge inverter is modeled as a variable voltage source using 3-level pwm voltages in each motor phase with a fundamental component, V_b . Two H-bridge voltage waveforms, Fig. 2-11 (a), (b) add with the grid line voltage, Fig. 2-11 (c) to form the line voltage delivered to the motor, Fig. 2-11 (d): two H-bridge voltages result in a 5-level pwm voltage in the motor line voltage with a pwm frequency up to four times the bridge switching frequency, Fig. 2-11 (e). The fundamental component of the motor line voltage, V_{Lm} determines the fundamental phase voltage delivered to the motor and is denoted V_m , with the per-phase component of the grid voltage denoted V_g , where line grid voltage is denoted as V_{Lg} .

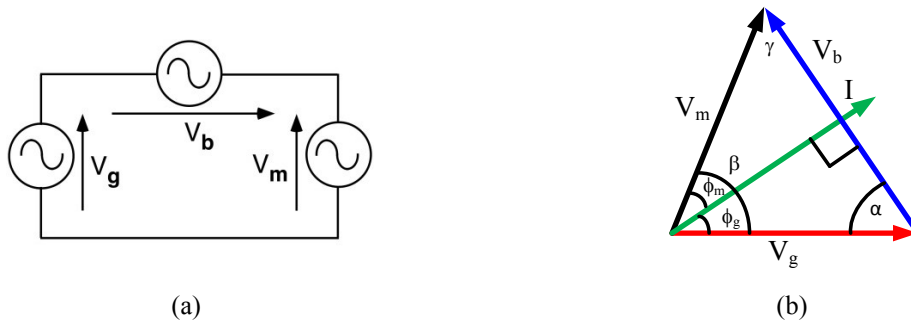


Fig. 2-10. Simplified system fundamental voltage single phase representation; (a) equivalent circuit, (b) vector diagram with angles labelled

When the per-phase voltage injected by the floating bridge, V_b , is zero, the grid voltage V_g and motor voltage V_m are equal and the stator current, lagging the stator voltage by ϕ_m . If a voltage V_b is injected by the floating bridge, the motor voltage is given by the vector summation between the grid and floating bridge voltage ($V_m = V_g + V_b$). As a result, the motor voltage and current are phase shifted relative to the grid supply voltage and the grid power factor may be improved, Fig. 2-12. By changing the floating bridge injected voltage, it is possible to adjust the motor voltage until the stator current is perpendicular to H-bridge voltage. Basic control of the motor voltage is achieved by changing the angle α of the floating bridge injected voltage relative to the grid voltage: generally the higher α the higher is the motor voltage and vice versa, Fig. 2-12. During a transient, the injected bridge voltage will change in magnitude if the current does not lie at 90° to the H-bridge voltage.

However, if the grid voltage magnitude and phase is known together with the H-bridge dc voltage, the angle α can be set by the controller to supply the motor at its desired voltage. Steady-state is reached when the current lies at 90° to the H-bridge voltage: representing a zero net power flow to the floating capacitor H-bridge: the H-bridge switching and conduction losses change this angle slightly depending upon the relative load power level.

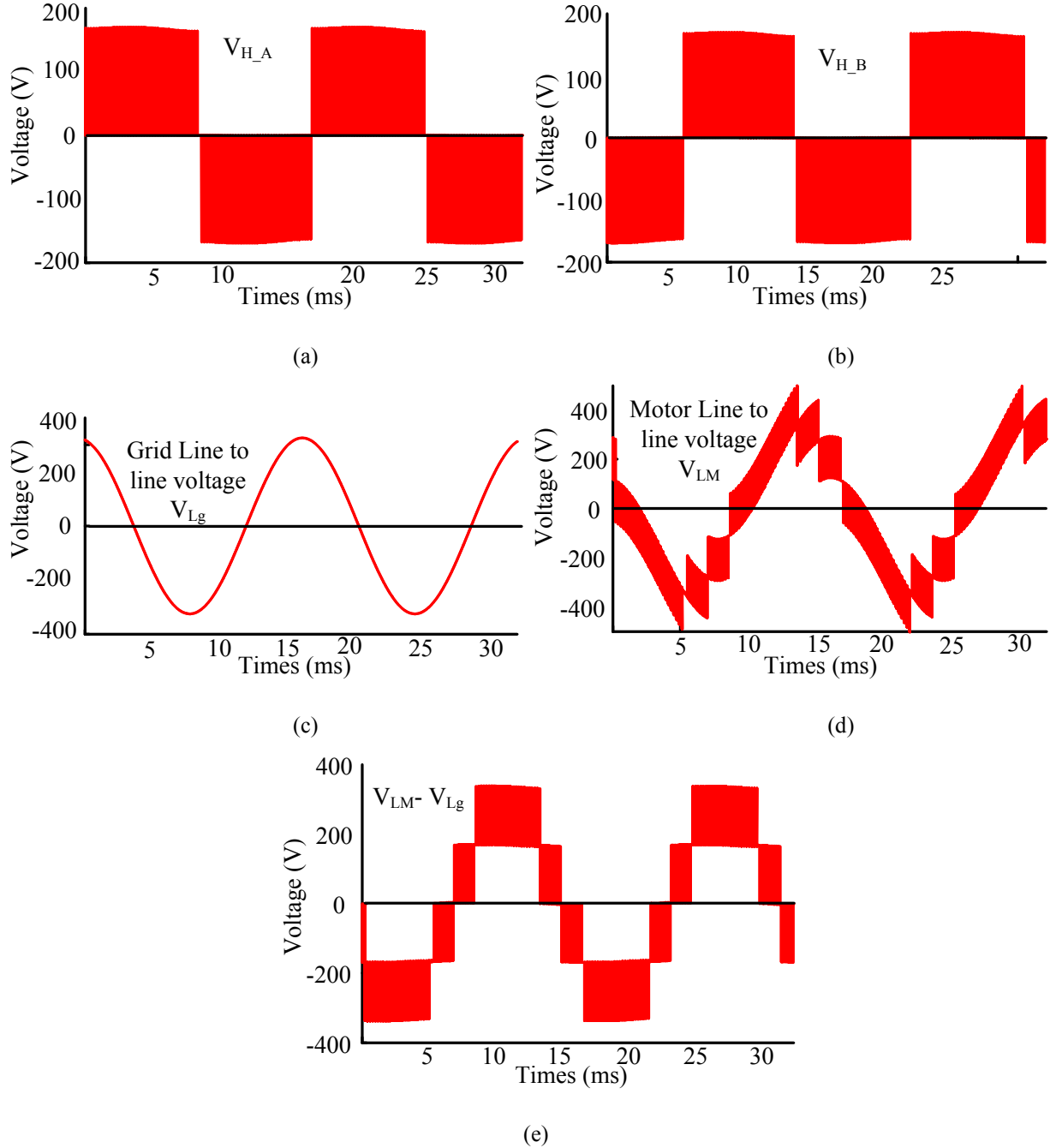


Fig. 2-11. Voltage waveforms; (a) Phase A and (b) Phase B of H-bridge output voltage, (c) grid line voltage, (d) motor line voltage component due to the H-bridges, (e) 5-level PWM waveforms generated by H-bridge

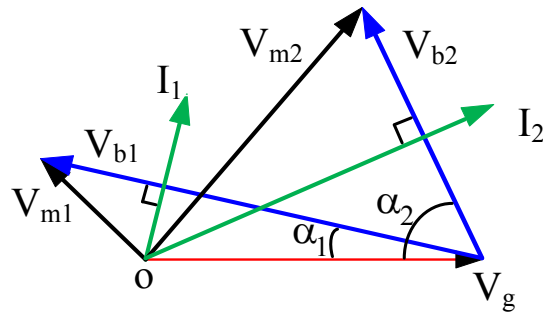


Fig. 2-12. Phasor diagram for floating capacitor H-bridge converter motor drive system

The voltage injection angle α , Fig. 2-11; can be controlled to deliver the desired motor voltage V_m to the motor, see Fig. 2-12:

- (a) reduce voltage: the motor voltage lower than the grid voltage, such as required for soft starting the motor, (V_{m1} in Fig. 2-12);
- (b) increase voltage: the motor voltage above the grid voltage, such as maintaining the motor voltage at its rated value when the grid voltage is reduced (V_{m2} in Fig. 2-12);
- (c) rated voltage: keeping the motor at rated voltage, when grid is equal to rated, Fig. 2-10(b).

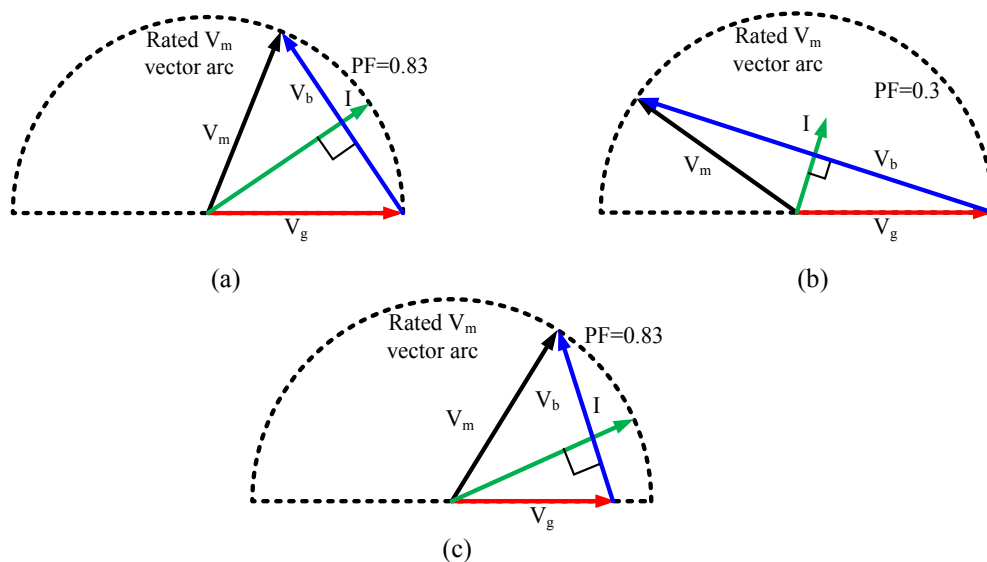


Fig. 2-13. Phasor voltage vectors: (a) $V_m = \text{rated}$, high load, (b) $V_m = \text{rated}$, light load, (c) $V_m = \text{rated} > V_g$, high load

Under rated voltage control, V_m follows a semicircle, Figs. 2-13(a), (b), in the voltage vector diagram, and α is changed to keep V_m fixed as the motor power factor changes: high at full load, Fig. 2-13(a), down to a low value under light load, Fig. 2-13 (b). Alternatively, if the grid voltage is lower than rated voltage, the motor voltage has to be boosted above the grid

voltage, Fig. 2-13(c). The vector diagrams in Fig. 2-13 demonstrate that the 3-phase H-bridge can deliver the desired motor voltage by changing α as long as the bridge capacitor voltage is allowed to change: the amplitude modulation depth m_a of the H-bridges is fixed at its maximum to limit the maximum dc capacitor voltage.

2.9 Voltage Vector Analysis

As the motor load changes, the motor characteristics determines the relationship between the motor voltage V_m , power factor $\cos\phi_m$, and power factor angle ϕ_m , Figs. 2-10 (b): the grid voltage V_g is assumed constant and the same as the motor rated voltage $V_{m,rated}$. During steady state operation, the system power factor angle as seen at the grid ϕ_g , H-bridge fundamental voltage V_b and the resultant dc voltage V_{dc} , can be predicted knowing V_g , V_m , ϕ_m .

For simplification, assume:

$$V_{m,pu} = \frac{V_m}{V_g} \dots\dots\dots 2-1$$

Using Fig. 2-10 (b), ϕ_m , ϕ_g and α are obtained from:

$$\cos \phi_g = V_{m,pu} \cos \phi_m \dots\dots\dots 2-2$$

$$\sin \alpha = V_{m,pu} \cos \phi_m \dots\dots\dots 2-3(a)$$

$$\cos \alpha = \frac{V_g^2 + V_b^2 - V_m^2}{2V_g V_b} \dots\dots\dots 2-3(b)$$

Knowing ϕ_g , ϕ_m the remaining angles in the vector diagram, Fig. 2-10 (b), are obtained using:

$$\beta = \phi_m + \phi_g \dots\dots\dots 2-4$$

$$\gamma = 90 - \phi_m \dots\dots\dots 2-5$$

The system behavior with changing load is presented using the motor equivalent circuit parameters for a 5 HP induction motor given in table 1 in chapter 1.

The grid voltage is assumed to be the same as the motor rated voltage, $V_{Lg}=V_{Lm}=230V$;

$V_g=V_L=230/\sqrt{3}=133V$, and the motor load is assumed to vary over a wide range, typically from 10 % to 100 % of rated. α is illustrated in Fig. 2-14 (a) as a function of the motor load in %. For completeness, γ and β are shown in Fig. 2-14 (b). Noting that the motor decides the relationship between V_m and ϕ_m as the motor load changes, ϕ_m and ϕ_g are shown in Fig. 2-14 (c).

α is increasing from under 10° at light load to close to 50° at high load. The controller uses α to deliver the desired motor voltage and Fig. 2-13 gives an insight as to how this is possible. For rated voltage control, the motor power factor is low under light load and high under high load, see ϕ_m in Fig. 2-14(c). Hence α is low under light load and high at high load, see

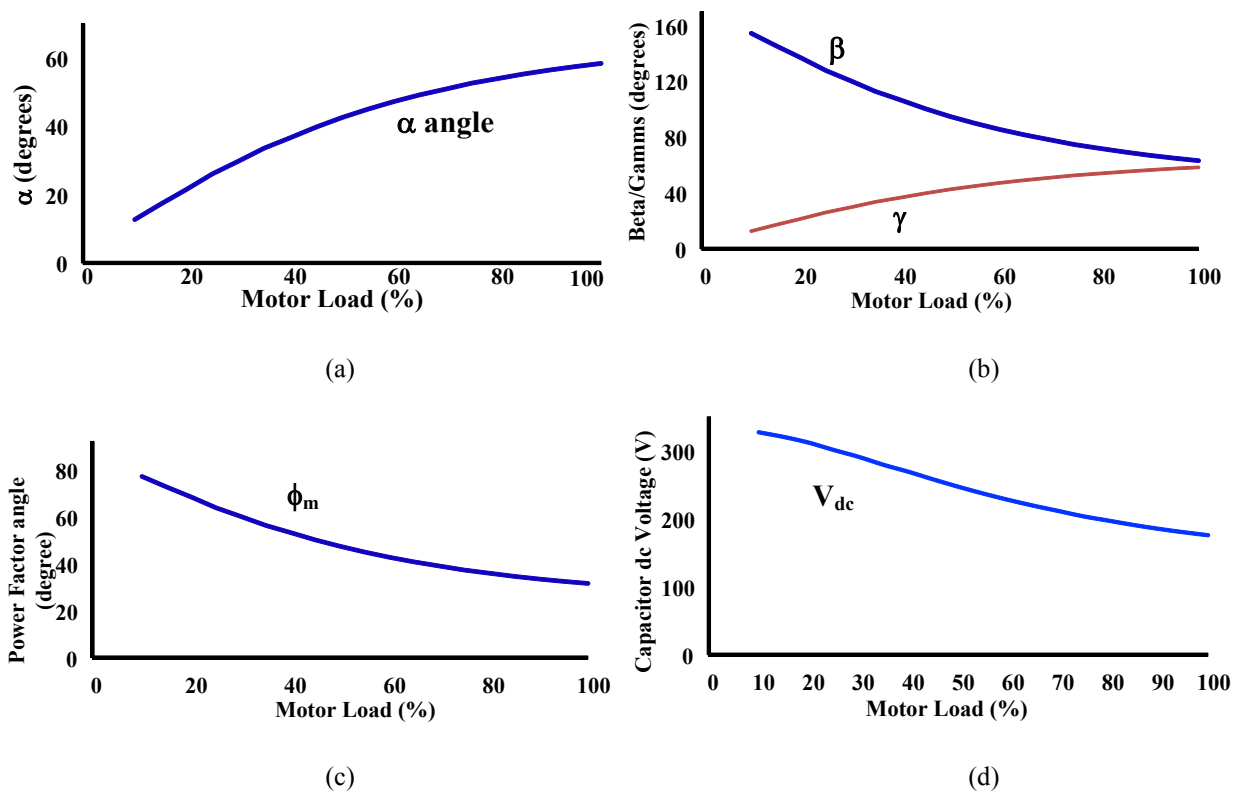


Fig. 2-14. System operations under 3-phase H-bridge configuration: a) control angle α , b) angles β and γ , c) power factor, d) capacitor dc voltage

Eqn. 2-3. Considering Fig. 2-13, α changes from a small value under light load to a high value at high load.

The linear relationship between $\cos \phi_g$ and $V_{m,pu}$, $\cos \phi_m$, see Eqn. 2-2, accounts for the decreasing magnitude of ϕ_g as the load increases in Fig. 2-14 (c). Note that ϕ_g is a leading angle

relative to V_g while ϕ_m is a lagging angle relative to the V_m . For rated voltage operation $V_{m,pu}$ is constant, but ϕ_m decreases with increasing load, hence ϕ_g decreases also.

With the various angles defined and assuming $V_g = V_{m,rated}$, the bridge injected voltage V_b can be predicted using Fig. 2-10 (b), and can be expressed in two ways:

$$V_b = V_g \frac{\cos(\alpha - \phi_m)}{\cos(\phi_m)} \dots\dots\dots 2-6(a)$$

$$V_b = \sqrt{V_g^2 - (V_m \cos \phi_m)^2} + V_m \sin \phi_m \dots\dots\dots 2-6(b)$$

The capacitor dc voltage is minimized by keeping the bridge pwm amplitude modulation depth at maximum, resulting in the bridge capacitor voltage fluctuating with V_b , and given by:

$$V_{cap} = \frac{\sqrt{2} V_b}{m_a} \dots\dots\dots 2-7$$

V_{cap} is plotted in Fig. 2-14 (d) and decreases with increasing load.

These expressions are useful in determining the theoretical system and motor performance when the motor characteristics are known: e.g. system VARs, power factor, and bridge capacitor dc voltage stresses.

2.10 Conclusion

Several power electronics solutions for providing a motor soft start and var control are described. A 3-phase H-bridge system is described that provides multilevel output voltages. The 3-phase H-bridge is described as providing a series voltage injection between the as supply and the motor. Motor voltage control is explained with vector diagrams and mathematical equations are derived to predict the system behavior.

Chapter 3

3 Soft Start

The motor soft-start function of the 3-phase H-bridge is described for starting 3-phase squirrel cage induction motors supplied from the utility grid. The process is based upon the 3-phase H-bridge injecting a fundamental voltage in series between the grid and the induction machine terminals. The motor starting current control described is based upon controlling the angle of the injected voltage relative to the grid voltage in order to control the magnitude of the voltage injection, hence the voltage delivered to the motor. The pwm amplitude modulation depth of the H-bridges is kept at maximum and the bridge dc voltages are allowed to fluctuate to change the magnitude of the voltage injection. An algorithm is described that accurately predicts the magnitude of the dc capacitor voltages before motor starting; hence over-voltage problems can be avoided. Experimental results show that the proposed system and controller can successfully soft start a standard squirrel cage induction machine under different modes and load conditions.

3.1 Introduction

The soft-start current control employed means that the motor voltage is reduced below its rated value to control the motor current, and is zero at the moment of starting: the H-bridge injected voltage is used to achieve this. Hence, no motor inrush current occurs and the motor current is made to ramp up from zero and then controlled at a desired level during the starting period. In addition, an auxiliary safety mechanism is also included so that excessive motor heating during soft start can be avoided.

The current control algorithm presented in this thesis was developed after experience gained from an initial motor voltage estimation PI control algorithm was developed [90-91]. However, this control involved a Park's transformation of the motor current, which was sensitive to interference from system disturbances and current harmonics caused by switching of the

power electronics. Effective tuning of the two PID controllers proved to be a difficult task [90-91].

The proposed motor starting current controller algorithm described in this thesis, was developed to determine the induction motor terminal voltage more directly [90-91], open loop voltage control, based upon direct measurement of the grid voltage and the H-bridge injected voltage vectors; the latter is determined by feedback of the average H-bridge dc voltages and the angle of the voltage injection being used. A closed-loop PI current control approach is used to determine the demand motor voltage required reducing a current error signal to zero; the demand current profile is preset by the controller.

3.2 Motor Voltage Control

The basic function of the controller presented is to regulate the phasor angle α , so that motor voltage can be controlled. The geometrical principle behind the proposed alpha angle control is shown in Fig. 3-1.

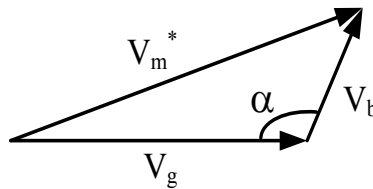


Fig. 3-1. Vector diagrams for the proposed alpha angle control

Control operation assumes that the rms value of the grid voltage V_g can be measured. The average of the three bridge dc voltages can be used to determine the effective series injected bridge ac voltage:

$$V_{dc}^{ave} = \frac{V_{dc}^a + V_{dc}^b + V_{dc}^c}{3} \dots\dots\dots 3-1$$

Averaging the three dc capacitor voltages lowers the effect of the 120 Hz ripple voltage in each bridge. The theoretical fundamental component of the voltage injected by the H-bridge can be estimated from Eqn. 2-7.

$$|V_b| = m_a \frac{V_{dc}^{ave}}{\sqrt{2}} \dots\dots\dots 3-2$$

Note that, m_a represents modulation index of the H-bridge. The pwm method used in this paper uses zero-sequence signal injection to increase the modulation index. The theoretical upper limit for m_a using zero-sequence injection is 1.15. In reality, m_a is fixed and set to be slightly lower ($m_a=1.12$).

V_m^* represents the reference signal for induction motor terminal voltage. The procedure of a current limited soft-start function is to ramp up the motor voltage rapidly from zero until a pre-set desired current limit is reached, and then the motor voltage is held constant to control the current at its desired pre-set level. Upon reaching full-speed, the motor current naturally falls down to its full-speed running level.

3.3 Controller

There are two basic categories of soft-starting methods: voltage ramp starting and current limit starting, Fig.3-2. Voltage ramp starting is the simplest form of soft starting in which the voltage supplied to the motor is increased progressively. The voltage ramp allows the applied motor voltage to increase from zero to 100% over an adjustable period of time, Fig.3-2(a). For current limit starting, Fig.3-2(b), the controller will sense the motor current and alter control signals in order to adjust the motor voltage to whatever value is necessary in order to maintain the current at the desired level at all time during starting and running conditions.

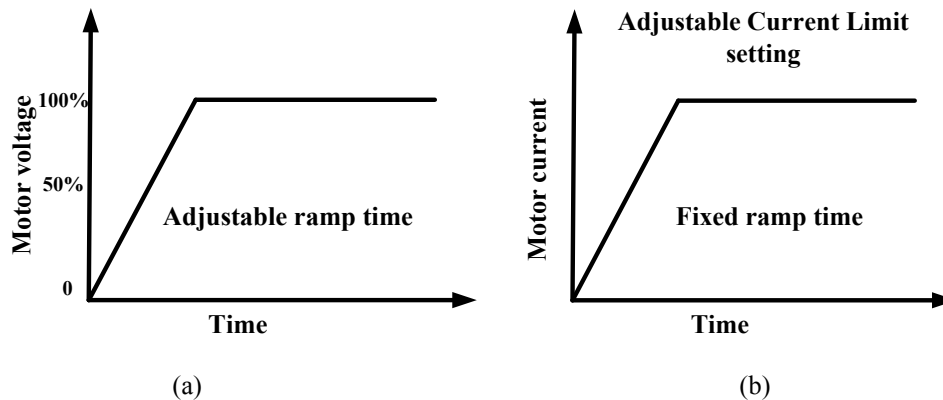


Fig. 3-2. Reduced voltage starting; a) voltage limit, b) current limit soft start

As most of today's soft starter manufactures offer both options in one, voltage ramp starting is also added in this thesis as an alternative soft start option, thus there is a flexibility to decide which soft-starting method is going to be employed before starting the motor. In this way,

the starting characteristics can be improved to provide a more healthy start for both the motor and the connected equipment.

As motor torque is proportional to square of voltage applied [60], reducing starting motor voltage essentially reduce starting torque for the motor. This means if current limit for soft start is set too small, the starting capability of the motor is severely reduced, resulting two possible scenarios: a) the machine may stall, remain at zero speed b) the machine may start but fail to accelerate to its running speed, causing it to run at that sub-synchronous speed. If either of the above scenarios happens, excessive motor heating will result, which may lead to premature motor winding failure [92]. So, a thermal limit timer is used as auxiliary safety mechanism to protect against damage due to over-temperatures during soft start. The threshold for the timer has a nonlinear relationship with the maximum allowable current limit, which is adopted according to the typical induction motor thermal limit curve shown in [93].

The proposed schematic diagram for soft start is given in Fig.3-3.

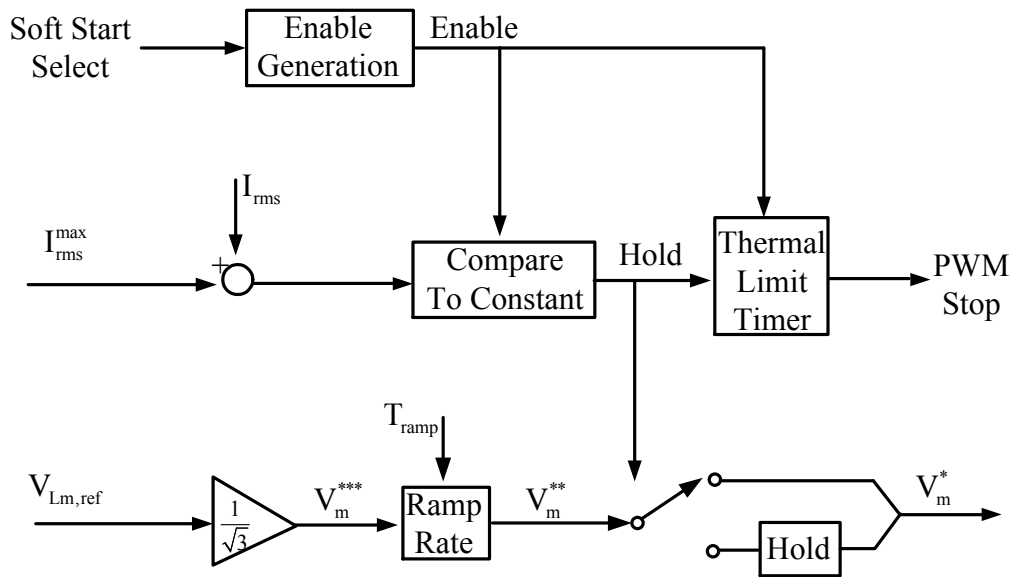


Fig. 3-3. Schematic diagram for soft start

The steady state operating motor voltage, $V_{Lm,ref}$, as well as maximum allowable root-mean-square (RMS) current magnitude I_{rms}^{max} during soft start is defined in the controller. If the actual motor current I_{rms} is below the desired maximum, the output from the ramp rate v_m^{**} is passed through as the motor voltage reference signal v_m^* . If the actual RMS motor current I_{rms}

exceeds its maximum allowable limit i_{rms}^{max} , a hold function is initiated, which locks v_m^* to the most recent value of v_m^{**} until the induction motor reaches steady-state speed and the actual motor current i_{rms} falls below its desired maximum. If the actual soft start time exceeds the threshold specified by motor thermal limit timer, the power electronics automatically turns off; abandoning the soft start process and a warning signal is generated in the human machine interface (HMI).

3.3.1 Control Block Diagram

V_m^* is a function of the desired soft start mode being assumed, PI or PID control is not required, which makes the tuning of the controller much easier, Fig. 3-4. The reference signal for α^* is derived from Eqn. 2-3 (b). A phase correction signal ϕ_{corr} was set at 5° in the experimental system to take into account various signal phase delays, such as PWM signal generation delays, but mainly the 5 kHz clocking frequency of the dSPACE controller ($= 200 \mu S = 4.3^\circ$). An absolute block is used to keep angle α positive during start-up. A PLL is used to track the grid voltage angle (θ), which is used to perform the inverse Park's transformation converting the dq0 frame modulation signals d_d, d_q, d_0 into to abc frame modulation signals d_a^*, d_b^*, d_c^* . Next, triangle intersection implementation of SVPWM [94], is used to obtain the modified modulation signals $d_a^{**}, d_b^{**}, d_c^{**}$ which include the zero-sequence signal. Finally, comparison of the modified modulation signals $d_a^{**}, d_b^{**}, d_c^{**}$ with level-shifted multi-carrier signals yields the gating signals D_a, D_b, D_c for the H-bridges. Thus, five level pwm line voltage waveforms are achieved [95-96].

3.4 Maximum Bridge DC Voltage Prediction

Maximum bridge dc voltage prediction is implemented since it is power factor dependent and has the potential to reach high values. The bridge modulation index is fixed at $m_a=1.12$. This means that H-bridge dc capacitor voltage has a linear relationship with the bridge ac voltage injected.

If per unit (p.u.) value is used, where the rms grid phase voltage is the base voltage ($V_{g,pu}=1.0$) and ϕ_m is power factor angle of the motor, the mathematical equation for ac voltage (p.u.) injected by the H-bridge converter can be obtained from Eqn. 2-6 (b)

$$V_{b,pu} = \sqrt{1 - (V_{m,pu} \cdot \cos \phi_m)^2} + V_{m,pu} \cdot \sin \phi_m \dots\dots\dots 3-3$$

Eqn. 3-3 shows that the bridge ac injected voltage is closely related to two factors:

- a) Motor terminal voltage $V_{m,pu}$,
- b) Motor fundamental power factor angle ϕ_m .

Assuming the grid voltage V_g is set at 1 p.u., then during a soft start, the per-unit motor terminal voltage increases gradually from 0 to 1.0 p.u. Using Eqn. 3-3, the trend for the bridge injected voltage under various motor power factor angles (ϕ_m from 0^0 to 90^0) is plotted in Fig. 3-5.

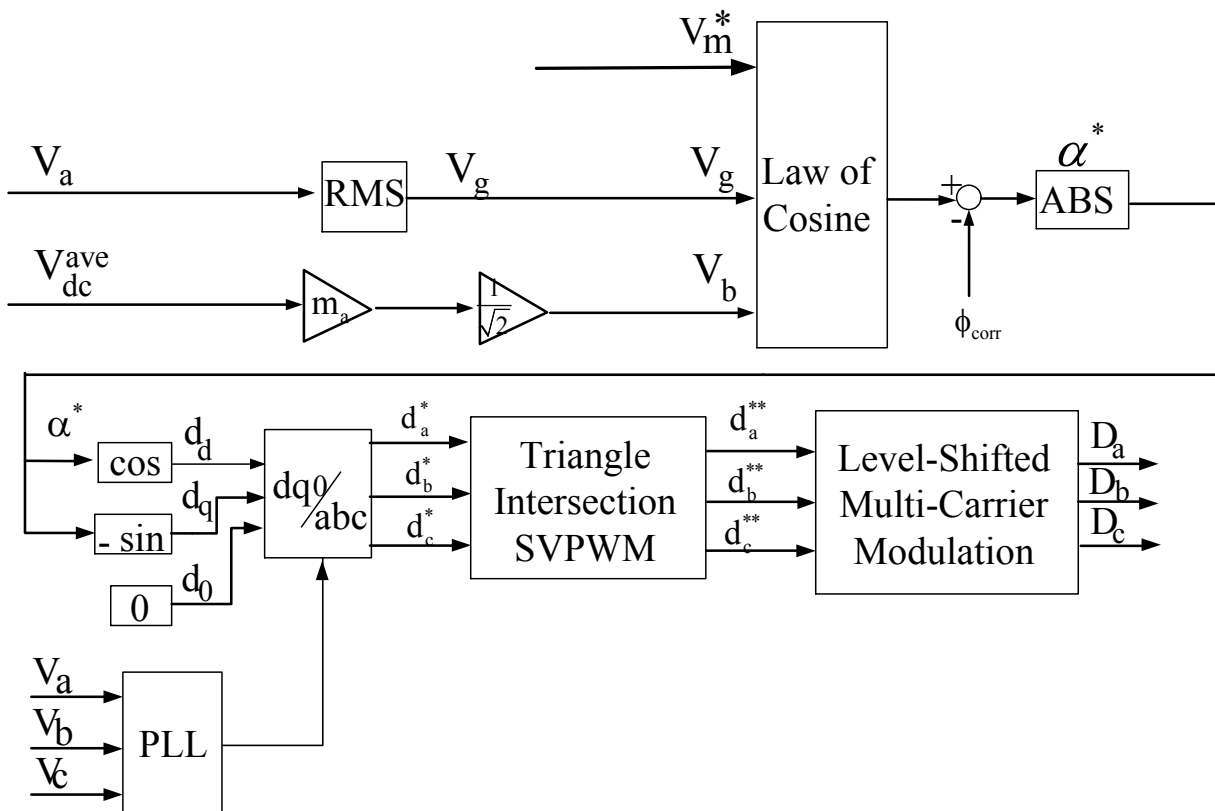


Fig.3-4. Control block diagram.

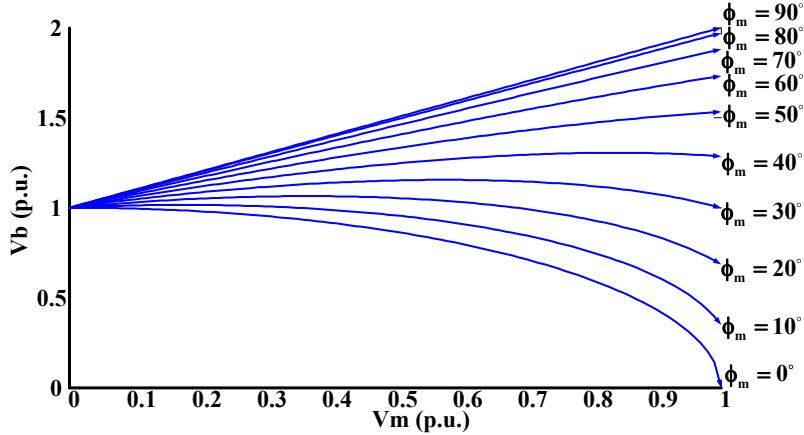


Fig. 3-5. H-bridge ac voltage trend under various induction motor power factor angles

The proposed system can realize soft start of induction motor, in which the motor terminal voltage increases gradually from 0 to 1.0 p.u. . It can be seen from Fig. 3-5 that during any soft start process, the H-bridge ac voltage always starts from 1.0 p.u. Generally, the heavier the induction motor is loaded, the smaller is induction motor power factor angle. There are three scenarios to be considered:

A) Heavy motor load ($\phi_m \leq 20^\circ$): ac voltage injected by H-bridge decreases as soft start progresses ($V_{m,p.u}$ increases gradually from 0 to 1.0 p.u).

B) Medium motor Load ($20^\circ < \phi_m < 40^\circ$): With increase in motor terminal voltage, ac voltage injected by H-bridge first goes up and then goes down.

C) Light motor Load ($\phi_m > 40^\circ$): voltage injected by H-bridge shoots up with increase in motor terminal voltage.

Light motor load condition is more of a concern in terms of bridge dc voltage because an increasing ac voltage injection puts more demand on dc capacitor voltage. At extreme high induction motor power factor angles ($\phi_m \geq 70^\circ$), voltage injected by H-bridge curvatures tend to approximate a straight line. This is because at high power factor angles, the following equations hold:

$$\cos\phi_m \approx 0 \text{ and } \sin\phi_m \approx 1 \dots\dots\dots 3-4$$

Putting value of $\cos\phi_m$ and $\sin\phi_m$ into Eqn. 3-3, ac voltage injected by H-bridge can be expressed as:

$$V_{b,pu} \approx V_{m,pu} + 1 \dots\dots\dots 3-5$$

Eqn. 3-5 shows when the induction motor is close to no load condition, the ac voltage injected by H-bridges tends to shoot up linearly with increase in motor terminal voltage. As a consequence, the dc capacitor voltage also increases linearly as soft start progresses. This means although the behavior of H-bridge dc capacitor voltage has a rather complex pattern under various induction motor load conditions, a simple representation of the worst case scenario for dc capacitor voltage before motor starting can be established. Therefore, maximum bridge dc voltage prediction algorithm is developed which is being included in control algorithm.

3.5 DC Capacitor Charging

In order to generate an artificial voltage vector that is able to counteract with the grid voltage, the dc capacitor voltage of the H-bridge should be charged to an appropriate magnitude before a soft start begins, otherwise, a mismatch between the grid voltage and bridge voltage may cause excessive motor currents. Therefore, the initial charging process for DC capacitor is investigated. Assuming a balanced operation condition between the grid and induction motor, the neutral points between the grid and a Y-connected induction motor stator windings should have the same voltage potential. Therefore, the per-phase equivalent circuit of the 3-phase H-bridge converter is illustrated in Fig. 3-6.

During the initial capacitor charging process, the IGBT switches of the H-bridge are turned off, leaving only antiparallel diodes conducting currents. Therefore, Fig. 3-6 (a) can be further simplified as Fig. 3-6 (b): From Fig. 3-6(b), it is obvious that during the initial capacitor charging process, the proposed system is equivalent to a single-phase diode rectifier without a load connected to it.

Due to anti-parallel diodes of the H-bridges, the dc capacitor voltage of the H-bridge can be naturally charged without special charging circuits before a soft start begins. Since the naturally charged dc capacitor voltage level is approximately the same as grid peak voltage, an artificial voltage vector that is able to counteract with the grid voltage right after a soft start is possible.

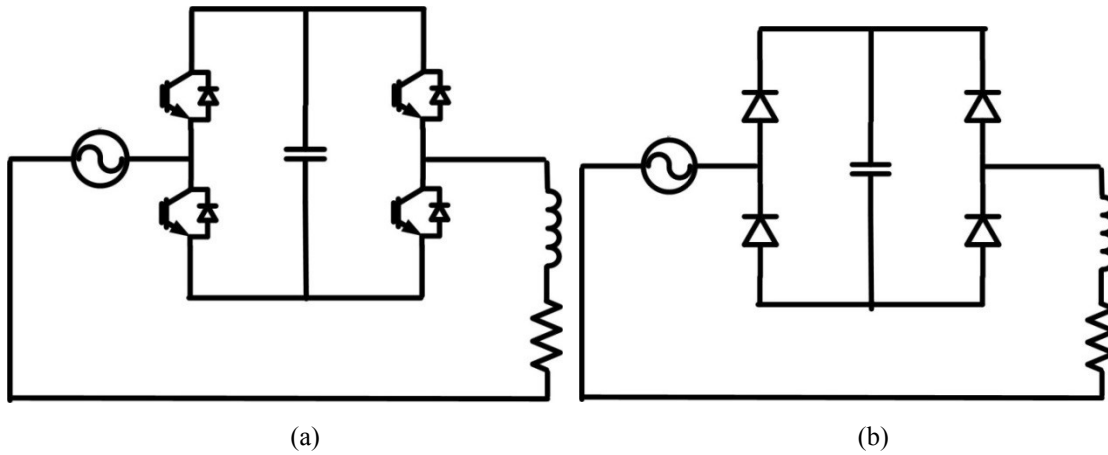


Fig. 3-6. Per-phase (a) equivalent circuit of the proposed system and (b) equivalent circuit during initial capacitor charging process

3.6 Dc Capacitor Ripple Voltage Modeling

For the proposed system, there exists dc capacitor voltage ripple due to energy fluctuation within the H-bridges. To quantify this dc capacitor voltage ripple, energy analysis is carried out. It should be noted that for the whole analysis process, the motor current vector I is used as the reference for the phasor coordinate.

Assuming a balanced system, since the H-bridge converters are connected in series with induction motor, the bridge current is the same as motor current, which can be expressed as:

$$I_A = \sqrt{2}I_{rms} \sin(2\pi f_s t) \dots\dots\dots 3-6$$

As already mentioned the voltage vector injected by the H-bridge is roughly 90 degrees leading the motor current vector. Therefore, the bridge voltage of phase A can be expressed as (V_b represents the RMS value for bridge voltage):

$$V_A = \sqrt{2}V_b \sin(2\pi f_s t + \frac{\pi}{2}) \dots\dots\dots 3-7$$

It should be noted that although the actual voltage injected by the H-bridge is a PWM waveform, to simplify the analysis, only the fundamental frequency component is considered. The instantaneous power flow from/to the Phase A of H-bridge can be expressed as:

$$P_A = V_A I_A = 2V_b I_{rms} \sin(2\pi f_s t + \frac{\pi}{2}) \sin(2\pi f_s t) = V_b I_{rms} \sin(2\pi 2f_s t) \dots\dots\dots 3-8$$

Eqn. 3-8 implies that: a) the average net power to the H-bridge is zero; b) the instantaneous power flow from/to the H-bridge is fluctuating at twice the grid fundamental frequency (120 Hz). For an individual H-bridge, the only component that can absorb electrical energy is the dc capacitor. Therefore, it can be concluded that due to this fluctuating power flow, the dc capacitor is constantly being charged and discharged, causing a ripple voltage on the dc capacitor, as is shown in Fig. 3-7.

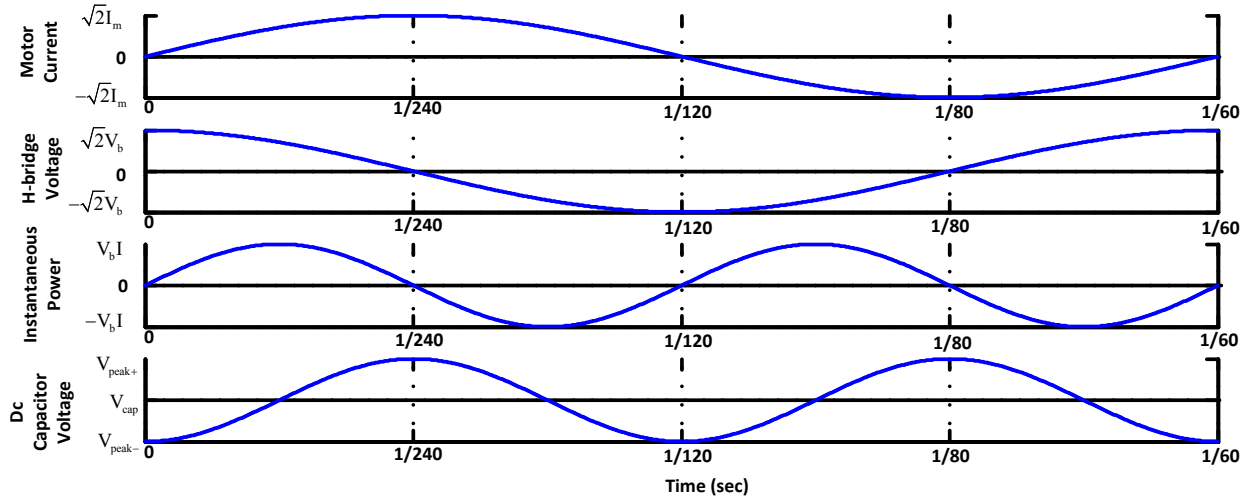


Fig. 3-7. Waveforms of different aspects of the H-bridge system

To quantify the ripple voltage, the energy stored in the capacitor during the charging period can be calculated as:

$$W_{\text{charge}} = \int_0^{240} P_A dt = \int_0^{240} V_b I_{\text{rms}} \sin(2\pi 2f_s t) dt = \frac{V_b I_{\text{rms}}}{120\pi} \dots\dots\dots 3-9$$

On the other hand, the energy stored in the dc capacitor during the charging period can also be calculated by the initial and final capacitor voltage level difference as (C represents the capacitance of DC capacitor):

$$W_{\text{charge}} = \frac{1}{2} (V_{\text{peak}+}^2 - V_{\text{peak}-}^2) C = \frac{1}{2} (V_{\text{peak}+} + V_{\text{peak}-}) (V_{\text{peak}+} - V_{\text{peak}-}) C = 2CV_{\text{cap}} \Delta V \dots\dots\dots 3-10$$

From Eqn. 3-9 and 3-10, the magnitude of dc capacitor ripple ΔV can be calculated as:

$$\Delta V = \frac{V_b I_{\text{rms}}}{240\pi C V_{\text{cap}}} \dots\dots\dots 3-11$$

Using Eqn. 3-2 , dc capacitor ripple ΔV can be calculated as:

$$\Delta V = \frac{m_a I_{rms}}{240\sqrt{2}\pi C} \dots\dots\dots 3-12$$

Assuming a fixed modulation index, Eqn. 3-12 indicates the magnitude of dc capacitor voltage ripple in the H-bridge is proportional to motor current and inversely proportional to the capacitance. Since the motor current is determined by motor load condition, the only factor that can reduce the dc capacitor ripple is to increase the capacitance of the dc capacitor, Fig. 3-8. For 100% ripple voltage minimum capacitance value is 0.163mF.

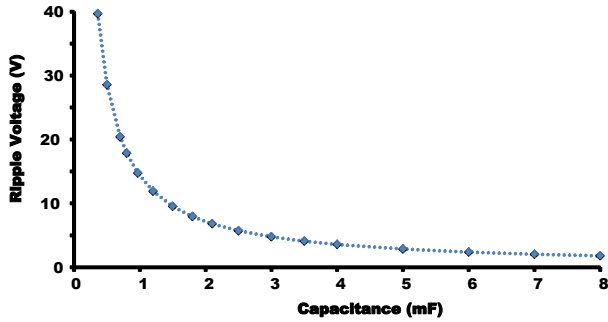


Fig. 3-8. Effect of capacitance on ripple voltage

3.7 Simulation Results

Simulation model is very useful to predict system behaviour before experimental validation and it also helps to recognize system performance without real world complexity. A MATLAB based simulation is used to verify the proposed H-bridge floating capacitor converter configuration. To verify steady state and soft start operation active device model is used. The parameter used in induction machine model is same as given in table 1.

Two different load settings are used to present simulation results: 50% load and 100% load, Fig. 3-9. The pre-set current limit is set to 3p.u. and load is set to square of speed. Simulation results show that the proposed control can soft start the induction motor within limited current settings, Fig.3-9 (c) and (d) . With the same current setting the higher load takes more time to reach steady state. As current limit soft start method is used, motor voltage ramp stops and stays at constant voltage when current reached maximum set value, Fig.3-9 (g) and (h). Thus, reference voltage generated by soft start controller limit the inrush current. As bridge

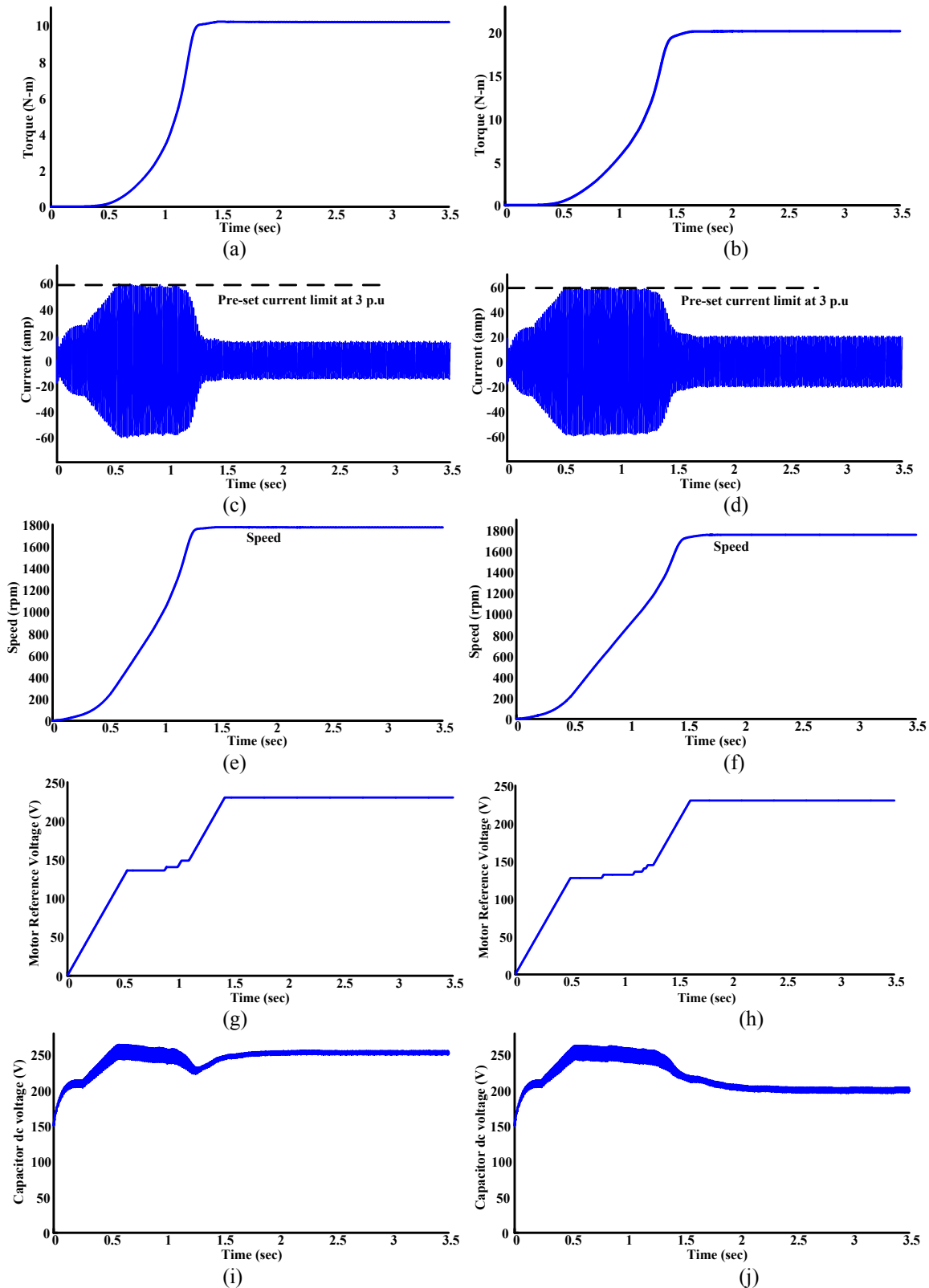


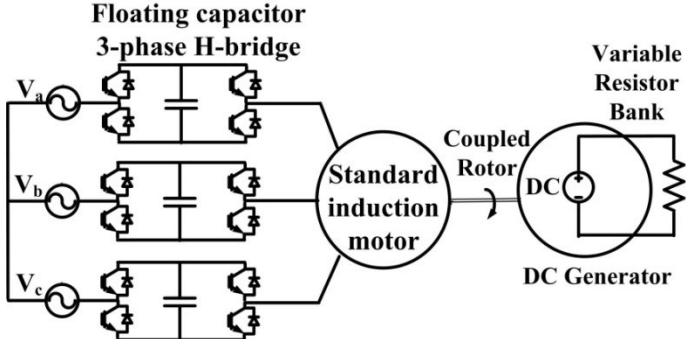
Fig. 3-9. System operation-torque: (a) half load; (b) full load, motor current: (c) half load; (d) full load, speed: (e) half load; (f) full load; motor reference voltage: (g) half load; (h) full load, capacitor dc voltage: (i) half load; (j) full load

voltage is pre charged and set from 1p.u., so voltage across the motor starts from zero, motor and grid power factor angle starts from zero reaches higher point and comes down as motor reach steady state. As the load increase motor power factor angle decrees (power factor increases), so as bridge voltage decreases with increasing load, Fig. 3-9. The simulated results show for full load capacitor voltage is lower compare to half load condition.

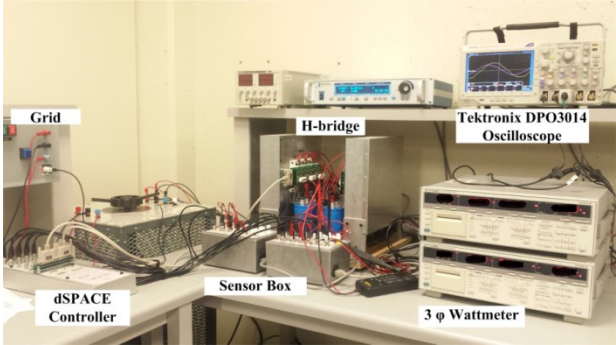
Simulated results presented here is very well agreement with theoretical prediction and also validate the concept before real time testing.

3.8 Experimental Setup

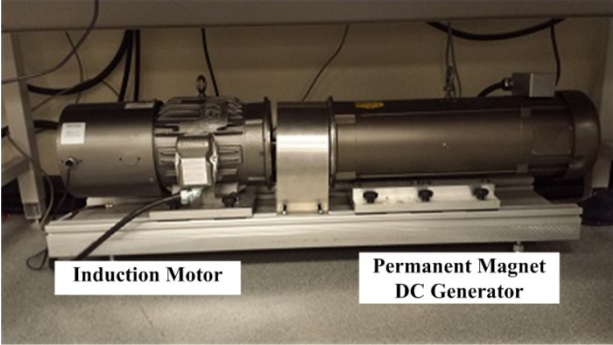
A 230V 5 HP motor-generator set is used as the test platform, as is schematically shown in Fig. 3-10 (a).



(a)



(b)



(c)

Fig. 3-10. Experimental test facility; (a) schematic for test platform, (b) controller with power electronics, (c) induction motor-dc generator set

From Fig. 3-10 it can be seen that three single-phase H-bridges are installed between the grid and the induction motor. A permanent magnet dc generator is mechanically coupled with the

induction motor and a variable resistor bank is connected to the dc generator armature terminals to act as a variable load. The actual experimental test facility is shown in Fig. 3-10 (b) and (c).

In the soft start test results, available 3phase supply is used, in the lab the line to line voltage is 208 V. The converters used in the experiment are custom made IGBT based power converters. The Semikron (SKiM306GD12E4) IGBT modules are used. The single H-bridges were made up of 2 separate inverter legs each with a 4mF dc capacitor with a voltage rating of 500VDC. Through parallel connection, the equivalent capacitance in each H-bridge is 8mF. Lower value capacitance can be used in the experiment but produces higher ripple voltage, say 1 mF capacitor produces 15V voltage ripple.

The induction motor is an inverter duty motor, has 4 poles and is rated at 5hp 60Hz, and parameters are provided in Table II. DC generator and resistor bank is used as load. The dc machine is rated at 5HP 180 V dc, 21.6A, 1750 rpm, type 3681P TEFC, design B, with a nominal efficiency of 84%. The variable resistor bank is rated at 250V with a resistance range from 7.81Ω to 83.3Ω.

TABLE II. INDUCTION MOTOR-2 PARAMETERS

P_{rated}	=	3.7	kW	R_s	=	0.562	Ω
$I_{s,\text{rated}}$	=	13.6	A	R_R	=	0.3	Ω
$V_{s,\text{rated}}$	=	230	V	X_s	=	0.544	Ω
f_s	=	60	Hz	X_R	=	0.766	Ω
p	=	4		X_M	=	18.34	Ω

The proposed control algorithm is implemented on a dSPACE CLP1104 platform, with a sampling frequency of 5kHz and a switching frequency of 7.5 kHz.

3.9 Experimental Results

Experimental testing is carried out to determine various aspects of the proposed system.

3.9.1 Current Limit Soft Start

Pre-setting the motor starting current at appropriate desired per-unit level, soft starting of a standard induction motor is implemented with a wide range of load conditions. Fig. 3-11 shows the starting voltage, current and speed under different starting procedures.

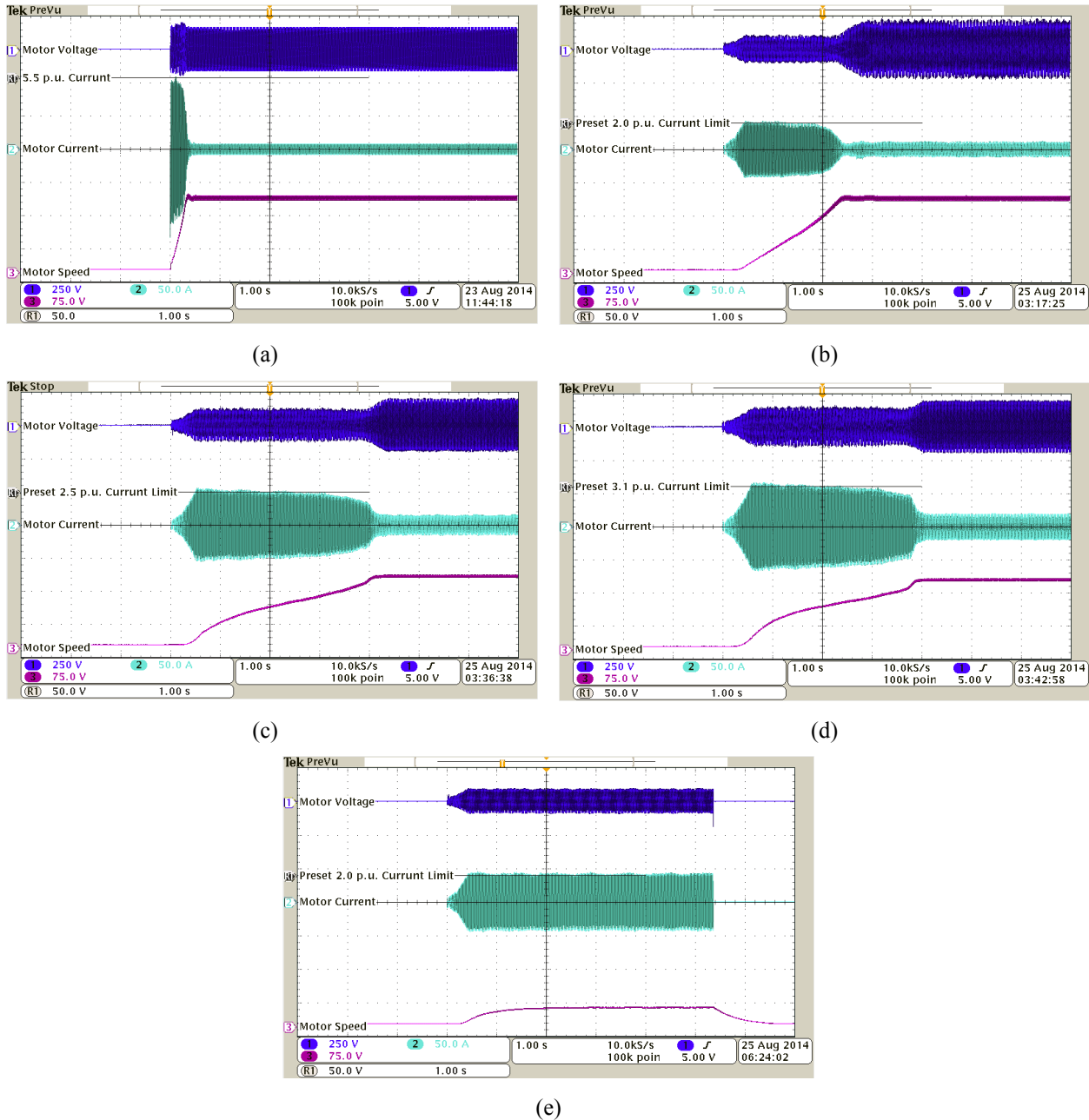


Fig. 3-11. Current limit soft-start: different conditions; (a) full-voltage; no load, (b) 2.0 p.u. motor current limit; no load, (c) 2.5 p.u. urrent limit; half load, (d) 3.1 p.u. current limit; full load, (e) 2.0 p.u. current limit; full load

The full voltage direct on-line start results in an inrush peak current of about 105 A, approximately 5.5 times peak rated motor current, Fig. 3-11 (a). In contrast, a soft start, Figs 3-11(b-d), results in limited motor currents and longer acceleration times. The reference signal (R1) in Figs. 3-11 (b-e) represents the motor starting current limits. The peak system current stress is the pre-set desired current level chosen for the starting procedure. Direct online starting, Fig. 3-11(a), results in a very rapid motor acceleration, in contrast, Fig 3.11 (e) presents a scenario where the current limit is set too low, the motor shaft rotates fails to accelerate to rated speed and the controller shuts down. If the current limit is set too low, the starting capability of the motor is reduced, resulting in two possible scenarios: a) the machine may stall and remain at standstill; b) the machine may start but fail to accelerate to its running speed, causing it to run at that sub-synchronous speed, Fig. 3-11 (e). If either of the above scenarios happens, excessive motor heating will result. To solve this problem, a thermal limit timer is used as auxiliary safety mechanism to protect against damage due to over-temperatures during soft start. The thermal limit timer is able to detect the abnormality during start up process and trip the power electronics, abandoning soft start process. It should be noted that for illustration purpose, the threshold for the thermal limit timer in Fig. 3-11 (e) is much lower than the time value specified by [93].

3.9.2 Voltage Ramp Soft Start

A second starting procedure has the motor voltage ramped at a pre-set constant rate starting from zero, the effect of selecting different ramping rates is illustrated in Fig. 3-12. This approach illustrates the motor voltage control capabilities of the system; see Fig. 3-12.

In comparison with the current limit soft start, the voltage ramp soft start can lower the initial inrush current, resulting in longer acceleration times. However, larger peak currents usually occur as the motor voltage is ramped up to higher values. Ramp time plays an important role in determining the magnitude of peak motor current in this starting mode and care must be taken to select an appropriate ramp time.

It should be noted that current requirement for the IGBTs is more than 100% rated motor current so that heavy motor load can be started. Although oversizing the IGBT is a common

practice for motor drives. In fact, the applicability of the proposed H-bridge system depends on the stiffness of the grid, and torque requirement of the load.

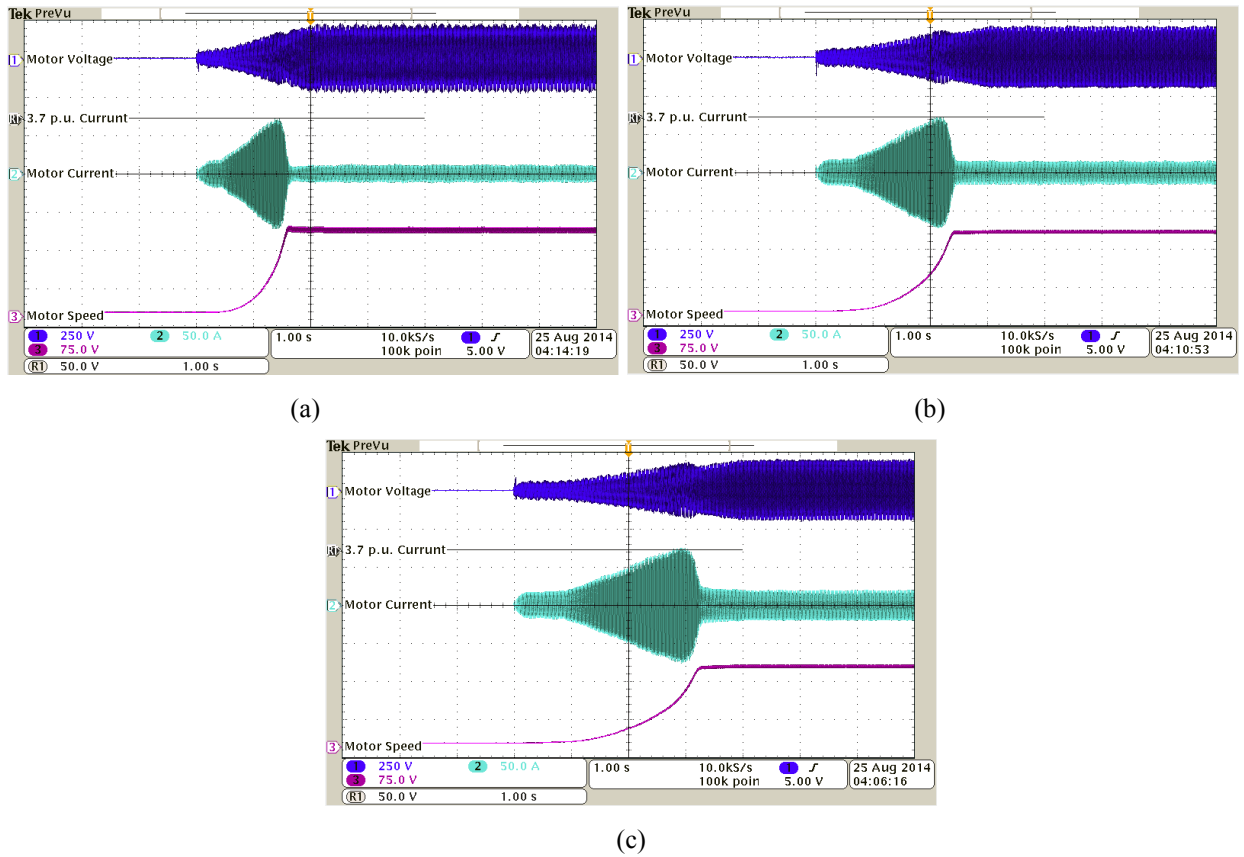
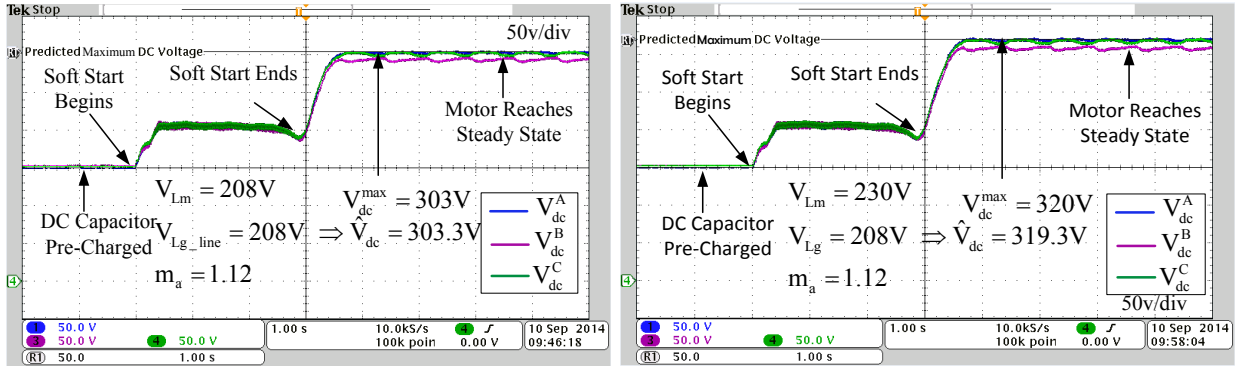


Fig. 3-12. Voltage ramp soft-start results; (a) 2 second ramp time; no load condition, (b) 3 second ramp time; half load condition, (c) 4 second ramp time; full load condition

3.9.3 Bridge Dc Voltage Prediction

The performance of the proposed bridge dc voltage prediction algorithm under current limit soft start mode is shown in Fig. 3-13, where actual dc capacitor voltages of the three H-bridges are drawn together. The reference signal (R1) in Fig. 3-13 represents the predicted dc voltage under no load condition, which is pre-determined before motor starts. It can be seen that maximum dc capacitor voltage can be accurately predicted under different motor and grid voltage configurations.



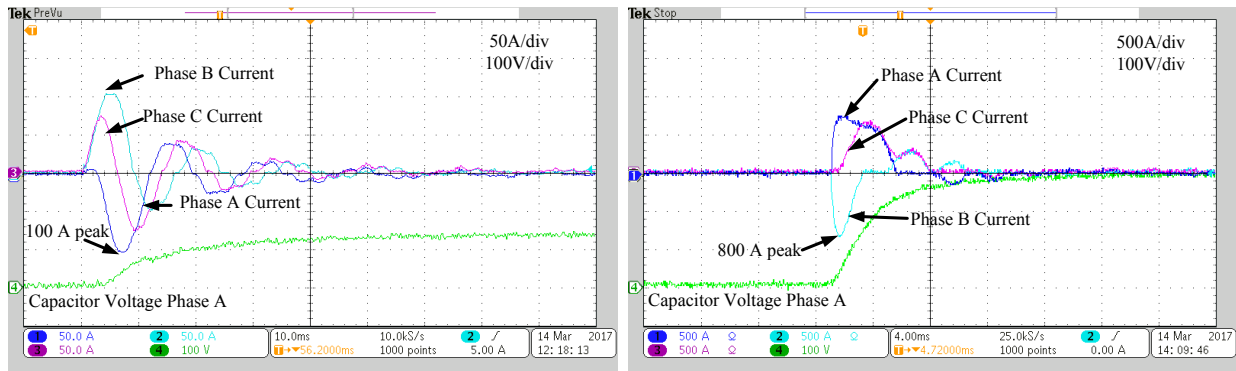
(a)

(b)

Fig. 3-13. Comparison between predicted and actual maximum dc voltage with no load condition; (a) $V_{Lm}=208V$; $V_{dc}=303.3$, (b) $V_{Lm}=230V$; $V_{dc}=319.3$

3.9.4 Peak Inrush Current for Capacitor Charging

Peak current stress of the diode during capacitor charging is shown in Fig. 3-14. The starting inrush current is limited by impedance of the H bridge converter and motor and it decays within few cycles. The capacitor voltage rises exponentially and no overshoot on capacitor voltage is observed. But for a VFD the voltage across the capacitor is two times of the H bridge voltage and also limited by only impedance of the rectifier circuit, Fig. 3-14 (b). The inrush current in VFD is almost eight times higher than the inrush current experienced by the proposed system.



(a)

(b)

Fig. 3-14. Inrush current for capacitor charging (a) H bridge system (b) VFD

3.9.5 Leading Power Factor

The proposed H-bridge system can operate continuously leading instead of lagging power factor. Fig. 3-15 shows relationship between grid phase voltage (V_g) and motor current (I) under rated motor voltage ($V_{m,rated}=230V$).

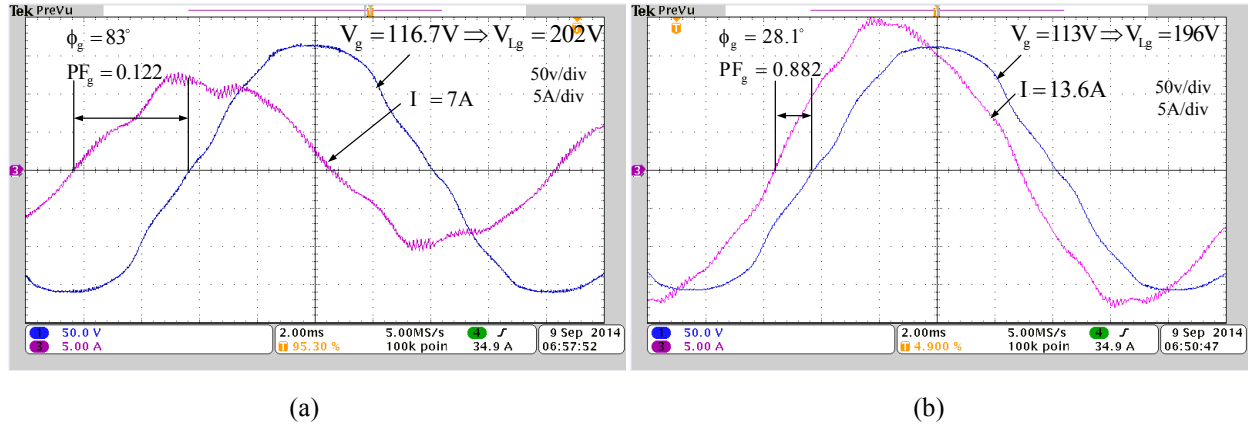


Fig. 3-15. Relationship between grid phase voltage and motor current under rated motor voltage: (a) no load, (b) full load

3.9.6 Five Level Line to Line PWM Voltage Generation

Under the proposed system, motor line to line voltage has five levels, as can be seen from Fig. 3-16. This reduces the dV/dt stress on the motor.

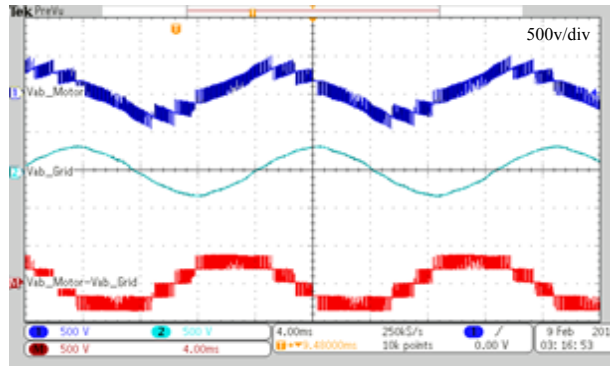


Fig. 3-16. Line to line PWM voltages generated by the proposed H-bridge system

In Fig. 3-16, motor voltage is the end result between grid voltage and bridge voltage. Therefore, grid line voltage is subtracted from motor line voltage so that perfect five level line-to-line PWM voltages generated by H-bridge can be observed.

3.9.7 Conclusions

This chapter presents a power electronics system to regulate voltage supplied to a standard squirrel cage induction motor. In summary:

- The proposed system does not require LCL filters and can supply five level line-to-line PWM voltages to motor terminals.
- The system can generate VARs without increasing IGBT current ratings on active front-end side converter.
- The peak inrush current for capacitor charging is eight times lower compared to VFD.
- The controller shows stable operation under transient condition; during starting and load change condition.
- The experimental results clearly demonstrate that the proposed system can provide flexible and more importantly, steady soft start solutions under different motor load conditions.
- Also, bridge dc capacitor voltage can be accurately predicted under a wide range of system configurations. These evidences suggest the proposed system merits further investigation.

Chapter 4

4 Series Voltage Compensation

A series compensation scheme for an induction motor is presented with inherent voltage sag ride through capability. By injecting a series voltage in each phase, a 3-phase H-bridge can manipulate the voltage supplied to a motor, increasing its tolerance of grid voltage sags. A controller is described for the 3-phase H-bridge to compensate for voltage sag ride-through conditions. Mathematical analysis of the proposed system is used to quantify both the voltage sag ride-through and the reactive power generation that results. This analysis shows that voltage sag tolerance is closely related to the motor power factor, hence also the machine. The voltage injection scheme has an inherently leading grid power factor under steady state, hence generates VARS into the grid over a wide range of load conditions. Moreover, unity power factor operation of the system as seen from the grid is possible and the reactive power generation capability can also be accurately quantified. A 5 HP experimental testbed is used to validate both the grid voltage ride through capability feature and the reactive power generation characteristics.

4.1 Introduction

Electrical grid voltage sags are a significant industrial power quality concern; according to a survey result across the U.S., voltage sags and short-duration power outages are responsible for 92% of power quality problems faced by industrial customers. These power interruptions often impose severe cost penalties in plant shutdowns for many industries. When directly grid connected, induction motors (and the industrial processes they drive) are one of the industrial components that are more sensitive to voltage disturbances. With an incidence between 61% and 87%, voltage sags are the main cause of voltage disturbances in industrial systems [99]. Voltage sags are normally caused by faults on the power system but can also be caused by energizing of heavy loads or starting of large motors. A survey of over 2000 events in the US found that the majority of voltage sags had a magnitude of around 80% of rated voltage and duration of less than 7 cycles [100]. When the induction motor terminal is directly subjected to voltage sag, the motor

current can increase significantly and large mechanical torques may occur that cause damage to the motor shaft or equipment connected to the shaft. In addition, inrush current at the instant of voltage recovery may trip over-current protection, thus causing a significant system downtime and associated costs [101].

The voltage sag sensitivity of an induction motor still exists when the motor is connected through a conventional VFD. The reported sensitivity threshold levels to grid voltage sag for a conventional VFD vary from 50–60% to 80–90% of rated voltage, with duration sensitivities of less than 5–6 cycles [59]. Field records of voltage sags and subsequent VFD shutdowns, indicates voltage sags with duration of 12 cycles or more and having a voltage magnitude below 80% of rated voltage will shut down a VFD [102]. Even if the motor is completely unloaded, the VFD still remains very sensitive to voltage sags [59]. For ride-through capability improvement, VFD manufacturers responded with new mitigation techniques. One of these is to try to maintain the intermediate dc link voltage from reaching the low voltage state that causes a shutdown by the use of the kinetic energy from the motor load [103]. By modifying and controlling the switching algorithm of the inverter and taking into account some inertia in the motor and the load, power can be fed back to the dc bus during the supply voltage dip. With this feature, the VFD can continue to work without stopping and resume normal operation after the grid voltage sag. However, a comparison test of five VFDs from five different manufacturers demonstrated that such ride-through capability of VFDs were not the same [104]. Moreover, it has been shown in [104] that even the best VFD under test could not cope with symmetrical voltage sag at 80 % voltage with either 60 or 300 cycles of duration. [105-106] describe a voltage sag compensator, used for critical loads, consisting of a three-phase voltage source inverter (VSI) and a coupling transformer for serial connection. When the grid is at its nominal level, the compensator is bypassed. During grid voltage sags, the compensator injects the required compensation voltage through the coupling transformer. However, long detection time (typically within 4ms) and large inrush currents can trigger the over-current protection which leads to compensation failure [106].

One of the power converters that have gained importance in current years is the Back-to-Back (BTB) converter. It is used in renewable energy systems (based on Wind Turbines (WT) [107] or Distributed Generation (DG) system [108]), HVDC systems [109-110] and in motor drive systems [111]. The performance of the BTB converter can also be affected by the variable conditions of the electrical grid system; voltage unbalance and voltage sags are the main source of

voltage disturbances in this type of system. The unbalanced grid voltage and voltage sag conditions causes instability in the dc-link voltage which can cause loss in power transfer or generate over-currents that damage the power devices and active protection [112]. For DG systems, the entire transmission and distribution systems can lead to instability when electrical disturbances appear in the grid [108]. In HVDC systems, high-power electronic converters are desired to operate with relatively low switching frequencies (maximum 9–15 times the line frequency, and even lower for multilevel converters). The low switching frequency operation of VSI systems imposes control limitations in the case of power system faults and disturbances when they may be needed the most. Presently installed operating systems, the ride-through capability is obtained either by using passive element design or a change in the control mode or using over rated power electronics devices [109]. Most of the control solutions to mitigate voltage unbalance are based on either the rotating-frame solution [112], or the stationary-frame solution [113-114]. The major disadvantage of the rotating-frame solutions is the complexity, which causes a high computational burden [114]. Again, low-pass, band stop, and notch filters are used in control algorithms to detect a voltage sag in the system but their response can be too slow [107]. For the BTB converter to inject reactive power to grid or to use in a motor drive application [111], appropriate filters (either L or LCL) have to be inserted between the grid and the front-end rectifier: note that filter inductors are also commonly used at the drive output terminals. On the contrary, the proposed system inherently generates VARS to the grid without requiring a grid supply reactor, which has the effect of reducing the system overall cost. Despite many attempts to compensate the reactive power of a grid-connected induction machine, the majority of these technologies cannot provide voltage sag rid-through capability. Examples are: a) reactive current injection such as capacitor bank or STATCOMs [39]; b) parallel auxiliary windings in the machine [115]; c) rotating converters [116]; d) open-winding induction machine with one terminal connected to a power electronic converter [69]. The proposed system is compatible with standard power distribution practices and therefore has potential in retrofit applications. Significant voltage sag tolerance has been demonstrated by the proposed 3-phase H-bridge system.

4.2 Grid Voltage Sag Tolerance

The series voltage injected by the H-bridge can be used to compensate for grid voltage sag and thus decouple the motor from the effects of the voltage sag. There is a limit to which the power electronics can compensate for a voltage sag: defined as the critical condition. The nature of the voltage sag compensation is described and the voltage sag limit s_{\min} , and the grid minimum voltage $V_{g,\min}$, for this compensation is defined in relation to the motor rated operating voltage, $V_{m,\text{rated}}$, motor power factor, PF_m , and the nominal grid voltage, $V_{g,\text{rated}}$. The behavior of the system under voltage sag is illustrated using the phasors in Fig. 4-1.

To illustrate the voltage sag ride-through capability of the system two important assumptions are made:

- (a) The load condition on the induction motor remains unchanged.
- (b) The induction motor terminal voltage is kept at its rated value by the H-bridge controller.

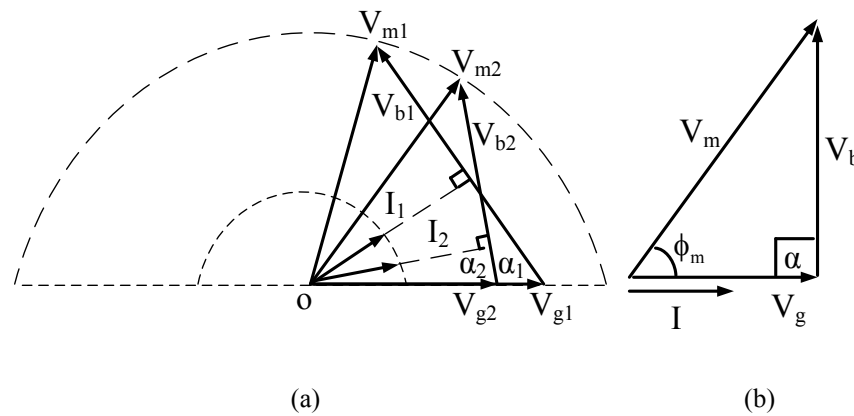


Fig. 4-1. Phasor diagram illustrating the system response to grid voltage sag; (a) during voltage sag: V_{g1} goes to V_{g2} , (b) critical condition.

Under these assumptions, if the grid voltage is reduced, from V_{g1} to V_{g2} , Fig. 4-1 (a), the angle α increases from α_1 to α_2 . As the motor is operating at its rated voltage under constant load, the motor fundamental current angle ϕ_m will remain the same. As a result, the trajectories of motor voltage V_m and motor current I will travel along the loci as arcs centered on point O. As the severity of the sag increases and V_g is reduced, the angle α , will increase until a critical condition is reached, where $\alpha = 90^\circ$ illustrated in Fig. 4-1 (b). Under the critical condition

shown in Fig. 4-1 (b), the motor current I and grid voltage V_g are in phase with each other and the system is operating with unity power factor at the grid interface without consuming VAR. The severity of voltage sag that the proposed H-bridge system can ride-through without consuming VAR is determined by the magnitude of the motor power factor angle ϕ_m under the critical condition, see Fig. 4-2.

For an induction motor with a constant motor terminal voltage, different load conditions will result in a different motor fundamental power factor angle ϕ_m . Considering Fig. 4-2, it can be seen that the shape of the right angle triangle obviously changes with ϕ_m . Therefore, the magnitude of V_g under the critical condition, and thus the voltage sag ride-through capability of the system, will be a function of ϕ_m . Under a no-load condition, since the magnetizing current forms a major component of the motor current, the motor power factor may be as low as 0.1–0.3 [117], which results in a high value for ϕ_m ($=75^\circ$ to 85°), see Fig. 4-2. Therefore, a small grid voltage, V_{g1} , can be boosted with the help of a bridge voltage V_{b1} to maintain the motor at rated terminal voltage V_{m1} . This means that if an induction motor is operating under very light load, the grid voltage sag can go as low as 10-30% of the rated motor voltage whilst still maintaining the induction motor at its rated voltage. However, under normal conditions (80–100% of the full-load), the motor power factor (PF_m) increases to typically 0.8–0.9 [48]. This means that the grid voltage sag that may be endured may lie in the range 80-90% of the rated motor voltage.

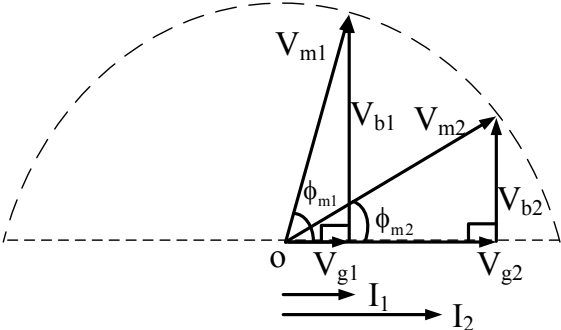


Fig. 4-2. Effect of the motor power factor angle ϕ_m on the critical condition for the permissible maximum voltage sag compensation

Expressing these conditions mathematically, the voltage sag ride-through capability depends on the motor fundamental power factor, and can be expressed as:

$$V_{g,\min} = V_{m,\text{rated}} \cos \phi_m = V_{m,\text{rated}} PF_m \dots\dots\dots 4-1$$

$V_{g,\min}$ represents the minimum grid voltage that the proposed H-bridge induction motor drive system can cope with. $V_{m,\text{rated}}$ represents the rated induction motor voltage, which is assumed to be kept constant and can be obtained from nameplate of the motor. PF_m represents the motor power factor, which is determined by the motor load condition. This relationship is confirmed in this work using experimental results.

The proposed 3-phase floating H-bridge system is compatible with standard power distribution practices and has great potential in retrofit applications. In both the industrial and tertiary sectors in the Europe Union, the average induction motor power factor is low, at $PF_m=0.57$ [118]. Therefore, if retrofitted with the proposed 3-phase floating H-bridge system, a symmetrical grid voltage sags of 60% indefinitely relative to the rated induction motor terminal voltage. Depending on the grid voltage applied, the severity of the voltage sag (in percentage) that the proposed H-bridge system can cope with is calculated as:

$$s_{\min} = \frac{V_{m,\text{rated}} PF_m}{V_{g,\text{rated}}} \times 100\% \dots\dots\dots 4-2$$

s_{\min} represents the severity of voltage sag relative to the nominal grid voltage; $V_{g,\text{rated}}$ represents the rated grid voltage. As an example, if the motor is operated at a rated voltage of 230 V with a power factor of 0.82 (= full load), then operating from a grid voltage of 208 V gives a value for s_{\min} at 0.91: if the motor power factor is 0.3 (light load), then s_{\min} becomes 0.33.

4.3 Motor Fundamental Current Angle Estimation

The voltage sag ride-through capability of the 3-phase floating bridge system, and predicting a value for s_{\min} , depends upon the knowing the motor power factor. PF_m varies with the motor load conditions and direct measurement of this quantity is not feasible practically due to the voltage PWM waveforms experienced at the motor terminals and noise interference. One solution is to apply a low-pass filter on feedback signals, however this may experience noise problems, attenuation, signal delays, and introduce phase shifts in the motor voltage being monitored. These effects may have a negative impact on the accuracy of the power factor measurement. Alternatively, the motor power factor angle, ϕ_m , during nominal grid steady-state operating conditions can be estimated if the power factor angle ϕ_g at the grid can be measured reliably. The controller is designed to monitor the utility grid parameters accurately using a PLL, and the grid

voltage and current can be monitored reliably and are natural signals to use in the controller. Consider Fig. 4-3, using a phase-locked-loop (PLL) to track the grid voltage angle θ , measurement of the grid three-phase currents using Park's transformation can then be used to obtain the grid current I angle, $\phi_g = \tan^{-1} \frac{I_q}{I_d}$.

Assuming that the bridge losses are negligible, V_b is approximately at 90° degrees relative to I (known error angles can be used to correct for any differences):

$$\alpha = 90^\circ - \phi_g \dots\dots\dots(4-3)$$

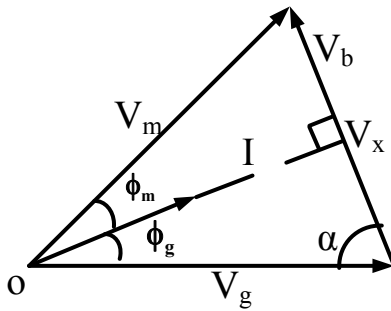


Fig. 4-3. System vector diagram under nominal steady-state operating conditions to predict the motor fundamental power factor angle

Applying the law of cosines and using phase quantities, the motor terminal voltage can be obtained as:

$$V_m = \sqrt{V_g^2 + V_b^2 - 2V_g V_b \cos \alpha} \dots\dots\dots 4-4$$

Now, it is possible to construct an imaginary voltage vector V_x aligned with I, Fig. 4-3. The length of the imaginary voltage vector V_x is

$$V_x = V_g \cos \phi_g \dots\dots\dots 4-5$$

Finally, given that V_b is approximately at 90° relative to V_x , the motor fundamental power factor angle ϕ_m can be estimated as

$$\phi_m = \cos^{-1} \frac{V_x}{V_m} = \cos^{-1} \left(\frac{V_g}{V_m} \cos \phi_g \right) \dots\dots\dots 4-6$$

This relationship is verified in this work with experimental results. Assuming a measured grid phase angle of 30° , $V_{Lg} = 208 \text{ V}$, $V_{Lm} = 230 \text{ V}$ (using line voltage equivalents), then $\phi_m = 38.4^\circ$, and the maximum, or critical, voltage sag from Eqn. 4-2 has $s_{min} = 0.87$.

4.4 Reactive Power Generation

Under both nominal system operating conditions and under conditions of grid voltage sag, the system current leads the grid voltage, see Figs. 4-3. This represents var generation into the grid and analysis is presented to predict the var generated under nominal and voltage sag conditions.

The voltage injected by the H-bridge (V_b) phase shifts the induction motor terminal voltage (V_m) so that it is leading the grid voltage (V_g), Fig. 4-3. As a result, the induction motor current vector (I) also leads the grid voltage (V_g), generating VARS instead of consuming. Taking into account the fact that the voltage vector V_x is in phase with I , the power factor of the proposed 3-phase floating H-bridge system as seen at the grid terminals can be expressed as:

$$PF_g = \cos \phi_g = \frac{V_x}{V_g} \dots\dots\dots 4-7$$

In steady state, the grid leading power factor (PF_g) is proportional to the motor fundamental power factor, lagging, as long as the grid and motor voltage are kept constant (Eqn. 2-4). This means that with an increasing motor load, the motor and the utility grid fundamental power factor increases. The relationship in Eqn. (2-4) is confirmed in this work using experimental results. In steady state, the proposed system supplies reactive power to the utility grid and thus improve the overall system var requirement. During grid voltage sags, V_g obviously decreases and the grid fundamental power factor also decreases. The VARS that are generated into the grid can be calculated as:

$$Q = 3V_g I \sin \phi_g \dots\dots\dots 4-9$$

$$Q = 3I \sqrt{(V_g)^2 - (V_m)^2 (PF_m)^2} \dots\dots\dots 4-10$$

Under constant motor voltage operation, as the motor load increases, both the motor current I and motor power factor PF_m increases. Eqn. 4-10 implies that if the utility grid voltage

remains constant and the proposed H-bridge system can maintain the motor terminal voltage at its rated value, then a load increase does not necessarily result in an increase or decrease of the VARS being generated. Eqn. (4-10) and the effect of load change is investigated further using experimental results.

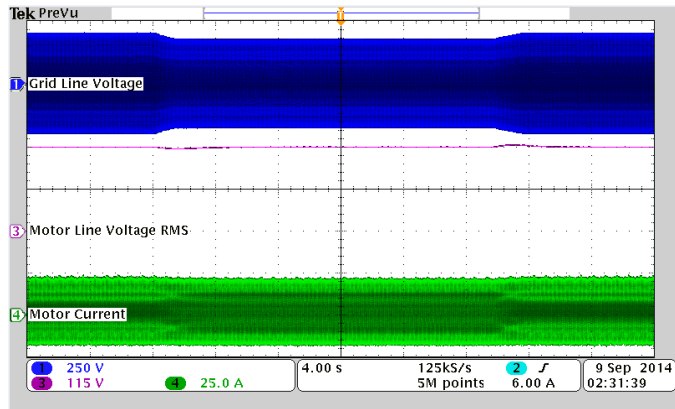
However, consider a voltage sag, if the motor voltage and its load is assumed constant, the motor current is constant. Assume a motor line voltage of 230V, current of 13.6 A, and PF_m 0.82 lagging. Comparing a nominal grid voltage of 208V, with a 5% sag condition of 197.6 V, the grid VARS generated change from 1633 VA to 1551.54 VA, with ϕ_g changing from leading by 24.9° to leading by 17.4° , as expected from Fig. 4-1. These trends are investigated further with experimental results.

4.5 Experimental Validation

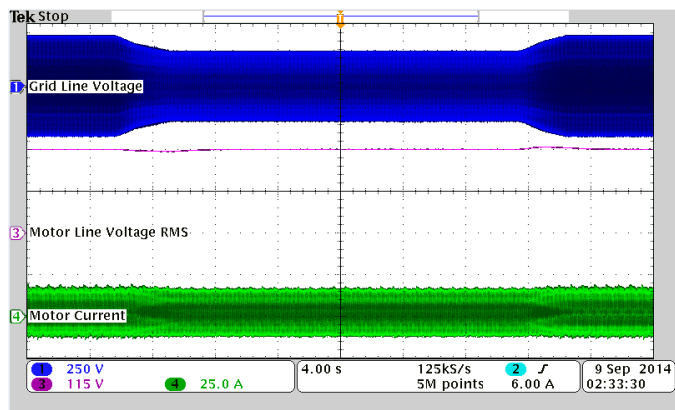
Same motor-dc generator set up being used in this part. A variac is used to step down the input voltage to emulate the three phase voltage sag.

4.5.1 Voltage Sag Tolerance

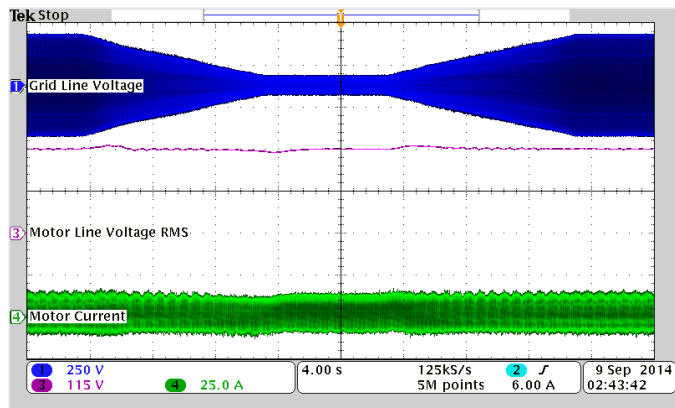
The experimental 3-phase floating H-bridge and motor system was proven capable of boosting the motor voltage to its rated value (230V) when operated from a 208 V grid, and maintained the rated motor voltage under voltage sags of various magnitudes (depending on the motor load conditions), see Fig. 4-4. Under a full load condition, the motor operated at 0.76 power factor lag, with rated voltage sustained at voltage sag of 176.5 V, Fig. 4-4 (a). When the motor was under half load, it operated at a 0.58 power factor lag and with a grid voltage dip down to 137.5 V, Fig. 4-4 (b). Under no load condition, the motor operated at 0.15 power factor lag and the system tolerated maximum voltage sag down to 32 V, Fig. 4-4 (c).



(a)



(b)



(c)

Fig. 4-4. Voltage sag ride through performance: (a) full-load, voltage sag 85% of rated grid voltage (b) half-load, voltage sag 66% of rated grid voltage (c) no load, voltage sag 16% of rated grid voltage

In brief, the experimental results in Fig 4-4 show:

Induction motor terminal line voltage can be maintained at its rated value (230V) for significant periods of time (no less than hundreds of cycles) during voltage sags under various load conditions.

The magnitude of the motor current stays the same during voltage sag.

The lower the motor load, the deeper the voltage sag that can be tolerated whilst maintaining rated motor voltage.

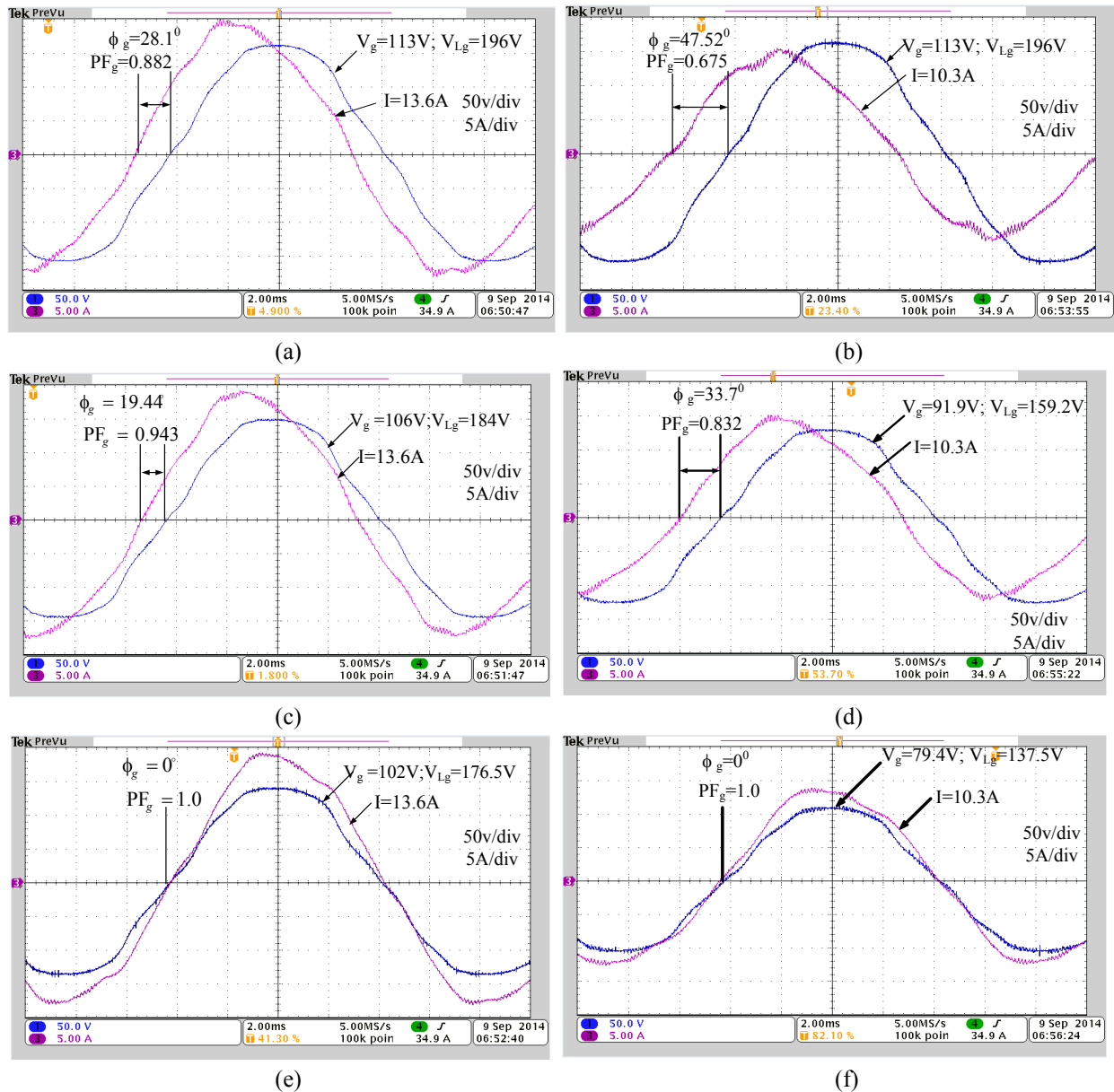


Fig. 4-5. Reactive power generation of the proposed H-bridge induction motor drive system under full load condition ($I=13.6A$, $PF_m=0.76$); (a) $V_g=196V$, (c) $V_g=184V$, (e) $V_g=176.5V$, under half load condition ($I=10.3A$, $PF_m=0.581$); (b) $V_g=196V$, (d) $V_g=159.2V$, (f) $V_g=137.5V$

Another set of experimental results are presented to demonstrate voltage sag critical condition. Experimental results for two different load conditions are taken under different grid voltages: full load ($I=13.6\text{A}$, $\text{PF}_m=0.76$); half load ($I=10.3\text{A}$, $\text{PF}_m=0.581$), see Figs.4-5. In these results, motor terminal voltage is boosted to its rated value (230V) by the 3-phase H-bridge. For each load setting, the motor power factor remains the same for each set of results as the motor voltage is unchanged. Figs. 4-5 are actually another way of representing the phasor diagram shown in Fig. 4-1 (a). In all situations, the critical condition is reached when the grid fundamental power factor becomes unity, Figs. 4-5 (c).

To validate the concept of voltage sag tolerance as identified in Eqn. 4-1, the motor power factor angle under various load conditions were recorded using the estimation technique described in section 4-3. A FLUKE 39 power meter was used to monitor the induction motor terminal voltage. A variac was used to simulate symmetrical voltage sags of different magnitudes. Close attention was paid to record the deepest voltage sag without collapsing of the induction motor terminal voltage ($V_{Lm} = 230 \text{ V}$). The experimental results of maximum voltage sag agreed very well with theoretical predicted values, see Fig. 4-6 (a).

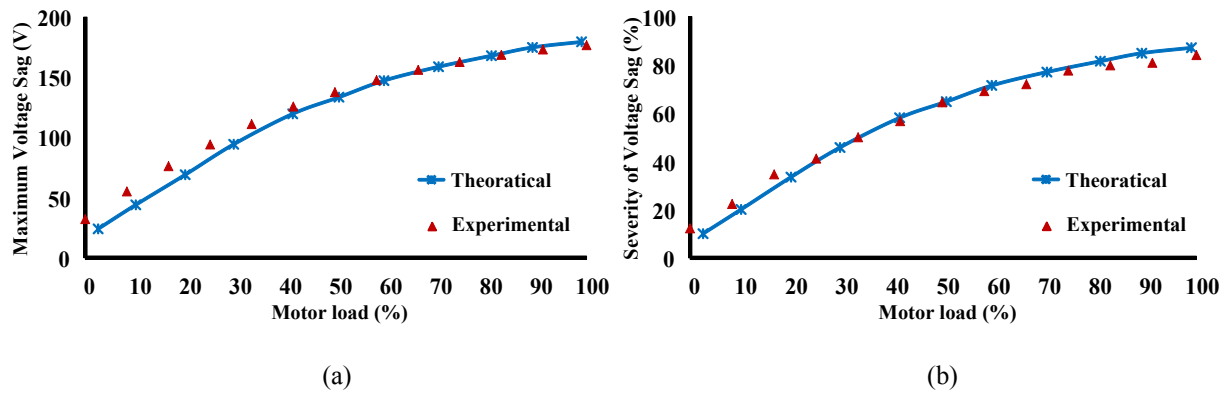


Fig. 4-6. Comparison between theoretical and experimental values of; (a) maximum voltage sag, and (b) severity of voltage sag whilst maintaining rated motor voltage.

To demonstrate the maximum voltage sag tolerance, s_{min} is plotted % in Fig. 4-6 (b). Under maximum load conditions, the proposed power electronics system can tolerate a s_{min} of 82%: a voltage sag up to 18% of the rated grid voltage for continuous periods.

4.5.2 Reactive Power Generation

Reactive power generation capability of the proposed H-bridge system under constant grid voltage ($V_{Lg} = 208V$), constant motor terminal voltage ($V_{Lm} = 230V$), but under variable motor load conditions (from no load to full load) are shown in Fig.4-8. Under fixed grid voltage and constant motor voltage, the grid reactive power generation depends on the motor fundamental power factor (Eqn. 4-10). Fig. 4-7 compare predicted and experimentally recorded of the grid fundamental power factor angle. Experimentally the grid and motor fundamental power factor angle was measured from a FLUKE 39 power meter. Experimental and predicted values for the motor fundamental current angle (ϕ_m), Fig. 4-7 (a), were in good agreement.

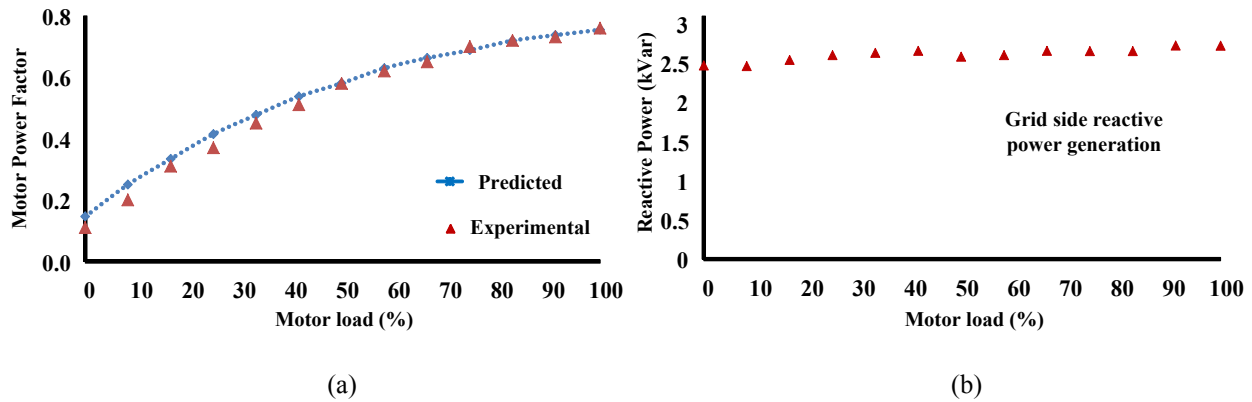


Fig. 4-7. Comparison of: (a) the motor power factor, (b) reactive power generation trend as a function of the motor load condition

The experimental grid reactive var generation is plotted in Fig. 4-7 (b) and observed reactive power delivered to the grid remains relatively flat despite large variations in the motor load. This means approximately, the operation of the proposed 3-phase floating H-bridge and induction motor can be modeled as constant reactive power generator for the grid.

4.6 Conclusions

The voltage sag ride-through capability of a system containing an induction machine connected to the 3-phase grid via a 3-phase H-bridge is described in this chapter. The reactive power generation capability of this system is presented as a function of the motor load and the degree of grid voltage sag experienced. The key features described in this chapter are as follows:

- The effectiveness of the voltage sag ride-through capability of the proposed system is closely related to the motor power factor angle. Generally, the higher the induction motor load, the lower the tolerance of the system to grid voltage sags. The lowest tolerance happens when the induction motor is fully loaded when the motor power factor is at its highest.
- Theory is presented that allows the largest voltage sag to be predicted, or alternatively the lowest grid voltage, to be predicted whilst maintaining the motor at its rated voltage.
- Unity power factor operation of the proposed H-bridge system is possible, which also corresponds to the critical condition for the maximum voltage boosting of induction motor voltage. Further reduction in grid voltage beyond the critical condition results in the collapsing of the H-bridge dc capacitor voltages and consequently, collapsing of the induction motor terminal voltage.
- As the motor load is increased under constant motor voltage control, the power factor of the proposed H-bridge as seen at the utility grid increases with the motor power factor. However, the reactive power generated by the proposed H-bridge system remains relatively flat despite variations in the motor load, which means the proposed system can be modeled as constant reactive power generator for the grid.

Chapter 5

5 Performance Improvement of Induction Motors

PWM 3-phase H-bridge converters can be used as series voltage compensators for grid supplied induction motors to improve their steady-state operating performance. The voltage supplied to the motor can be increased or decreased relative to the grid voltage and especially useful when the motor is connected to a grid whose nominal voltage differs from the machine's rated value or that may fluctuate over time (sag or swell). By injecting a voltage in series with the grid supply, floating capacitor converters can set the motor voltage at a fixed desired value, above or below the grid voltage, under transient or continuous steady-state conditions, to allow the motor power losses to be decreased, hence improve the motor and system efficiencies. For applications where frequency control is not required, the proposed power electronics is more energy efficient than a VFD (VFD), hence a viable cost effective solution. Experimental tests are used to compare the proposed system with several alternatives, using performances such as: power losses and efficiency of the motor, power electronics and the system as a whole.

5.1 Introduction

The grid voltage to which an ac motor can be connected to are seldom precisely the motor rated values to which the motor was designed. Motors are designed with adequate tolerance level to guarantee reasonable performance over a range of supply voltages. But even within the tolerable voltage supply, variations in motor performance exist. The motor designer recognizes the fact that there are side effects and variations in operating costs when a motor is at voltages other than the precise nameplate conditions. Moreover, the nameplate data does not state additional qualities of the electric supply which may also derate the motor performance. When a voltage supply comprises considerable amounts of extraneous noise it is referred to as being dirty. It is also said to be polluted and [119] defines eight types of electrical pollution: e.g. voltage level variations from nominal; frequency variations; voltage unbalances between phases; distortions in sine wave voltages and currents. These electric pollutants contribute to a reduction

in the performance of equipment to which they are connected. Each pollutant results in a rise in the total operating costs of the system. These cost increases may lie in several areas, such as - reduction in motor efficiency, increased capital costs by a) use of oversized motors b) complex control schemes c) oversized system plan; motor burnouts; power factor capacitor failures; production interruptions. Since modern motors are designed to make better use of materials than before, they can be less able to accommodate a wide range of operating conditions. These conditions often result in sizing motors at power levels higher than required for the load demand. Even small efficiency improvements will produce very large energy savings. New NEMA high performance motor gave less satisfactory results when running under rated conditions [31].

Pulse Width Modulated (PWM) 3-phase H-bridge converters examined in this chapter achieves higher energy savings and lower current harmonics than is possible using traditional soft-starters. The proposed system has a significant performance advantage over traditional soft-starters/VFD: the motor voltage can be increased or decreased relative to the grid voltage during transients and steady-state operation. This introduces many features, but relevant to the topic of this chapter, the motor efficiency can also be improved under high as well as light loads; independent of utility voltage fluctuations.

Experimental data are used to assess and compare the steady-state performance of the motor, power electronics and the system as a whole, over a wide range of motor load conditions. Data for several situations of interest are presented:

1. Operating the motor at rated voltage when operating from a lower grid voltage.
2. Comparing the proposed system performance with the alternative of using a VFD.
3. Operating the motor at maximum motor efficiency under variable load conditions by changing the motor voltage.

5.2 Experimental Setup

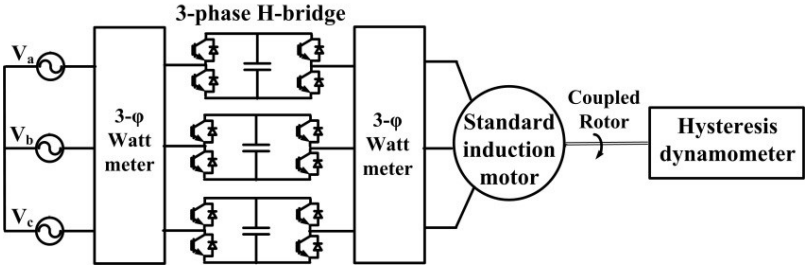
A 230V 5 HP motor-dynamometer set was used as the test platform, where the 3-phase H-bridge was located between the grid and the induction motor, Fig. 5-1(a).

The general purpose NEMA premium induction motor used had the following ratings: 5 HP, 60Hz/50Hz; 4 poles; 230V/460V; 12.6A/6.3A; 89.5% efficiency; 1760 rpm; 0.83 power

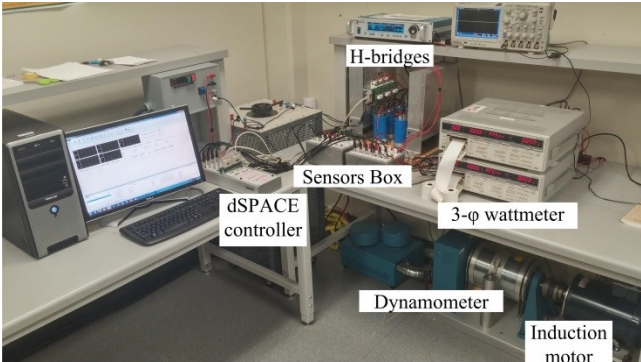
factor. The same power electronics Semikron (SKiM306GD12E4) IGBT modules were used. A MAGTROL hysteresis dynamometer was used as a load, where a frictionless load torque is provided independent of the shaft speed. The MAGTROL DSP 6000 dynamometer was used as the motor load controller, Fig. 5-1.

5.3 Induction Motor Performance

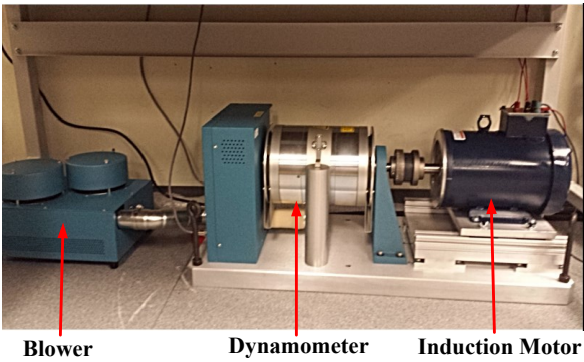
With the motor operated at the grid frequency, three different systems were chosen for experimental performance comparisons: direct grid connected; “conventional” VFD; 3-phase H-bridge. Efficiency, losses, and output power were chosen as the main factors for steady-state performance comparisons over a wide range of motor loads. The motor efficiency was determined from direct measurement of the electrical input and mechanical



(a)



(b)



(c)

Fig. 5-1. Experimental setup; (a) block diagram, (b) 3-phase H-bridge system with a dSPACE controller, (c) Induction motor with dynamometer

output powers: known as the direct method in the IEC 60034-2-1 [120] and Method A in IEEE Standard 112 [121]. Various operating conditions are referred to by the line voltages used (V_{Lm} , V_{Lg} , V_{Lb}), but the equivalent phase voltages (V_m , V_g , V_b) are used in the phasor vector diagrams

(e.g. 208V line = 120 V phase, 230V line = 133V phase). The experimental results show that the 3-phase H-bridge has numerous performance benefits over a direct grid connection and a VFD.

5.3.1 3-phase H-bridge vs Direct Grid: Motor Voltage = Rated

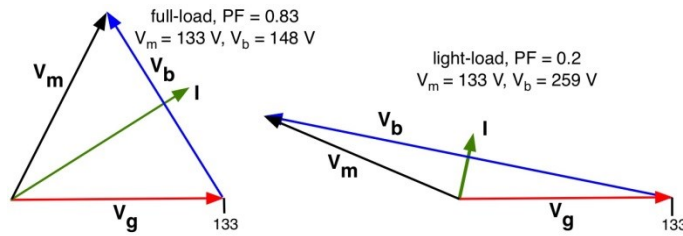
To validate that the motor performance is not degraded by using the proposed 3-phase H-bridge, the motor was supplied with a 3-phase 230V supply using a variac powered from a 208 V 3-phase supply, hence $V_g = V_m = 133$ V. Two cases were considered: (a) direct grid connected, (b) 3-phase H-bridge, see Fig. 5-2. The vector diagram in Fig. 5-2 (a) shows how the V_b can be changed in magnitude and phase relative to V_g in order to keep the motor supplied at 230 V ($V_m = 133$ V) as the motor load and power factor changes, see V_b & V_m in Fig. 5-2(a).

It should be noted that for the direct grid connection, the motor voltage drooped from 230 V under light load to 225 V at full-load. Since the 3-phase H-bridge naturally operates with a leading grid power factor, Fig. 5-2(a), a lower grid voltage droop is experienced (230 V to 226V) when using the H-bridges. Experimentally, it is verified that motor operating characteristics (Fig. 5-2) are the same. Hence:

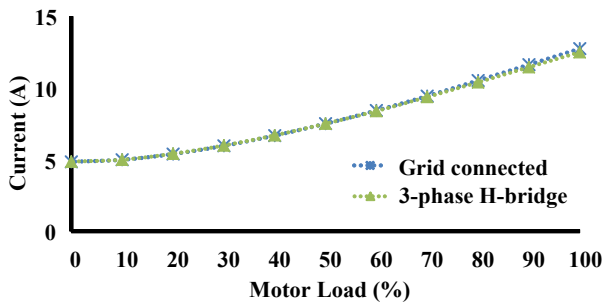
- The motor performance is not compromised when using the 3-phase H-bridge rather than the direct grid connection.
- The 3-phase H-bridge can be considered a viable motor controller because it provides extra functionality in terms of soft-start, chapter 3; voltage sag compensation, chapter 4; and an improved motor performance when using a variable motor voltage control strategy.

5.3.2 3-phase H-bridge vs Direct Grid: Motor Voltage < Rated

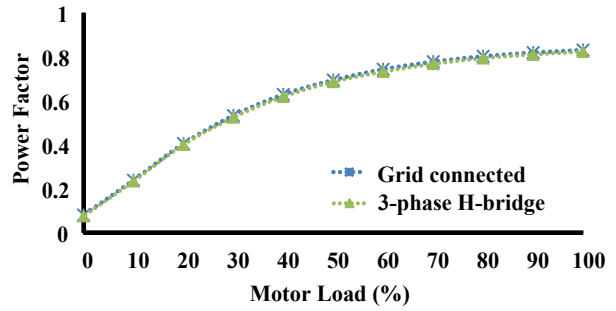
To examine the effect of operating an induction motor from a grid voltage that differs from the motor rated voltage, experimental tests were undertaken using a grid voltage lower than the motor rated voltage. Two cases were considered: (a) direct grid connected ($V_{Lg} = V_{Lm} = 208$ V), (b) 3-phase H-bridge ($V_{Lg} = 208$ V, $V_{Lm} = 230$ V), see Fig. 5-3.



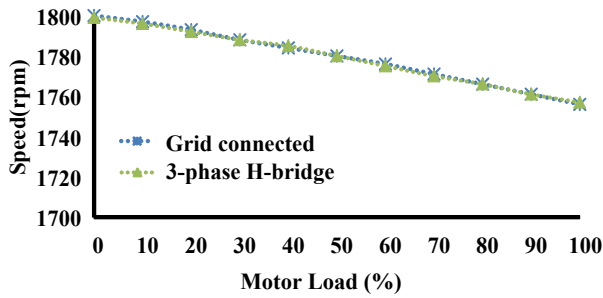
(a)



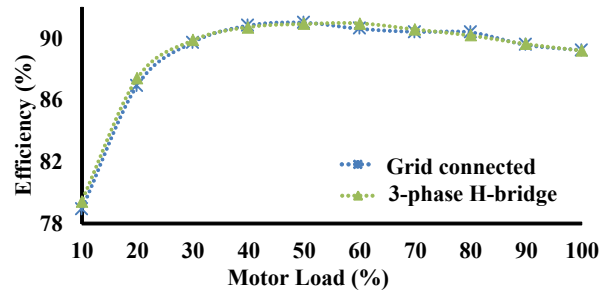
(b)



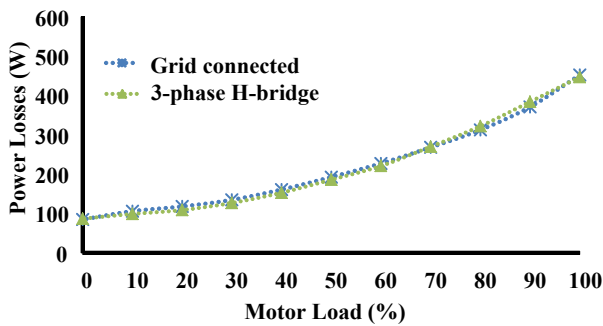
(c)



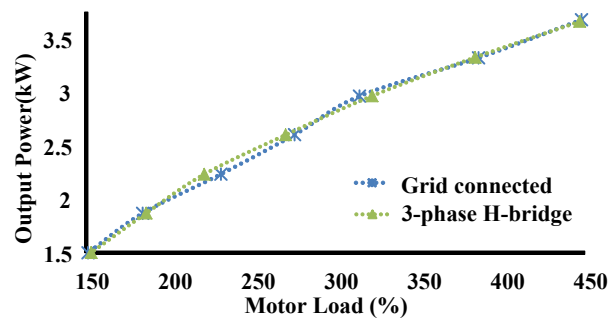
(d)



(e)

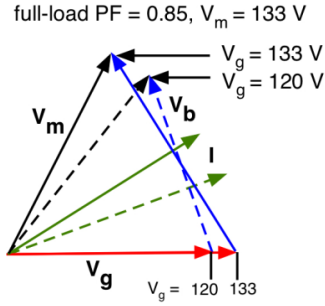


(f)

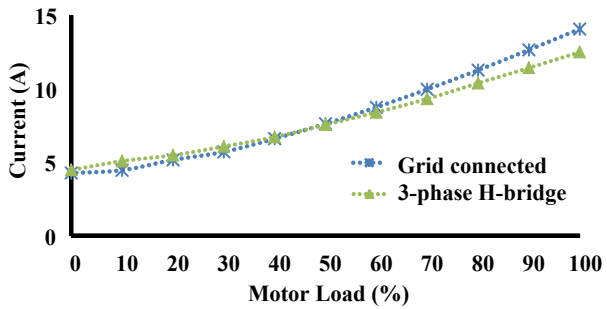


(g)

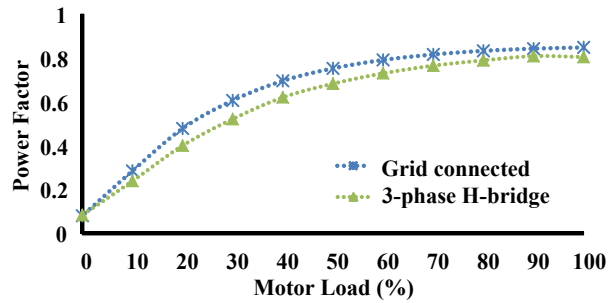
Fig. 5-2. Experimental motor performance comparison ($V_{Lg}=230V$, direct grid connection: $V_{Lm}=230V$, 3-phase H-bridge: $V_{Lm}=230V$): (a) voltage vectors for the motor at full-load and light load, (b) motor current, (c) power factor, (d) speed, (e) efficiency, (f) power losses, (g) output power



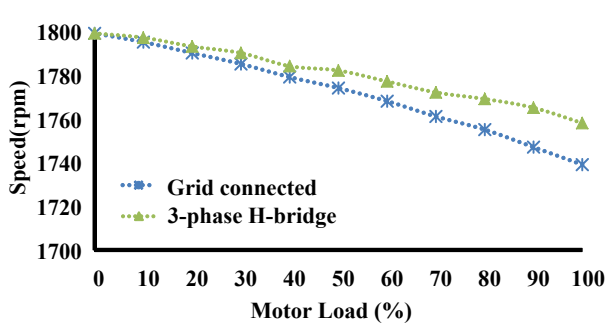
(a)



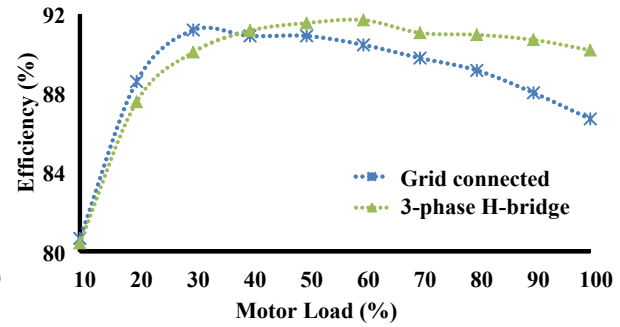
(b)



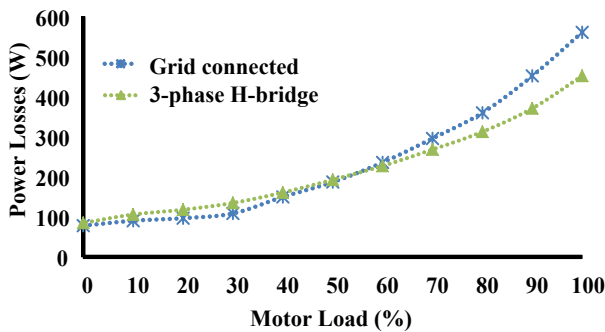
(c)



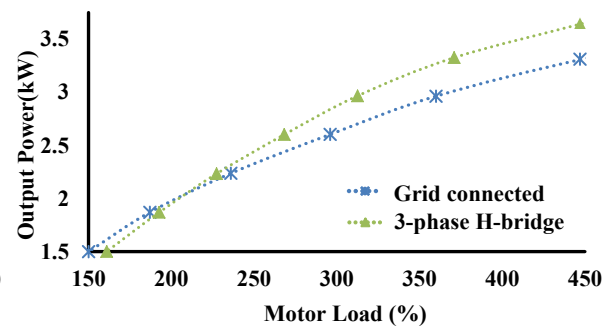
(d)



(e)



(f)



(g)

Fig. 5-3. Experimental motor performance comparison ($V_{Lg} = 208$ V, direct grid connection: $V_{Lm} = 208$ V, 3-phase H-bridge: $V_{Lm} = 230$ V); (a) vector diagram, (b) motor current, (c) power factor, (d) speed (e) efficiency (f) power losses (g) output power

Fig. 5-3 (a) illustrates how the magnitude and phase of V_b changes relative to V_g in order to keep the motor voltage constant at 230 V ($V_m = 133V$) when the grid voltage changes from 230 V to 208 V ($V_g = 133$ to 120V). The experimental results reveal that the motor performance is improved by using the 3-phase H-bridge. Motor current is reduced by 10%, Fig. 5-3 (b), power factor is reduced so as speed droop, Fig. 5-3(c)-(d). At full-load: the motor efficiency differs by 3%, Fig. 5-3(e); the motor losses differ by 100 W ($\approx 20\%$), Fig 5-3 (f). Hence, when operating directly from a lower than rated supply voltage, an induction motor has to be de-rated to limit the motor losses and temperature rise [122, 123] or can be operate the motor with 13% increase in output power, Fig. 5-3 (g) Since the 3-phase H-bridge can deliver rated voltage to the motor, it's losses and temperature rise are not elevated when using a lower than rated grid voltage. This is a significant result which can affect the operational life-time of the motor's stator winding [124-125].

5.3.3 3-phase H-bridge vs VFD

The VFD considered for comparison used a diode rectifier input and a PWM inverter output stage. This drive type was used as it has the largest market share ($> 90\%$) in the low-voltage industrial drive market [11]. However, this VFD suffers from system voltage drops and contrasts with the ability of the 3-phase H-bridge to boost the motor voltage when operating from a lower grid voltage. Hence these two systems were compared using $V_{Lg} = 230$ V to improve the performance of the VFD: (a) VFD: $V_{Lg} = 230$ V ($m_a = 1.12$), constant V/f control, (b) 3-phase H-bridge: $V_{Lg} = 230$ V, $V_{Lm} = 230$ V.

Experimental results reveal that the motor performance is improved for all motor load levels when using the 3-phase H-bridge, with the improvement being more significant at high loads, Fig. 5-4. At full load motor efficiency is improved by 1.5%, Fig. 5-4 (a) and loss is reduced by 12% Fig. 5-4 (b). Also the motor is de rated by 7% of output power for the same loss, Fig. 5-4 (c). This is caused by the 3-phase H-bridge being able to keep the motor at its rated voltage, whilst the VFD output voltage is naturally less than the grid and droops as the motor load increases.

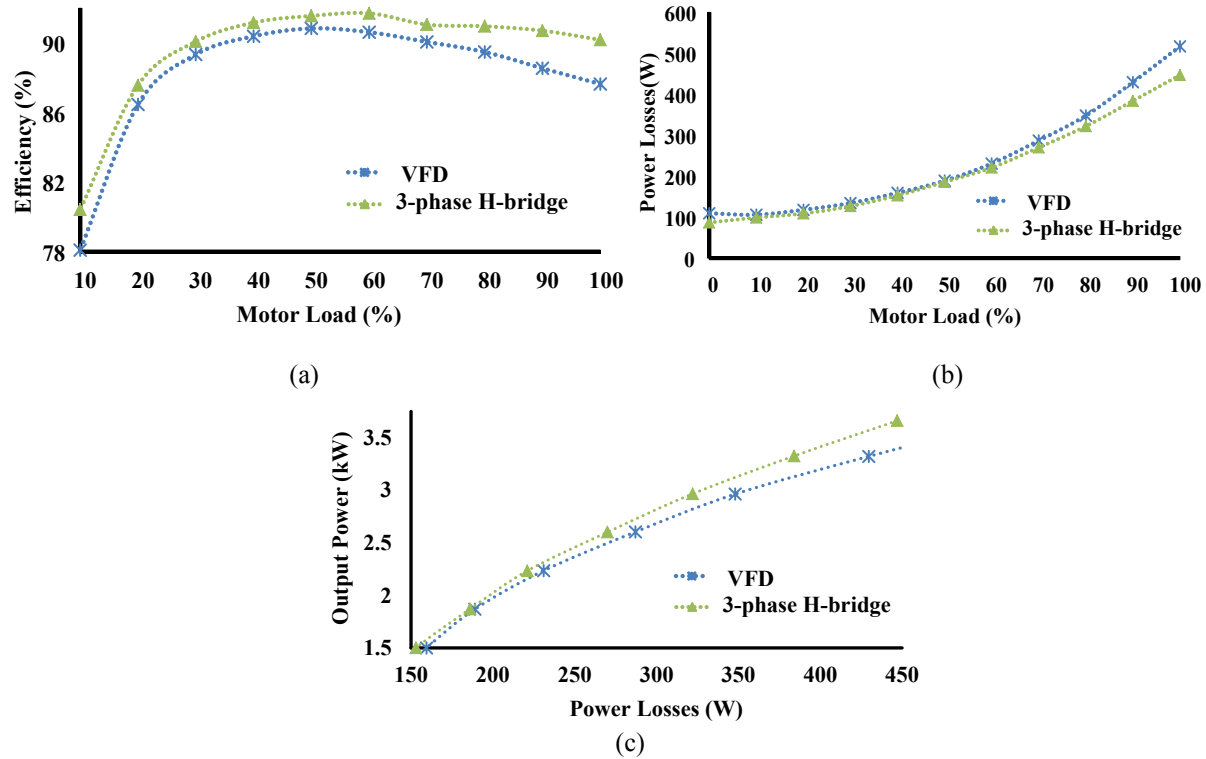


Fig. 5-4. Experimental motor performance comparison ($V_{Lg} = 230V$, VFD: $V_{Lm} = 225-214V$, 3-phase H-bridge: $V_{Lm} = 230V$): (a) efficiency, (b) power losses, (c) output power

Note that it is common practice for a VFD to be operated from a higher grid voltage, say 480 V for a 460 V motor, to compensate for system voltage drops. Alternatively, a BTB converter drive can boost the motor voltage above the grid similar to the 3-phase H-bridge [11]. However, several factors make the power electronics used in the BTB converter drive less desirable than the proposed system. The BTB converter needs an input reactor/filter (L or LCL) between the grid and front-end converter. This not only adds cost, weight in the system but also introduces additional losses in the system. In addition, the boosted dc link voltage naturally puts more stress on the semi-conductor devices, which could result in more switching losses in power electronics. In contrast, the proposed 3-phase H-bridge does not need passive filters and can easily boost motor voltage using a much lower dc voltage.

5.3.4 Power Electronics

Two experimental configurations are compared: (a) VFD: $V_{Lg} = 230V$, $V_{Lm} = \approx 225-214V$, (b) 3-phase H-bridge: $V_{Lg} = 230 V$, $V_{Lm} = 230 V$.

The “conventional” VFD was not able to supply the grid voltage to the motor at any load

level, varying in the range $V_{Lm} = 225$ to $214V$. The 3-phase H-bridge on the other hand has a voltage boost capability and can guarantee that the machine be supplied at rated voltage even though the grid voltage was roughly the same as the rated motor voltage and also experienced a small droop with increasing load.

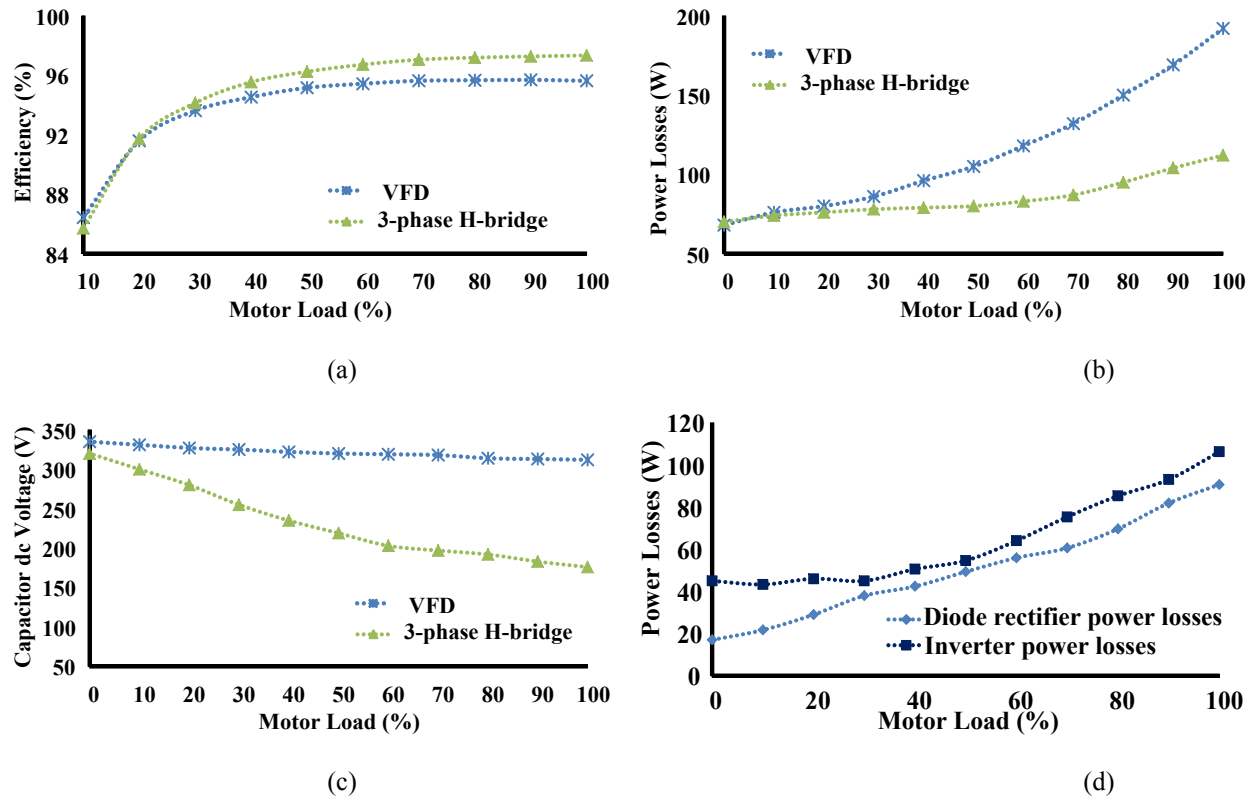


Fig. 5-5. Experimental power electronics performance comparison ($V_{Lg} = 230V$, VFD: $V_{Lm} = 225-214V$, 3-phase H-bridge: $V_{Lm} = 230V$): (a) efficiency, (b) power losses, (c) dc voltage, (d) VFD rectifier & inverter losses

The power conversion efficiency of the power electronics is higher; hence the power losses lower, for the 3-phase H-bridge when compared with the VFD over the complete range of the motor output power, Figs. 5-5 (a), (b). Under full load conditions the 3-phase H-bridge has a 3% higher efficiency, 96% compared with 93% for VFD, with a measured power electronics loss of 112 W compared with 198W for the VFD: representing a 43% lower power loss in the power electronics. The higher efficiency of the H-bridge can be attributed to several factors. The dc voltages in the 3-phase H-bridge is lower than for the VFD, varying in the range from 320 V under light load down to 160 V at full load, while for the VFD the dc voltage remains high around 325V, Fig. 5-5(c). This results in the 3-phase H-bridge switching losses to be lower than for the VFD. The VFD also operates the motor at a lower voltage (214V versus 230V), so the

system currents are higher, producing higher conduction losses [126-127]. This current difference is even higher for the VFD diode rectifier due to supply current harmonics.

The higher conduction and switching losses in the VFD should also be considered with the fact that the VFD is often operated with an input and an output 3-phase reactor. The VFD 3-level PWM output voltages, with voltage steps as high as 325V, should be compared with the 3-phase H-bridge where a higher frequency 5-level pwm voltage is present using lower voltage steps, as low as 160 V at full-load. Lastly, the power losses for a “*conventional*” VFD can be separated between the diode rectifier and the pwm inverter, see Fig. 5-5(d). Using these results, when assuming a BTB converter drive is used at the same 325 V dc-link voltage, the BTB converter would have a total loss at full load of around 212 W (106 *2 W). This compares with 112W for the 3-phase H-bridge. This means that the BTB converter drive using the same number of switches would have at least 90% higher losses than the 3-phase H-bridge. Note that the BTB converter drive would also normally be operated with a slightly higher dc voltage, hence increasing this estimated power loss difference.

5.3.5 3-phase H- Bridge and a Variable Motor Voltage

Under fixed frequency and variable motor load, the motor power conversion efficiency can be maintained at its maximum by changing the motor voltage [128, 129]. In order to achieve this over the range from full load to light load, the 3-phase H-bridge can supply the motor with a voltage greater than or lower than the grid voltage. The 3-phase H-bridge system is able to change the motor voltage to cope with a high voltage at a high load and a high power factor, versus a light load with a low voltage and a low power factor, see the voltage phase vectors shown in Fig. 5-6 (a) Experimentally three cases are presented using the 3-phase H-bridge: (a) $V_{Lm} = 208$ V, (b) $V_{Lm} = 230$ V, (c) $V_{Lm} =$ variable.

To maximize the motor power conversion efficiency, the H-bridge output voltage was altered to achieve the lowest motor input power while the dynamometer maintained a constant motor output mechanical power; hence minimizing the motor losses for each pre-set motor load. This procedure was repeated for each motor load setting. Note that results at the maximum motor load for the motor could not be obtained as the motor voltage was approaching its saturation limits.

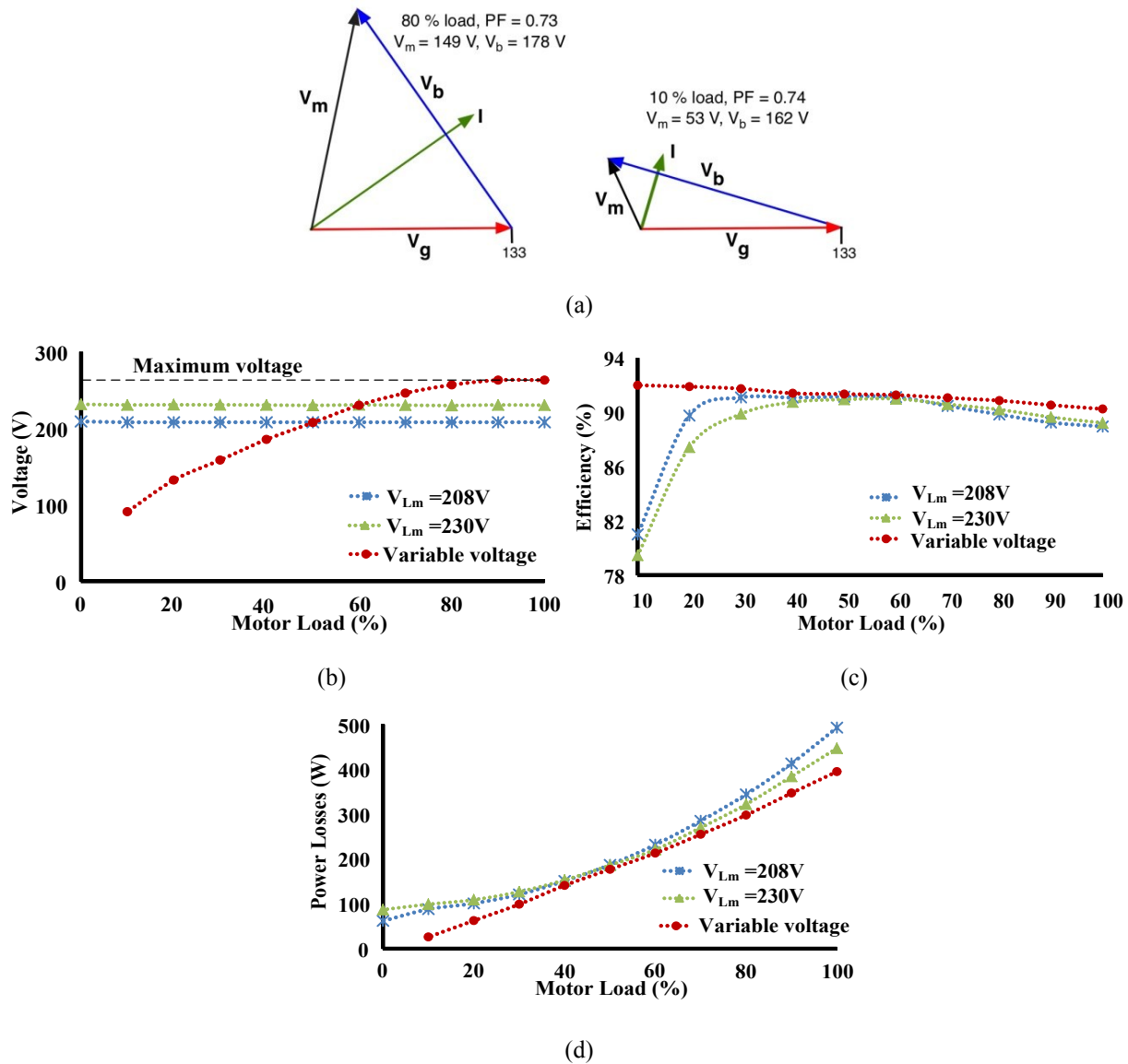


Fig. 5-6. Experimental motor performance comparison for the motor performance using the 3-phase H-bridge ($V_{Lm}=208$ V, 230V, variable): (a) voltage vectors, (b) motor voltage, (c) efficiency, (d) power losses

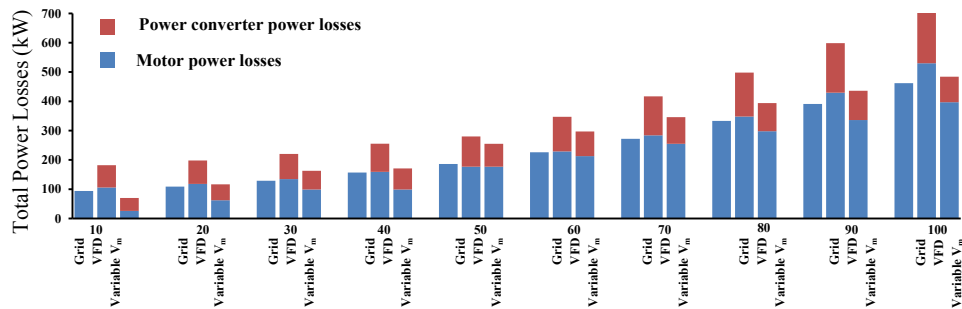
The motor performance is improved when using variable voltage operation, compared with the two fixed voltage cases, over the entire range of motor loads, see Figs. 5-6 (b),(c),(d). The motor performance approached that obtained with the two fixed voltage modes in the middle power range as the motor voltage required to lower the motor losses corresponded to the two fixed voltage cases: compare the motor voltages in Fig. 5-6(b) with the performances plotted in Figs. 5-6 (c), (d).

The efficiency improvement is more significant at low power settings: 10% difference at

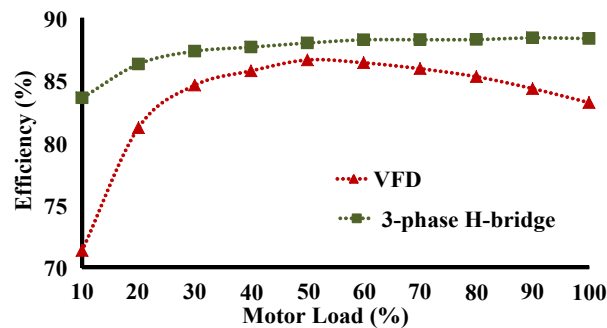
the lowest setting: 1% difference at the highest setting, Fig. 5-6 (c). 50W (12%) lower power losses were achieved at the highest load setting with 70W (15%) difference at the lowest power setting, Fig. 5-6 (d).

5.3.6 Total System Performance

Experimental results are presented representing the steady-state total system performance, relating to the output power of the machine relative to the input power delivered by the grid. Power electronics can be placed between the grid and the motor to improve the system performance under specific circumstances, (e.g. soft-start, sag compensation and grid VAR generation) but the power electronics themselves add to the total system losses in steady-state operation.



(a)



(b)

Fig. 5-7. System performance comparison; (a) motor, power electronic and total system losses, (b) system efficiency, 3-phase H-bridge vs VFD

The performance of three different systems is presented: (a) direct grid connected ($V_{Lg} = V_{Lm} = 230V$), (b) VFD connected ($V_{Lg} = 230 V$, $V_{Lm} = 225-214 V$), (c) 3-phase H-bridge ($V_{Lg} = 230V$, $V_{Lm} = \text{variable}$). The results illustrate that variable motor voltage control using the 3-

phase H-bridge has a superior performance relative to using a VFD but also a comparable performance with the direct grid connection, see Fig. 5-7.

The 3-phase H-bridge achieves the lowest motor and power electronic losses over the complete range of the motor loads, with the VFD producing the highest overall losses of the three systems examined, see Fig. 5-7(a). At full load, the 3-phase H-bridge overall system has 22% lower losses when compared to the VFD. Note that a BTB converter regenerative drive with the same number of switches will have higher losses.

The 3-phase H-bridge system achieves the lowest motor loss. This has several implications. First, the motor will operate at the lowest temperature, increasing its lifetime expectancy. The 3-phase H-bridge has the lowest power electronic losses which either results in a smaller more compact system design because of the lower cooling requirements, or alternatively, it can result in a lower operating temperature for the power electronics, hence a longer lifetime expectancy.

The benefits of the 3-phase H-bridge over direct grid connection is not that obvious from the results presented in Fig. 5-7(a), generally, total system losses are slightly higher for the 3-phase H-bridge due to the losses in the power electronics that does not exist for the direct grid connection. However, similar total system performances can be achieved as the 3-phase H-bridge can lower the motor losses by using a variable motor voltage control strategy. This partially compensates for the losses in the power electronics. The differences between the two systems are relatively small and the 230 V direct grid connected results represent the ideal situation. In a practical situation neither the grid voltage may not be the same as the motor rated voltage, may fluctuate, nor can the grid voltage be adjusted for improved motor performance under variable load. In these situations, the 3-phase H-bridge can be said to improve the system performance.

In addition, the 3-phase H-bridge system can also realize both a soft-start feature, and compensation for grid voltage sags. Both of these features contribute to increasing the motor lifetime expectancy due to the lowering of the electrical and mechanical stress on the motor. For instance, an induction motor can experience unplanned breakdown due to direct online starting resulting in expensive process downtimes [130].

Another benefit of the 3-phase H-bridge is its grid VAR generation capability. As a result, grid voltage sags produced by the motor load can be reduced and compensation is also possible

for the reactive power generated by other loads, hence, improving the overall power factor of the grid.

Finally, voltage sag is one of the power quality problems that can cause serious economic loss due to malfunction of equipment [131]. The 3-phase H-bridge can maintain the motor voltage during grid voltage disturbances (voltage sags or swells). As a result, downtimes can be avoided or reduced and productivity increased.

When all these factors are to be taken into consideration, it can be concluded that in applications, the proposed H-bridge system is a competitive choice over a direct grid connected machine and the VFD or BTB converter drive.

5.4 Conclusions

The steady-state performance of a smart grid connected induction motor is presented when operating with constant supply frequency. A power electronic system using floating bridge converters is used to improve the operation of the motor. The experimental performance of the power electronics, motor and total system is presented with respect to power losses, system efficiency and the motor output power. In summary:

- The performance of the motor is not compromised when the motor is operating with the PWM 3-phase H-bridge converter.
- The proposed system is demonstrated to have a higher performance over the direct grid connection when the grid voltage is not the same as the motor rated voltage: reducing the losses hence temperature rise of the motor.
- The 3-phase H-bridge confirmed improves performance over the VFD. The overall system loss is reduced by 12% and motor performance is higher by 7%.
- Variable motor voltage control can lower or increase the motor voltage relative to the grid and hence can be used to lower the machine losses over its entire load range. These performance benefits should be considered in addition to the soft-start and voltage sag compensation capabilities.

Chapter 6

6 Variable Motor Voltage Control

The proposed 3-phase floating H-bridges is inserted between the utility grid and an induction motor to inject a voltage in series with the grid voltage. The magnitude and phase of this voltage is used to control the motor voltage under steady state operation so as to lower the motor power losses over its entire load range. This is made possible because the 3-phase H-bridge can be used to both increase and decrease the motor voltage relative to the grid voltage as required. This feature affects the performance of the overall system, more specifically; the motor power conversion efficiency is improved, lowering its operating temperature and hence improving reliability and life time expectancy of the stator winding. A variety of motor voltage control options exist, the controller presented here is based on readily available machine nameplate data. This data is used to identify the motor output power associated with its maximum efficiency operating point when operated under rated voltage. This data is then used as the basis to control the motor voltage according to the square root of the measured motor input power. The controller and the performance of the 3-phase H-bridge are described. The relationship between the motor winding temperature rise and motor loss is also established. The benefits of the variable voltage control are assessed by comparing the motor performance with the machine operated at its rated voltage. The chosen controller also results in the H-bridge dc voltages being relatively low and constant over a wide load range, hence lowering the power losses and electrical stress in the power electronics. Both experimental results and theoretical predictions are used to illustrate the performance of both the 3-phase H-bridge and the motor.

6.1 Introduction

The electronic operating systems used with many induction motors are significant element in future industrial smart-grids, used as a means to achieve energy savings, reduce production costs, and provide grid voltage support. The power electronic, 3 phase H-bridge, can be used to control the motor voltage under a variety of situations [132-212]: limit the motor

starting current (Chapter 3); provide immunity to grid voltage sags and swells (Chapter 4); generate VARs into the grid for VAR compensation and voltage support; provide a buffer between the motor mechanical system and the grid to limit system oscillations (chapter 5); and lastly, to control the motor voltage to lower its energy losses. The latter feature is the subject of this chapter.

Many loss minimization control schemes for induction motors have been reported [133-134]. These techniques can be divided into three main categories: (a) model-based methods, (b) simple state control and (c) search control.

Calculation intensive model-based methods provide smooth and fast adaptation of the motor flux as long as the motor parameters are known: e.g. rotor speed or slip, core loss, main inductance saturation [135]. The less complex state control assumes certain quantities of the motor can be easily defined, such as displacement power factor or slip to operate motor at maximum efficiency. Alternatively, rotor slip frequency control requires a speed feedback. The constant power factor approach has a relatively fast response (<1 s) and is a good choice for industrial drives [136]. A real-time search method can be used to find the motor voltage that minimizes the motor input power for a constant load output power [137]. Theoretically, this method offers an optimal solution, however, this method is not popular as it has a slow response to load changes (>7 s) [4], difficulties tuning the algorithm and requiring precise load information.

The operation and performance of a 3-phase H-bridge is presented, where the motor voltage is controlled using a series voltage injection relative to the fixed frequency grid voltage. This resultant system is more energy efficient and cost effective when compared to other systems such as a VFD. The work presented in this chapter presents a novel controller for a 3-phase floating capacitor H-bridge system; to control the motor voltage hence its power conversion efficiency. The controller does not require speed feedback or machine parameters. The maximum motor power conversion efficiency is closely linked with a fixed speed, constant motor power factor, and more significantly, constant motor impedance. Hence, the motor voltage can be made to change with the square root of the measured motor input power to maintain maximum motor efficiency operation; noting to avoid saturation at the higher voltages. Since the motor voltage can be set above or below the utility grid voltage using the H-bridge system, the motor efficiency

can be improved over a wide load range irrespective of utility voltage fluctuations. Previous performance improvements [135] using voltage control did not use the proposed H-bridge system and reduced the applied voltage when the torque requirement of the load can be met with less than full motor flux. The ability of the floating H-bridge system to increase or decrease the motor voltage relative to the grid voltage is a significant feature of the system to maintain a high motor efficiency over a wide load range. For practical convenience, the system controller is implemented using parameters readily available from the motor nameplate data. The controller set the reference motor voltage based on input power. In chapter 5, the reference voltage is set by the user to maximize the motor power conversion efficiency. The results of extensive experimental performance testing of the motor and system as a whole compare favourably with theoretical predictions.

6.2 Motor Voltage Control

Two voltage control modes are chosen to highlight the benefits of variable voltage control using the 3-phase H-bridge over operating the motor at its rated voltage: (a) “*rated voltage control*”, V_{rated} , and (b) “*variable voltage control*”, V_{var} . The former control keeps the motor voltage constant at rated irrespective of grid voltage droops, sags or swells. The latter control requires the motor voltage to be greater than or less than the grid voltage and is chosen to minimize the motor losses, hence maximize the motor power conversion efficiency. The rated grid voltage is assumed to be the same as the motor rated voltage and the motor load is assumed to vary over a wide range, typically from 10 % to 100 % of rated.

If, as a starting point, changes in motor parameters caused by the varying flux level are neglected, the improvement obtained by varying stator voltage is easily demonstrated through equivalent circuit considerations. For a fixed input voltage the only variable quantity in the equivalent circuit of Fig. 6-1 is the slip s ; hence changes in load are accommodated by changes in s . With s varying, the motor terminal impedance and hence the power factor, current and efficiency all vary. If, as an alternative, an automatic voltage controller is used to maintain slip constant at some optimum value, the terminal impedance and hence the power factor and efficiency remain constant. Since, at a given slip, torque is proportional to voltage squared, the controller will in fulfilling its slip control function also provide a voltage proportional to the square root of the developed torque [137]. Hence, a motor voltage control can be envisaged that

maintains high motor power conversion efficiency where the motor voltage V_m is altered as the square root of the measured electrical input power P_{in} relative to rated input power P_{mo} . As the motor power changes, the motor input impedance Z_{ph} stays constant together with the input power factor, slip and rotor speed.

$$V_m = V_{m,rated} \sqrt{\frac{P_{in}}{P_{mo}}} \dots\dots\dots 6-1$$

For illustrative purpose, this chapter uses the equivalent circuit parameters for a 5 HP induction motor described in chapter 1.

An induction motor with the parameters has a maximum power conversion efficiency of 91% occurring at roughly 65% of the motor rated load.

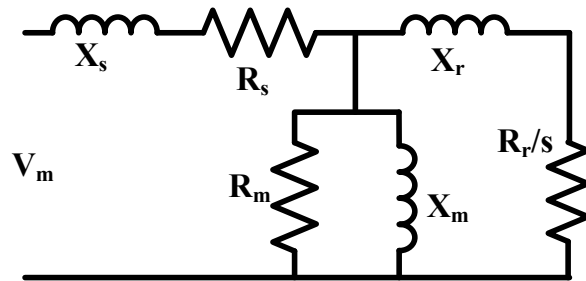


Fig. 6-1. Equivalent circuit of induction motor

The 3-phase H-bridge differs from previous methods reported [128, 62] as the motor voltage can be made to be greater than the grid voltage to improve the motor efficiency at high loads, and less than the grid voltage to improve the motor efficiency under light loads. Fig. 6-2 and 6-3 compares rated voltage control versus variable voltage control using equation 6-1. Temperature effects on motor efficiency are illustrated by black line in Fig. 6-3. Though it is assumed motor parameters are constant throughout motor load condition but in experiment it is observed temperature plays a vital role in motor's performance. So motor's parameters-resistance values are changed according to motor loss or temperature rise. Later of this chapter experimentally it is shown loss and temperature rise has linear relationship. Variable voltage control, using Eqn. 6-1, results in the motor power factor being constant at approximately 0.71, compared with rated voltage control where the power factor varies from 0.83 at full load, down to 0.1 under light load. Noting that the 3-phase H-bridge provides a series voltage injection V_b at 90° to the current, then the per-unit injected voltage $V_{b,pu}$ is shown in Fig. 6-2(b) as a function of

the motor voltage $V_{m,pu}$ using curves at motor power factor angles ϕ_m in 10^0 steps: $V_{b,pu}$ for V_{rated} and V_{var} control are also highlighted in the figure. Significantly, variable voltage control, V_{var} , largely results in a lower injected voltage, $V_{b,pu}$. This can be used advantageously to lower the power losses and electrical stresses in the power electronics by lowering their dc voltage. Unlike rated voltage control, variable voltage control maintains a balance between the current flowing through the motor magnetizing inductance and its rotor circuit. This balance lowers the motor input current under both light load and high load conditions, hence lowering the motor losses.

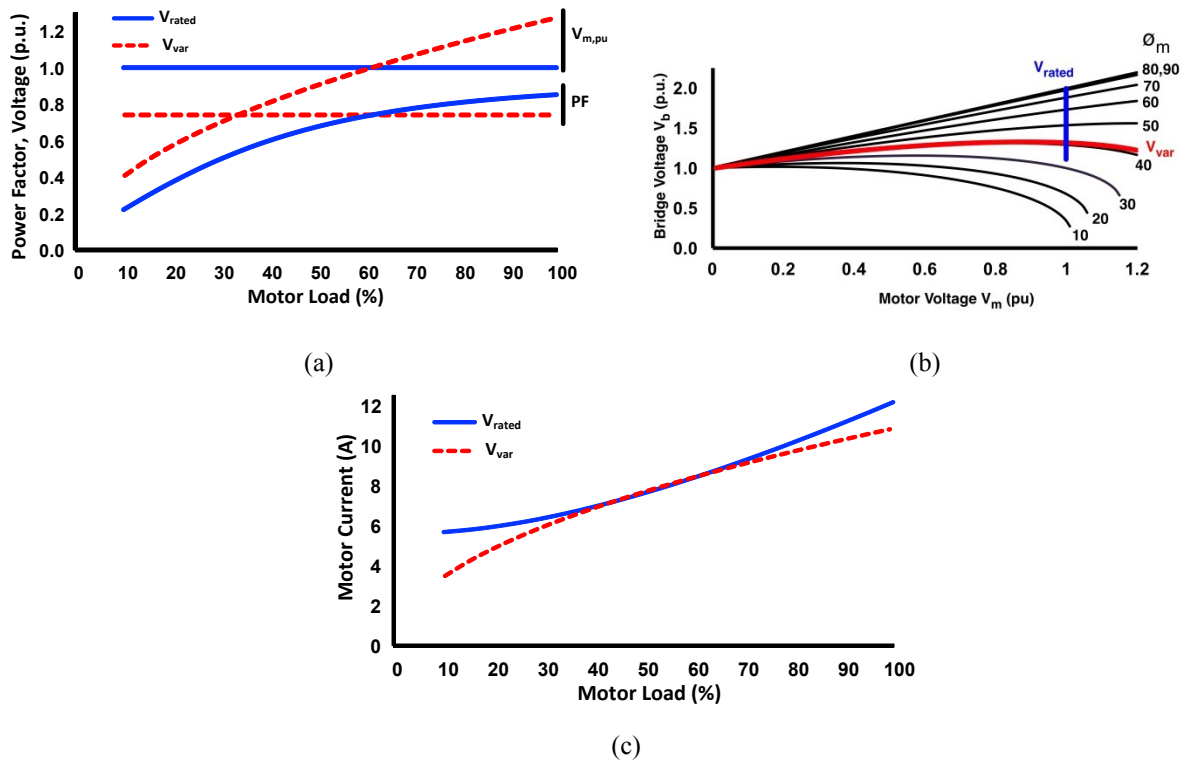


Fig. 6-2. Motor operation under rated and variable voltage control; (a) motor voltage and power factor, (b) bridge voltage as a function of the motor power factor angle, (c) input current

Theoretically variable voltage control results in the motor efficiency staying at the motor maximum over the entire load range, Fig. 6-3(a), if temperature variation is ignored. Considering temperature effect of motor's resistance value the efficiency curve is not constant anymore, increase at lower load and decrease at higher load. Rated voltage control results in much lower power conversion efficiencies under both high and light loads. These trends in the efficiency curves is reflected in the motor loss curves, Figs. 6-3(a) and 6-3(b).

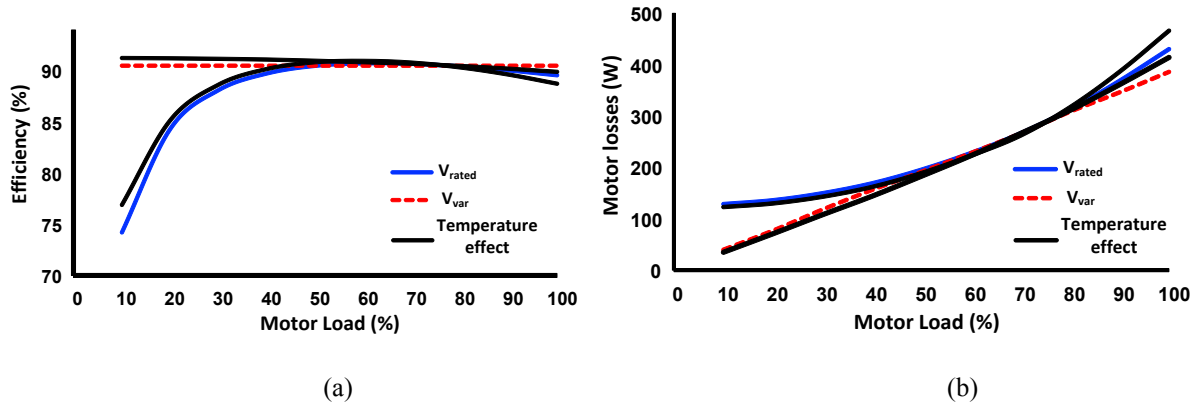


Fig. 6-3. Motor operation under rated and variable voltage control with temperature variation; (a) motor efficiency, (b) motor losses

6.3 3-phase H-bridge Control

For the 3-phase H-bridge to deliver the desired motor voltage, a motor voltage larger, equal to, or less than the grid voltage is required. The system voltage vectors required to achieve the two modes of motor voltage control are presented. Theoretical analysis of the vector diagrams is presented to predict both the angle α and magnitude of the injected voltage V_b . Performance curves for the 3-phase H-bridge are presented for both motor control modes. Given the motor parameters stated in chapter 1, the voltage injection angle α , Fig. 6-4(a), can be controlled to deliver the desired motor voltage V_m to the motor. For variable voltage control, the motor power factor is fairly constant, in the Figs. 6-4 (a), (b). Under high load, the motor voltage has to be boosted above rated, Fig. 6-4 (a), and reduced under light load, Fig. 6-4 (b), as given by Eqn. 6-1. The vector diagrams in Fig. 6-4 demonstrate that the 3-phase H-bridge can deliver the desired motor voltage by changing α as long as the bridge capacitor voltage is allowed to change.

Interestingly both control modes have α changing relatively close together increasing from under 10° at light load to close to 50° to 60° at high load, Fig. 6-5 (a). Though motor power factor varies from low value (0.1) to high value (0.83) under rated voltage operation, but with variable voltage control, motor is running under almost constant power factor, so the motor power factor is constant throughout the load range (neglecting temperature effect). The motor voltage is low under light load and high at high load, ϕ_m in Fig. 6-5(c). Hence α changes from a small value under light load to a high value under high load.

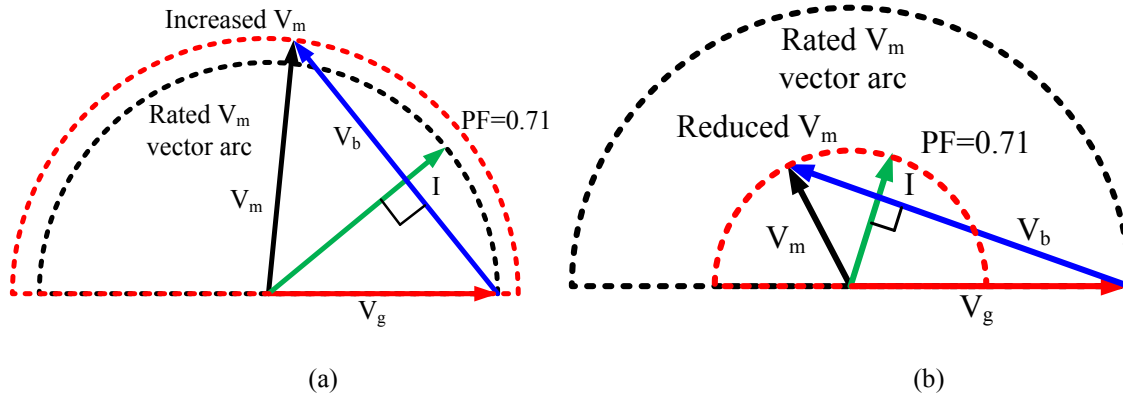


Fig. 6-4. Phasor voltage vectors: (a) $V_m >$ rated, high load, (b) $V_m <$ rated, light load.

For rated voltage control $V_{m,pu}$ is constant, but ϕ_m decreases with increasing load, hence ϕ_g decreases also. For, variable voltage control, ϕ_m is constant, but ϕ_g decreases with increasing load as $V_{m,pu}$ increases with increasing load, Fig. 6-5 (c).

V_{cap} is plotted in Fig. 6-5 (d) for both control cases assuming $V_{Lg} = 230$ V for the 5hp machine. An obvious benefit of the variable voltage control, operating with a constant relatively low power factor of 0.71, is that the capacitor voltage is fairly constant as the load changes and peaks at just over 200 V as compared with 340 V for the rated voltage control. This has many benefits in lowering the power electronics losses and electrical stresses, hence lowering temperature fluctuations.

For rated voltage control: ϕ_g is a leading angle relative to V_g while ϕ_m is a lagging angle relative to the V_m by the same amount. When $V_{g,pu} = V_{m,pu} = 1$ p.u, the Eqn. 2-2, 2-3 and 2-6 can be simplified as

$$\cos \phi_g = \cos \phi_m \Rightarrow PF_g = PF_m \dots\dots\dots 6-2$$

$$\sin \alpha = \cos \phi_m \dots\dots\dots 6-3$$

Hence:

$$V_{b,pu} = 2 \sin \phi_m \dots\dots\dots 6-4$$

For variable voltage control assuming: $\cos \phi_m = 0.71$, The Eqn. 2-2, 2-3 and 2-6 can be derived as

$$\cos \phi_g = \frac{V_{m,pu}}{\sqrt{2}} \dots\dots\dots 6-5$$

$$\sin \alpha = \frac{V_{m,pu}}{\sqrt{2}} \dots\dots\dots 6-6$$

Hence:

$$V_b = \sqrt{1 - \left(\frac{V_{m,pu}}{\sqrt{2}}\right)^2} + \frac{V_{m,pu}}{\sqrt{2}} \dots\dots\dots 6-7$$

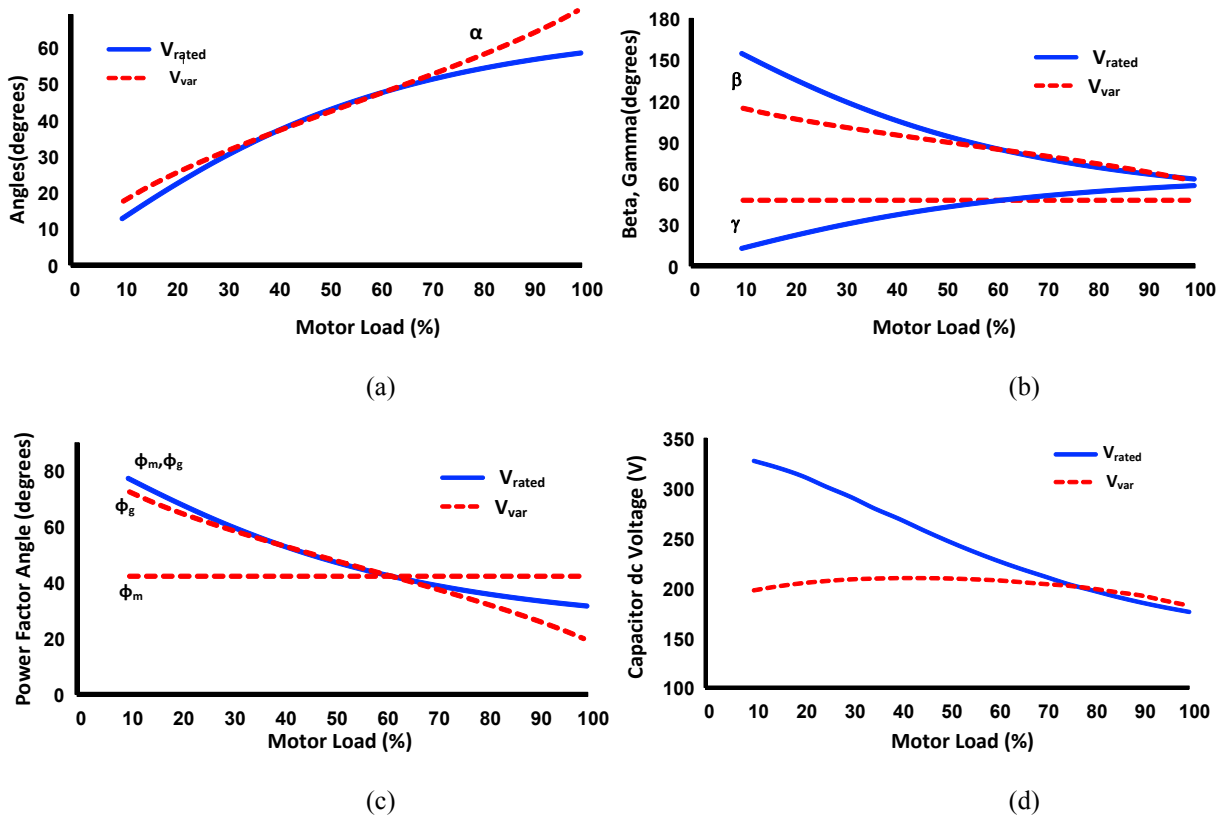


Fig. 6-5. Rated & variable voltage control;(a) control angle α (b) angles γ and β , (c) grid & motor displacement angles ϕ_g and ϕ_m , (d) capacitor dc voltage

6.4 Motor Voltage Controller

As mentioned, motor voltage control is achieved by changing the control angle α^* , Fig. 6-6. For constant voltage control, V_m^* corresponds to the motor rated voltage ($=V_{rated}=V_g$), for

variable voltage control V_m^* is given by Eqn. 6-1 to keep the motor operating at maximum efficiency. But in chapter 5, the variable voltage operation is a search method where the motor voltage is varied in predefined value till minimum loss in the motor is obtained for a specific load setting. The whole process is carried out for 10% to full load setting.

The input power P_{in} for Eqn. 6-1 is measured at the grid, though strictly this measurement also includes the power losses in the power electronics. The grid voltage is used by the controller PLL to provide the base reference frame for phase information. Both the current and voltage feedback signals measured at the grid are reliable low noise signals.

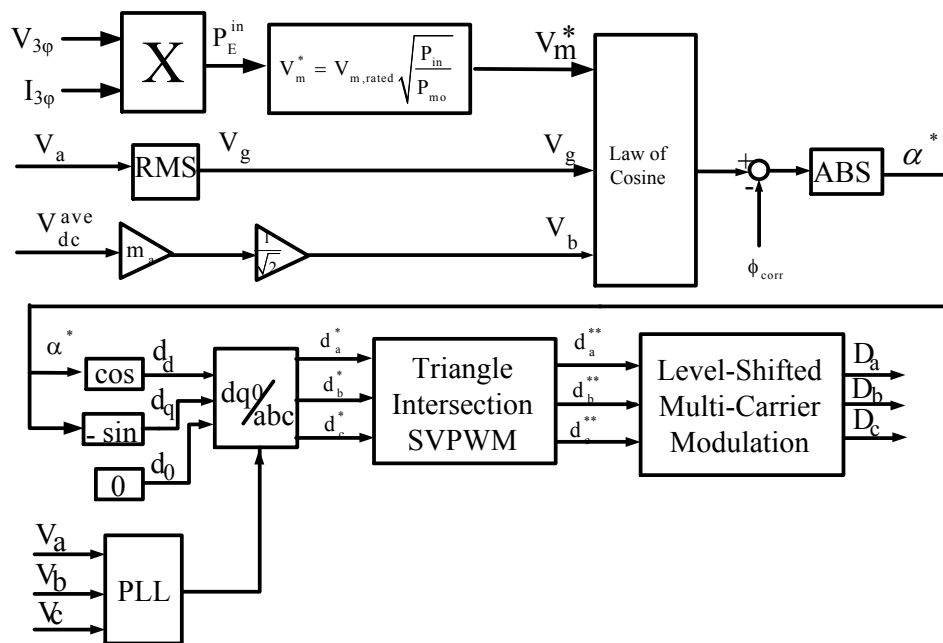


Fig. 6-6. Control block diagram for variable motor voltage control

6.5 Experimental Results

The system performance is compared over a wide load range between using rated voltage control ($V_{Lm} = 230$ V line; $V_m = 133$ V) and variable voltage control ($V_m = V_{var}$). The motor with the basic motor parameters defined in chapter 1 is used for testing. However, the theoretical motor performance curves were improved from those shown in section 6.2 as the motor equivalent circuit resistances were adjusted with the motor operating temperature for each load setting. Better agreement between experimental and theoretical predictions is achieved as a result. Section 6.5.5 describes the relationship between the motor losses and its temperature rise.

6.5.1 General Motor Performance

Good agreement was obtained between experimental and theoretical motor performance predictions for all the parameters presented in Fig. 6-7. The results confirm that the motor voltage controller illustrated in Fig. 6-4, and using α control as defined in equation 2-3(b), is a good method for directly controlling the motor voltage, Fig. 6-7 (a).

Variable voltage control improves the motor efficiency under high and light load levels, reducing the motor current and lowering the motor losses. For example, 7% reduction of the motor current is obtained under full load and 11% reduction under light load, Fig. 6-7 (b). The two controllers produce similar results in the mid power range as expected.

Variable voltage control has very slightly higher currents and efficiency in the mid power range, Fig. 6-7 (b), because machine data at 75% load was used in setting up the parameters associated with equation (6-1). This implies that under rated voltage, the motor efficiency probably peaks at a power level slightly below the 75% load setting. This did not occur in the theoretical results described in section 6.2 as motor equivalent circuit data was used to more accurately determine the machine maximum efficiency condition, which occurred at around 65% motor load level. Variable voltage control has a steadily decreasing efficiency as the motor power is increased, Fig. 10(c), compared with the flat characteristics in Fig. 2(c). This is caused by the temperature dependence of the motor resistance with the motor load. The variable voltage experimental currents, power losses and efficiency show good agreement between experimental and theoretical predicted results. The same parameters for rated voltage control are in close agreement with slightly higher differences.

Under light load, variable voltage control has a motor efficiency of 92 % as compared to 79% under rated voltage control; the difference in efficiency at full load is approximately 1%. Higher power conversion efficiencies are associated with lower motor losses and a lower temperature rise: around 10% loss reduction is possible at rated load, Fig. 6-7 (d). This increases the motor lifetime expectancy: note that the motor winding insulation life can be doubled for every 10°C reduction in average operating temperatures [122]. With accurate variable voltage control, the 3-phase H-bridge is also immune to non-optimal grid voltage and its sags and swells. These latter factors often lead to derating a motor [123] and using a motor with a larger frame

size [24]. Fig. 6-7(d) illustrates that with variable voltage control the motor power rating can be increased by 7% as a result of the lower losses experienced at high power levels.

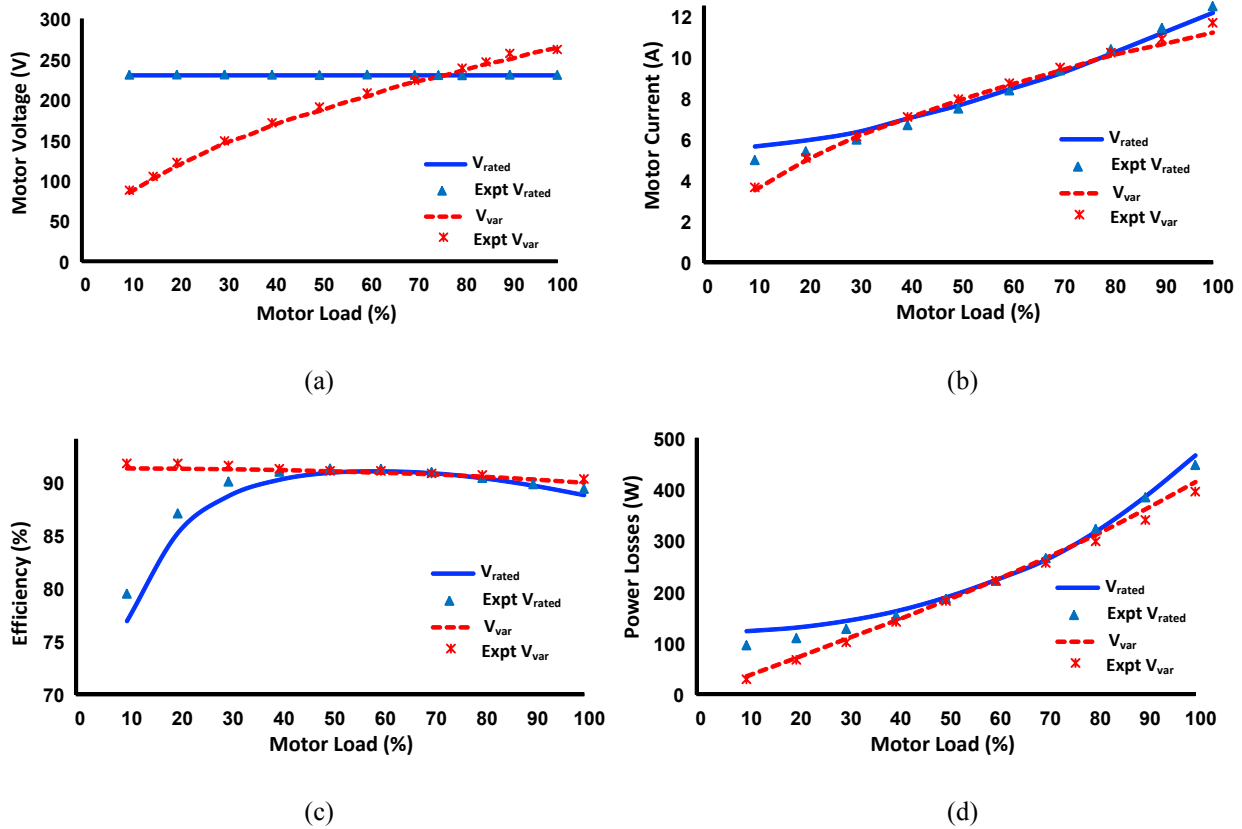


Fig. 6-7. Motor performance as a function of the motor output load in %; (a) motor voltage, (b) current, (c) efficiency, (d) power losses

6.5.2 Motor Reactive VARs and Rotor Speed

Variable voltage control is associated with operating the machine at its maximum power conversion efficiency and the machine having a constant input impedance, constant speed and constant power factor. The Experimental results presented in Fig. 6-8 confirm these conclusions with a good agreement between experimental results and theoretical predictions. For instance, the motor power factor is fairly constant and close to 0.75 to 0.8, with experimental results giving slightly lower values, see Fig. 6-8(c).

Rated voltage control has usual droop in speed with increasing load commonly associated with induction motors operated at constant voltage, Fig. 6-8(a): the motor droop in power factor as the load is decreased is also a classic characteristic associated with induction motors, Fig. 6-8

(c). With the torque speed curve for both controls is shown in Fig. 6-8 (b), which shows almost constant speed with variable torque under variable control whereas speed varies with different load under rated voltage control. For constant voltage control, motor operating at almost constant reactive VARs is caused by the magnetizing inductance drawing a constant current due to the constant supply voltage, Fig. 6-8 (d). This contrasts with the VARs decreasing almost linearly with decreasing load under variable voltage control: since the machine is operating at constant power factor, Fig. 6-8(b), then it is expected that machine VARs should decrease linearly with machine load.

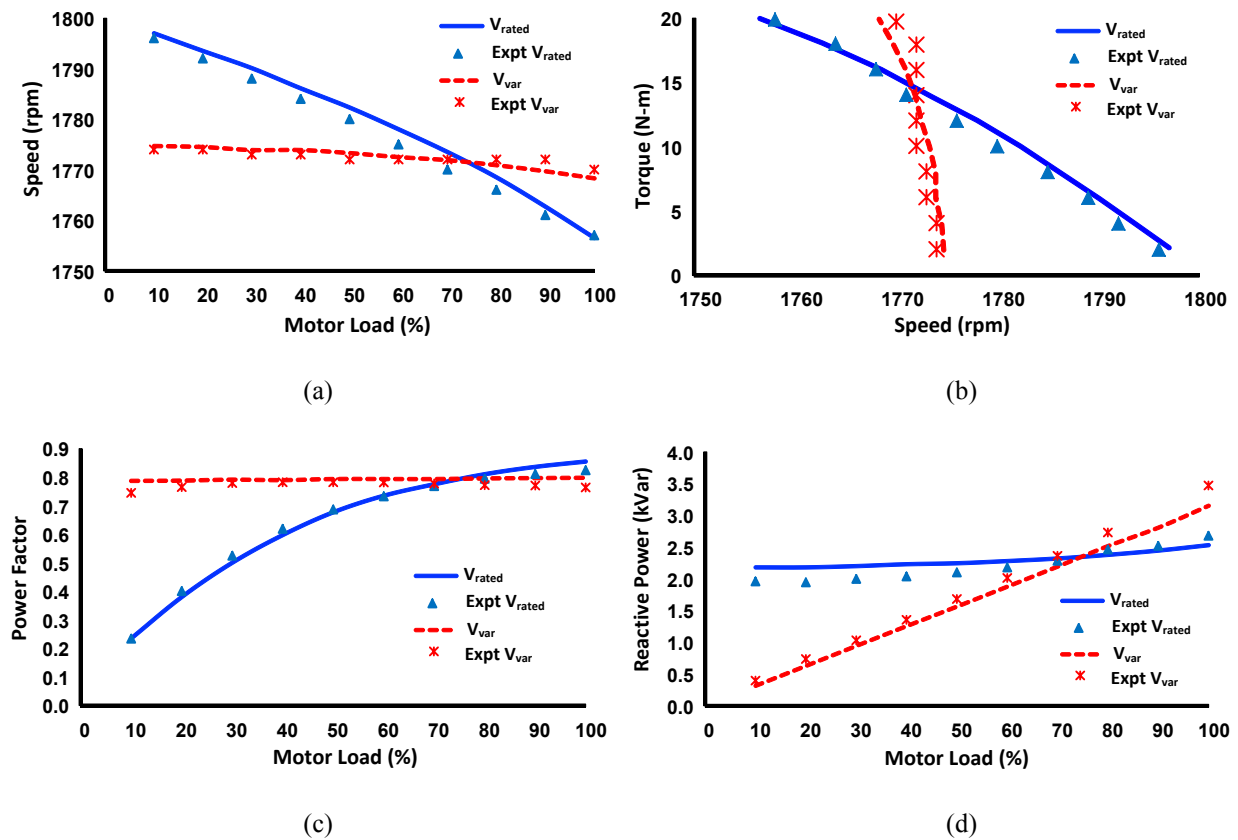


Fig. 6-8. Motor reactive power and speed curves: (a) rotor speed, (b) torque-speed, (c) power factor, (d) reactive power

6.5.3 Grid: Power Factor and VARs

The voltage injected by the 3-phase H-bridge V_b phase shifts the motor voltage V_m so that it leads the grid voltage V_g . The grid power factor decreases with the decreasing motor load for both motor controllers, Fig. 6-9(a), however the grid power factor is leading rather than the lagging power factor at the grid terminals. This can be expected for constant voltage control

since $|\phi_g| = |\phi_m|$ when $V_m = V_g$ and ϕ_g leads with ϕ_m lagging. For constant voltage control, the motor VARs are relatively constant, hence the grid VARs are also relatively constant, see Fig. 6-9 (b). For variable voltage control, firstly, the system power flow decreases linearly with the motor load as expected. Secondly, since the machine impedance is assumed constant and the motor voltage changes according to the square-root of the motor power, then the grid current hence grid apparent power changes according to the square root of the motor power. These two trends for the grid power and apparent power results in the curved relation for the grid VARs relative to the motor load, Fig. 6-9 (b).

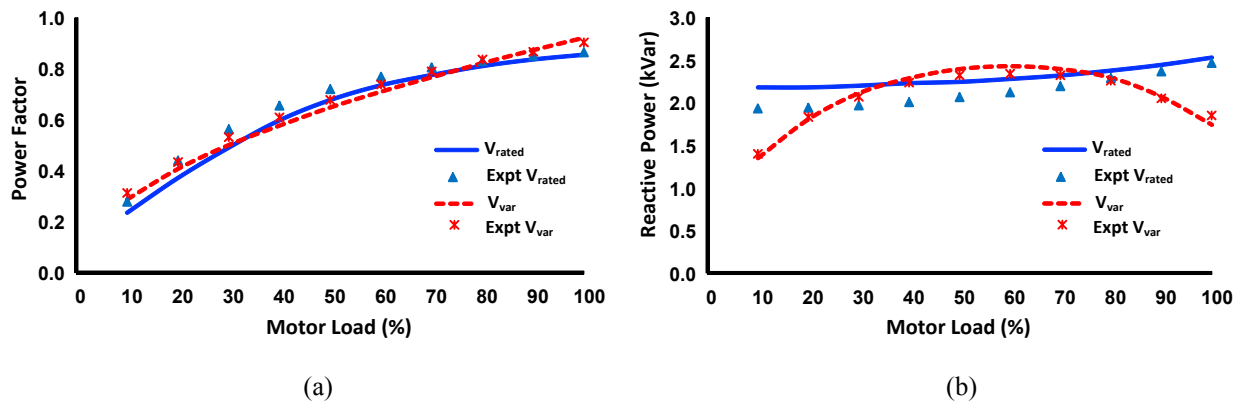


Fig. 6-9. Reactive VAR generation and grid Power Factor: (a) leading grid current, (b) grid power factor (PF_g), (c) grid VAR generation.

6.5.4 Temperature Dependence

The motor temperature rise is widely assumed to be proportional to its power losses. Experimental tests results prove this to be the case for the motor used in this study. The stator temperature rise is the most significant as the stator winding insulation lifetime deteriorates with temperature. The stator temperature rise was obtained by operating the motor from a 230 V supply for a few hours at each power setting, stopping and measuring the stator winding resistance within 30 secs of cutting the power to the machine. A linear relationship between the motor losses and temperature rise was obtained, with the motor rising to 60 °C at the motor rated conditions of 5 hp and 230 V respectively, see Fig. 6-10(a): the data for the machine quoted a 65 °C rise under rated conditions. The power losses obtained for both the rated and variable voltage control were then related to the stator temperature rise using the results from Fig. 6-10(a), see Fig. 6-10(b). The stator temperatures coincide in the mid motor load region, as expected from the

maximum efficiency condition used to set up the controller. Under rated power conditions (Torque=20 N-m), the variable voltage control produced a temperature rise of 7.5 °C less than rated voltage control, corresponding to a 75% increase in stator winding insulation lifetime expectancy according to [125]. Under light load (Torque=2 N-m), the variable voltage control produced a temperature rise 10 °C less than rated voltage operation, representing a 100 % increase in winding insulation lifetime if the machine were operated under this load continuously; however this result if for a very light load is less significant than the full-load result. Considering the same temperature rise obtained under rated power conditions for variable voltage control, rated voltage control produces approximately 7% less power: this represents a 7 % power derating.

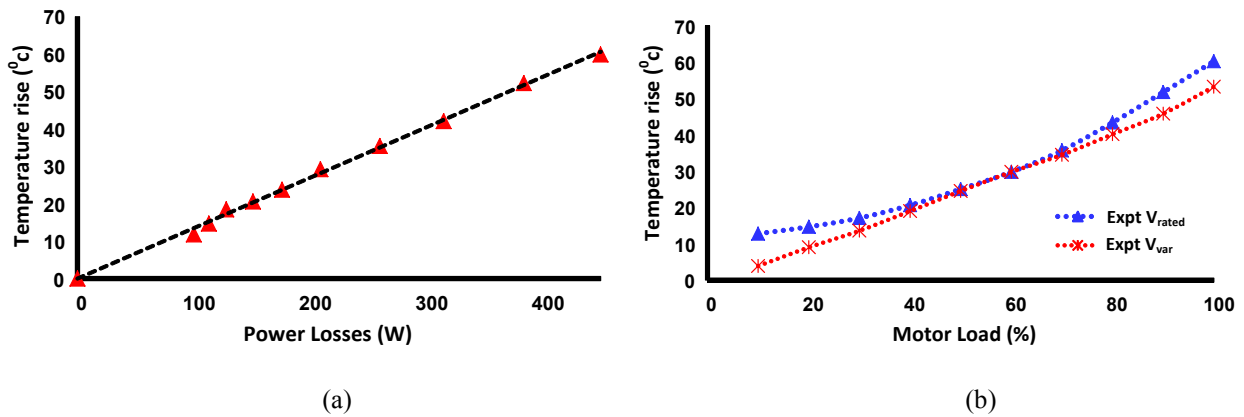


Fig. 6-10. Motor stator temperature rise dependence on losses; (a) stator temperature as a function of motor losses ($V_{Lm}=230$ V), (b) temperature rise comparison between rated and variable motor voltage

6.5.5 DC Voltage Reduction

The average H-bridge dc capacitor voltage can be predicted using equations (2-5) and (2-6) and illustrated in Fig. 6-2(b) via observing V_b . Relatively close agreements between predicted and experimentally measured values were obtained, see Fig. 6-11. The variable voltage control produces a relatively constant H-bridge capacitor dc voltage over the full motor load range, whereas the rated voltage control results in a wide variation, increasing with decreasing load. The latter characteristics is caused by the motor power factor decreasing with the motor load, see Figs. 6-2(a), (b) and 6-4(d). Variable voltage control has a relatively constant bridge dc voltage because the motor load power factor is fairly constant as the load changes. The lower bridge dc

voltage is advantageous as it produces lower stress on the power electronics and decreases its losses.

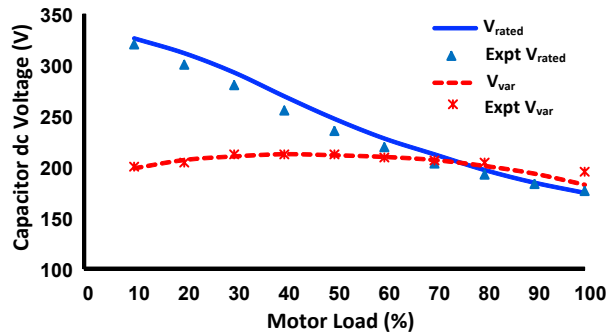


Fig. 6-11. Comparison of dc capacitor voltage

This result in Fig. 6-12 signifies that variable voltage motor control results in a constant voltage stress for the power electronics which is more desirable. Same voltage stress over a full load range allows lower rated device to be used. On the contrary, rated voltage operation results in a variable dc voltage stress (undesirable) in the capacitor. A transient response of the controller is demonstrated in Fig. 6-12. The load is being changed from 70% to 50% and back to 70% again. Despite the current envelopes change, DC capacitor voltage remains almost constant.

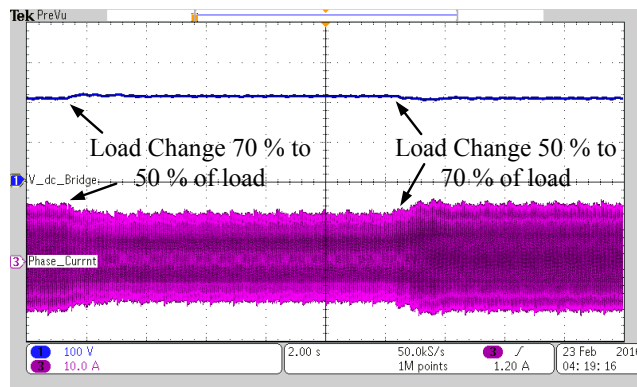


Fig. 6-12. Transient operation of the system

6.5.6 Power Electronics Performance

The power electronics losses were also monitored for this work. The total power losses in the power semiconductors are composed of switching losses and conduction losses. In this chapter, total loss of the power electronics including both switching loss and conduction loss is

calculated. It can be seen from Fig. 6-13 that the variable voltage operation produce lower losses and higher efficiency compare to rated voltage operation.

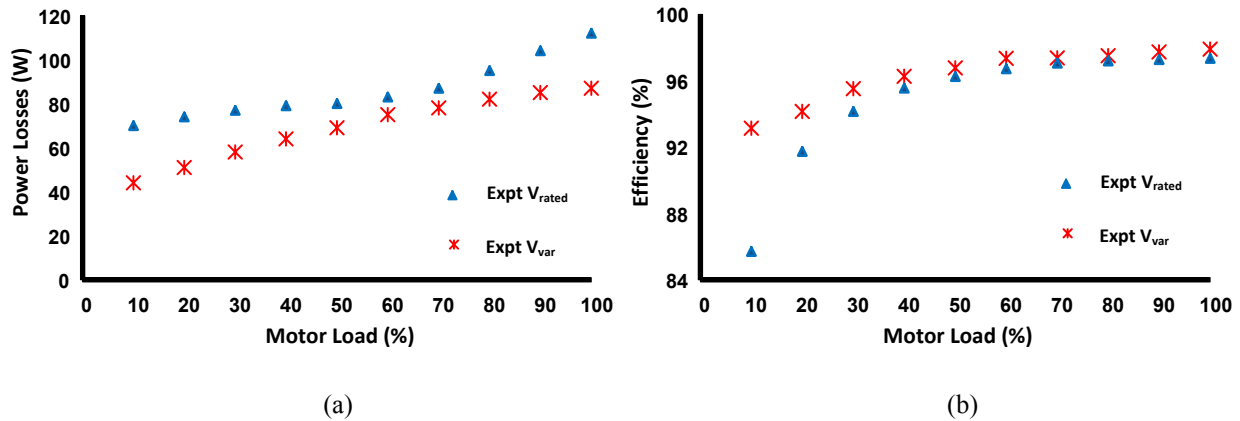


Fig. 6-13. Experimental; (a) H-bridge losses, (b) efficiency comparison

The cost of the power electronics can be closely linked to the cooling requirements for the system. Results in Fig. 6-13 show variable motor voltage control of the proposed H-bridge system can reduce losses in the power electronics by up to 31% and thus reducing the cost related to cooling requirements.

6.6 Conclusions

The performance of a 3-phase H-bridge system using floating dc capacitors is presented for controlling the voltage supplied to an induction motor under a wide range of steady-state load conditions. A variable voltage control is described that is based upon maximizing the motor operating efficiency, hence improving its reliability and lifetime expectancy: the motor voltage is made proportional to the square root of the measured motor input power. The controller was implemented using input parameters based upon readily available machine data, such as the motor performance at 75% output power, and corresponding to the maximum known motor efficiency condition without having to use more detailed motor modelling. The proposed variable voltage control produced:

- high motor power conversion efficiency over a wide load range. Higher efficiency improvement is achieved under light load condition compare to full load condition.

- reduced power losses and lower rms currents. With variable voltage control the motor power rating can be increased by 7% as a result of the lower losses experienced at high power levels.
- reduced temperature rise in the stator winding. Comparing variable voltage with rated voltage control, the motor temperature was reduced by 7.5 °C at the motor rated output power, and 10 °C lower under light load. Thus 75% increases in life time expectancy of stator winding while running the motor under rated condition.
- reduced electrical stress on power electronics. The variable voltage controller results in the H-bridge dc voltages to be relatively constant as the load changes at much lower levels than obtained when operating under rated voltage. This reduces the electrical stresses on the power electronics and improves their reliability and lifetime expectancy.
- constant motor speed. The machine speed was shown to be relatively constant over a wide load range around 1775 rpm.
- lastly, leading power factor to grid. The system naturally produces a leading grid power factor, hence generates VARs in to the grid.

For applications where frequency control is not required, the proposed 3-phase H-bridge system is a viable reliable cost effective alternative.

Chapter 7

7 Conclusion

The 3-phase floating H-bridge topology proves a simple and viable cost effective solution to motor voltage control. The power electronics can be used as a series voltage compensator to reduce start up transients or to improve steady state performance of an induction motor. The work described in this thesis is summarized with some concluding remarks. Some noteworthy suggestions for future extensions of the work are presented on system dynamic performance.

7.1 Summary

Power electronic converters can be acknowledged as the heart of modern power systems, especially with the development of renewable energy concepts. Inverters with lower losses are a key component in this regard. However, the resulting solutions should be low-cost and practicable to be thought of as acceptable solutions; e.g. without unnecessarily complex design needs.

This work presents a floating 3-phase H-bridge system that can inject a fundamental voltage in series with the grid voltage by using PWM switching. The voltage supplied to the motor is controlled, hence directly controlling the motor current and input power during starting. Comparing to a dynamic voltage restorer, the proposed system can inject series voltage with grid without a transformer and can maintain rated voltage during grid voltage sag. So the proposed system is cost effective and is able to perform stable voltage control with change in load condition. The motor voltage control is achieved by changing α ; increase α with increasing V_m and decrease α with decreasing V_m . Also as the system is slow in nature and the system is stable under the worst transient condition, the starting condition. So, there is no requirement for the dynamic equation of the controller and can be used fixed modulation index.

Similar to the BTB, this system employs 12 switches, however, the system is deemed desirable primarily because of the absence of input and output ac filter inductors and a much

lower dc link operating voltage. The variable voltage controller in the 3-phase H-bridge converter produces relatively constant and low capacitor dc voltage as the load changes, constant 325 V for VFD and 200 V for the proposed system. If variable voltage control is used during soft start and higher efficiency operation lower voltage value capacitor can be used. This is more cost effective and produces lower semiconductor losses and device electrical stress; hence the cooling requirements for the power electronics can be reduced. The overall system operating efficiency can be increased as a result with a higher power density.

Moreover, the proposed system can supply five level motor line pwm waveforms to the induction motor. This voltage compares with 3-level in a BTB system with much larger voltage steps and higher dV/dt stress on the motor. The pwm voltage steps in the system steps less than half that of the BTB or VFD (170 V for proposed system compare to 325 V for VFD for 230 V system under rated condition) and the motor induced average volt-secs (closely linked to iron losses in the motor) is much lower.

The motor voltage pwm frequencies are up to four times the device switching frequency as compared to double for the BTB converter; hence the motor current ripple is much lower with an associated lowering of the motor high frequency Cu losses; contrasting with the low frequency harmonics experienced in the MERS system [88]. The 3-phase H-bridge output pwm voltage waveforms can be said to be friendlier for motor cable connection and for the motor winding insulation. The system also has advantage over an open winding machine [66], because it is compatible with standard power distribution practices and therefore has potential in retrofit applications.

A flexible and stable soft start under different load conditions are examined and clearly demonstrate that bridge capacitor dc voltages can be predicted before motor start and thus ensure a safety feature of the proposed system. The system can provide flexible soft start solutions under variety of load conditions. The inrush current of the motor can be reduced to 63% compare to direct online starting. The proposed system can operate leading instead of lagging power factor and thus generate VAR instead of consumption and reactive power generation almost remains constant despite load variations.

Theoretically maximum sag compensations are established and experimentally verified. Voltage sag ride through capability directly related to motor power factor. Under rated voltage

operation, the lowest sag tolerance happens when the motor is fully loaded or the power factor is maximum. Even under rated load conditions, voltages sags of up to 18 % can be compensated continuously and under lower load condition this compensation reaches to 80%.

The experimental performance of the power electronics, motor and total system is also presented with respect to power losses, system efficiency and the motor output power. The proposed system is demonstrated to have a higher performance over the VFD. 43% lower losses are observed in the 3-phase H-bridge compare to VFD. An improved motor performance over the direct grid connection can even be achieved when the grid voltage is not the same as the motor rated voltage.

Variable motor voltage control can lower or increase the motor voltage relative to the grid and hence can be used to lower the machine losses over its entire load range. Motor losses and temperature rises in the stator winding show linear relationship and also the proposed system can increase stator lifetime expectancy by 75%. The motor voltage can be controlled with readily available motor name plate data and the proposed voltage control produced high motor power conversion efficiency over a wide load range, together with reduced power losses and lower rms currents.

It should be mentioned the proposed system cannot change the supply frequency of the voltage supplied to induction motor, thus cannot access the full torque-speed plane. The solution is only intended to be used in applications where fixed frequency control is not required, such as medium voltage (MV) motors used to drive fans, pumps, compressors, and conveyors.

7.2 Future work

Determining the minimum dc capacitance value that can be feasibly used is a very important design guide for the future engineering implementation. So, preparing a guideline for the minimum feasible capacitor size that can be used based upon the voltage, power, frequency and current ratings of the system is important. So, minimum capacitance requirement together with unbalance capacitance effects must be investigated together.

VFDs can operate the motor lower than the rated voltage so, maximum efficiency throughout the load range is not possible if the VFD is supplied from rated voltage. Since a dual inverter drive system can boost the motor voltage, neglecting saturation, proper investigation

must be carried out to operate the motor with higher efficiency using a dual inverter drive. Maximum efficiency is closely linked to a fixed motor impedance or slip. Operating the motor at maximum efficiency, results in a fixed speed droop. So speed control of the induction motor is possible without speed feedback, but this feature requires further investigation.

Grid connected modular H-bridge configuration can be viable solution in a medium voltage system. Modular structure can reduce the voltage rating of the power electronics but keep the current ratings same. So, modular or cascade H-bridge configuration can be studied for further investigation.

Voltage sag tolerance, symmetrical voltage drop of the proposed system is presented in the thesis. But unbalanced condition is not analyzed and also more detailed capacitor voltage control can be investigate to operate the H bridge under severe voltage sag condition. As an H-bridge is series connected with the grid, any unbalance in grid will contribute to unbalance in motor voltage and thus increase stator current, ripple voltage, reduce motor efficiency and increase motor losses. But with a VFD the effect may be more severe; the ac line current wave shape will become more single pulse shape-higher peak current. Increased line current flows through the diodes and associated capacitors of the rectifier, increasing the ripple voltage, reactive power and stress on these components. Moreover VFD may trip due over current and under voltage without showing any immediate and obvious fault. So proper investigation can show which topology is more robust under voltage imbalance and further research should be carried to focus this problem.

7.3 Concluding remark

This thesis explored the application of a 3-phase H-bridge converter in low voltage motor system. The series voltage injection with the grid manipulates the motor terminal voltage and improves the motor performance. The systems can soft-start the motor, tolerate symmetrical voltage sags and improve the motor efficiency using relatively simple control algorithms. Where frequency control is not required, this configuration can improve the overall system performance. Therefore, it is hoped this thesis contributed to improving performance of certain low voltage applications with minimal appreciable cost.

Bibliography

- [1] Stephen Chapman, *Electric Machinery Fundamentals*, 4th Edition, McGraw-Hill Science/Engineering/Math; 4 edition (Jan. 7, 2004)
- [2] Bimal K. Bose, *Modern Power Electronics and AC Drives*, Prentice Hall; 1 edition (Oct. 12, 2001)
- [3] Paul C. Krause , Oleg Wasynczuk , Scott D. Sudhoff, *Analysis of Electric Machinery and Drive Systems*, Wiley-IEEE Press; 2 edition (March 5, 2002)
- [4] F. Abrahamsen, F. Blaabjerg, J. K. Pedersen, P. Z. Grabowski and P. Thogersen, "On the energy optimized control of standard and high-efficiency induction motors in CT and HVAC applications," in *IEEE Transactions on Industry Applications*, vol. 34, no. 4, pp. 822-831, Jul/Aug 1998.
- [5] P. K. Choudhary and S. P. Dubey, "Efficiency optimization of induction motor drive in steady-state using Artificial Neural Network," *2016 International Conference on Computation of Power, Energy Information and Commuincation (ICCPEIC)*, Melmaruvathur,Chennai, India, 2016, pp. 295-302.
- [6] Z. Maljkovic, M. Cettolo and M. Pavlica, "The impact of the induction motor on short-circuit current," in *IEEE Industry Applications Magazine*, vol. 7, no. 4, pp. 11-17, Jul/Aug 2001.
- [7] N. Kumar, T. R. Chelliah and S. P. Srivastava, "Adaptive control schemes for improving dynamic performance of efficiency-optimized induction motor drives," *ISA Transactions*, vol. 57, pp. 301-310,2014.
- [8] C. Chakraborty and Y. Hori, "Fast efficiency optimization techniques for the indirect vector-controlled induction motor drives," in *IEEE Transactions on Industry Applications*, vol. 39, no. 4, pp. 1070-1076, July-Aug. 2003.
- [9] F. J. T. E. Ferreira; G. Baoming; A. T. de Almeida, "Reliability and Operation of High-Efficiency Induction Motors," in *IEEE Transactions on Industry Applications* , vol.PP, no.99, pp.1-1
- [10] M. K. Yoon, C. S. Jeon and S. K. Kauh, "Efficiency increase of an induction motor by improving cooling performance," in *IEEE Transactions on Energy Conversion*, vol. 17, no. 1, pp. 1-6, Mar 2002.
- [11] d e Almeida, A ; Ferreira, F.]. T. E.; Duarte, A : "Technical and Economical Considerations on Super High-Efficiency Three-Phase Motors" , *IEEE Trans. on Industry Applications*, Vol. 50, No . 2 , pp. I 274-1 2S5, 2 0 1 4 .
- [12] S. Lie and C. Di Pietro, "Copper die-cast rotor efficiency improvement and economic consideration," in *IEEE Transactions on Energy Conversion*, vol. 10, no. 3, pp. 419-424, Sep 1995.
- [13] D. T. Peters, E. F. Brush and J. L. Kirtley, "Die-cast copper rotors as strategy for improving induction motor efficiency," *2007 Electrical Insulation Conference and Electrical Manufacturing Expo*, Nashville, TN, 2007, pp. 322-327.

- [14] P. Pillay, V. Levin, P. Otaduy and J. Kueck, "In-situ induction motor efficiency determination using the genetic algorithm," in *IEEE Transactions on Energy Conversion*, vol. 13, no. 4, pp. 326-333
- [15] M.H. Rashid, *Power Electronics Handbook*, Burlington, MA: Elsevier, 2007
- [16] Surya Santoso; H. Wayne Beaty; Roger C. Dugan; Mark F. McGranaghan, *Electrical Power Systems Quality*, published by McGraw Hill, ISBN: 0-07-138622-X, 528 pages, 2003
- [17] Kay, J., Paes, R., Seggewiss, J., & Ellis, R. (1999). Methods for the control of large medium-voltage motors: application considerations and guidelines. *IEEE Transactions on Industry Applications*, 36 (6), 1688--1696.
- [18] M. J. Melfi and S. D. Umans, "Squirrel-Cage Induction Motors: Understanding Starting Transients," in *IEEE Industry Applications Magazine*, vol. 18, no. 6, pp. 28-36, Nov.-Dec. 2012.
- [19] Norman, "Starting characteristics and control of polyphase squirrel-cage induction motors," in *Journal of the A.I.E.E.*, vol. 45, no. 10, pp. 1003-1006, Oct. 1926.
- [20] A. J. Williams and M. S. Griffith, "Evaluating the Effects of Motor Starting on Industrial and Commercial Power Systems," in *IEEE Transactions on Industry Applications*, vol. IA-14, no. 4, pp. 292-305, July 1978.
- [21] A. H. Bonnett, "Analysis of Winding Failures in Three-Phase Squirrel Cage Induction Motors," in *IEEE Transactions on Industry Applications*, vol. IA-14, no. 3, pp. 223-226, May 1978
- [22] P. J. Collieran and W. E. Rogers, "Controlled Starting of AC Induction Motors," in *IEEE Transactions on Industry Applications*, vol. IA-19, no. 6, pp. 1014-1018, Nov. 1983.
- [23] R.F. McElveen;M.K. Toney, Starting High-Inertia Loads, *IEEE Transactions on Industry Applications*, Volume: 37, Issue: 1, pp. 137-144, 2001
- [24] G. Zenginobuz, I. Cadirci, M. Ermis and C. Barlak, "Performance optimization of induction motors during Voltage-controlled soft starting," in *IEEE Transactions on Energy Conversion*, vol. 19, no. 2, pp. 278-288, June 2004.
- [25] W. S. Wood, F. Flynn, and A. Shanmugasundaram, "Transient torques in induction motors due to switching of the supply," *Proc. Inst. Elect. Eng.*, vol. 112, no. 7, pp. 1348–1354, July 1965.
- [26] R. H. Daugherty, "Analysis of transient electrical torques and shaft torques in induction motors as a result of power supply disturbances," *IEEE Power App. Syst.*, vol. PAS-101, pp. 2826–2836, Aug. 1982.
- [27] A. A. Shaltout, "Analysis of torsional torques in starting of large squirrel cage induction motors," *IEEE Trans. Energy Conversion*, vol. 9, pp. 135–141, Mar. 1994.
- [28] F. M. Bruce, R. J. Graefe, A. Lutz and M. D. Panlener, "Reduced-Voltage Starting of Squirrel-Cage Induction Motors," in *IEEE Transactions on Industry Applications*, vol. IA-20, no. 1, pp. 46-55, Jan. 1984

- [29] X. Liang and O. Ilochonwu, "Induction Motor Starting in Practical Industrial Applications," in *IEEE Transactions on Industry Applications*, vol. 47, no. 1, pp. 271-280, Jan.-Feb. 2011
- [30] Massimo Ceraolo, Davide Poli "Fundamentals of Electric Power Engineering: From Electromagnetics to Power Systems" April 2014, Wiley-IEEE Press ISBN: 978-1-118-67969-2
- [31] P. Pillay, "Applying energy-efficient motors in the petrochemical industry," *IEEE Industry Appl. Magazine*, vol. 3 issue 1, pp. 32-40, 1997
- [32] E. B. Agamloh, "The Partial-Load Efficiency of Induction Motors" *Industrial Appl. IEEE Transaction on*, vol. 45, no.1, pp. 332-340, 2009.
- [33] S. N. Vukosavic and E. Levi, "Robust dsp-based efficiency optimization of a variable speed induction motor drive," *IEEE transaction on Industrial ElectroniCS*, vol. 50, no. 3, pp. 560-570, June 2003.
- [34] "Premium efficiency motor selection and application guide a handbook for industry" advanced manufacturing office, US department of energy.
- [35] J. Appelbaum, I. A. Khan, E. F. Fuchs and J. C. White, "Optimization of Three-Phase Induction Motor Design Part II: The Efficiency and Cost of an Optimal Design," in *IEEE Transactions on Energy Conversion*, vol. EC-2, no. 3, pp. 415-422, Sept. 1987.
- [36] B. Lu, D. B. Durocher and P. Stemper, "Predictive maintenance techniques," in *IEEE Industry Applications Magazine*, vol. 15, no. 6, pp. 52-60, November-December 2009
- [37] M. Zucker and J. J. Erhart, "Capacitors Near Loads? The Engineering Viewpoint," in *IEEE Transactions on Industry Applications*, vol. IA-21, no. 2, pp. 308-317, March 1985.
- [38] Y. Yao, A. Cosic and C. Sadarangani, "Power Factor Improvement and Dynamic Performance of an Induction Machine With a Novel Concept of a Converter-Fed Rotor," in *IEEE Transactions on Energy Conversion*, vol. 31, no. 2, pp. 769-775, June 2016.
- [39] M. Ermis, Z. Cakir, I. Cadirci, G. Zenginobuz and H. Tezcan, "Self-excitation of induction motors compensated by permanently connected capacitors and recommendations for IEEE std 141-1993," in *IEEE Transactions on Industry Applications*, vol. 39, no. 2, pp. 313-324, Mar/Apr 2003.
- [40] D. F. Miller, "Application Guide for Shunt Capacitors on Industrial Distribution Systems at Medium Voltage Levels," in *IEEE Transactions on Industry Applications*, vol. IA-12, no. 5, pp. 444-459, Sept. 1976.
- [41] E. Muljadi, T. A. Lipo and D. W. Novotny, "Power factor enhancement of induction machines by means of solid-state excitation," in *IEEE Transactions on Power Electronics*, vol. 4, no. 4, pp. 409-418, Oct 1989.
- [42] F. J. T. E. Ferreira and A. T. de Almeida, "Novel Multiflux Level, Three-Phase, Squirrel-Cage Induction Motor for Efficiency and Power Factor Maximization," in *IEEE Transactions on Energy Conversion*, vol. 23, no. 1, pp. 101-109, March 2008.

- [43] Larabee, J., Pellegrino, B., & Flick, B. (2005). Induction motor starting methods and issues. *Petroleum and Chemical Industry Conference, 2005. Industry Applications Society 52nd Annual* , 217--222.
- [44] G. Zenginobuz, I. Cadirci, M. Ermis and C. Barlak, "Performance optimization of induction motors during Voltage-controlled soft starting," in *IEEE Transactions on Energy Conversion*, vol. 19, no. 2, pp. 278-288, June 2004.
- [45] T. W. Jian, N. L. Schmitz and D. W. Novotny, "Characteristic Induction Motor Slip Values for Variable Voltage Part Load Performances Optimization," in *IEEE Transactions on Power Apparatus and Systems*, vol. PAS-102, no. 1, pp. 38-46, Jan. 1983.
- [46] N. Mohan, "Improvement in Energy Efficiency of Induction Motors by Means of Voltage Control," in *IEEE Transactions on Power Apparatus and Systems*, vol. PAS-99, no. 4, pp. 1466-1471, July 1980.
- [47] C. K. Duffey and R. P. Stratford, "Update of harmonic standard IEEE-519: IEEE recommended practices and requirements for harmonic control in electric power systems," *Industrial Applications, IEEE Transaction on*. vol. 25, pp. 1025–1034, Nov./Dec. 1989.
- [48] A. Gastli; M.M. Ahmed, ANN-Based Soft Starting of Voltage-Controlled-Fed IM Drive System, *IEEE Transactions on Energy Conversion*, Volume: 20, Issue: 3, pp. 497-503, 2005.
- [49] H.S. Rajamani and R.A. McMahon, "Induction motor drives for domestic appliances", *IEEE Transactions on Industrial Applications*, vol. 3, no. 3, pp. 21-26, 1997
- [50] D.W. Novotny and T.A. Lipo, *Vector Control and Dynamics of AC Drives*, 1997.
- [51] J. Holtz, "Pulsewidth modulation-A survey", *IEEE Trans. Ind. Electron*, vol. 39, no. 5, pp. 410-420, 1992
- [52] E.R.C. Da Silva, E.C. Dos Santos Jr. and C.B.O. Jacobina, "Pulse width modulation strategies", *IEEE Ind. Electronics Magazine*, pp. 37-45, 2011.
- [53] D. Nguyen, J. Hobraiche, N. Patin, G. Friedrich and J.-P. Vilain, "A direct digital technique implementation of general discontinuous pulse width modulation strategy", *IEEE Trans. on Ind. Electronics*, vol. 58, no. 9, pp. 4445-4454, 2011
- [54] B. Karanayil, M.F. Rahman and C. Grantham, "Online stator and rotor resistance estimation scheme using artificial neural networks for vector controlled speed sensor less induction motor drive", *IEEE Transactions on Industrial Electronics*, vol. 54, no. 1, 2007.
- [55] J.K. Kang and S.K. Sul, "New direct torque control of induction motor for minimum torque ripple and constant switching frequency", *IEEE Transactions on Industrial Applications*, vol. 35, pp. 1076-1082, 1999.
- [56] A.B. Jidin, N.R.B.N. Idris, A.H.B.M. Yatim, M.E. Elbuluk and T. Sutikno, "A wide-speed high torque capability utilizing overmodulation strategy in dtc of induction machines with constant switching frequency controller", *IEEE Transactions on Power Electronics*, vol. 27, no. 5, pp. 2566-2575, 2012.

- [57] J. Titus, J. Teja, K. Hatua and K. Vasudevan, "An Improved Scheme for Extended Power Loss Ride-Through in a Voltage-Source-Inverter-Fed Vector-Controlled Induction Motor Drive Using a Loss Minimization Technique," in IEEE Transactions on Industry Applications, vol. 52, no. 2, pp. 1500-1508, March-April 2016.
- [58] F. J. T. E. Ferreira, A. T. de Almeida, J. F. S. Carvalho and M. V. Cistelecan, "Experiments to observe the impact of power quality and voltage-source inverters on the temperature of three-phase cage induction motors using an infra-red camera," Electric Machines and Drives Conference, 2009. IEMDC '09. IEEE International, Miami, FL, 2009, pp. 1311-1318.
- [59] S.Z. Djokic; K. Stockman; J.V. Milanovic; J.J.M. Desmet; R. Belmans, Sensitivity of AC adjustable speed drives to voltage sags and short interruptions, IEEE Transactions on Power Delivery, Volume: 20, Issue: 1, pp. 494-505, 2005
- [60] Giannoutsos, S.V.; Manias, S.N. "A Systematic Power-Quality Assessment and Harmonic Filter Design Methodology for Variable-Frequency Drive Application in Marine Vessels" IEEE Transactions on Industry Applications, Volume: 51, Issue: 2, pp. 1909-1919, 2015.
- [61] Cuzner, R.; Drews, D.; Venkataramanan, G, "Power Density and Efficiency Comparisons of System-Compatible Drive Topologies", IEEE Trans. on Industry Applications, Volume: 51, Issue: 1, pp. 459-469, 2015.
- [62] E. Wemekinck, A. Kawamura, and R. Hoft, "A high frequency ac/dc converter with unity power factor and minimum harmonic distortion," in Proc. 7th IEEE PESC, 1987, pp. 264–270.
- [63] Reznik, A.; Simoes, M.G.; Al-Durra, A.; Muyeen, S.M. "LCL Filter Design and Performance Analysis for Grid-Interconnected Systems" IEEE Trans. on Industry Applications, Volume: 50, Issue: 2, pp. 1225-1232, 2014.
- [64] H. Stemmler and P. Guggenbach, "Configurations of high-power voltage source inverter drives", Proc. IEEE EPE Conf., vol. 5, pp. 7-14.
- [65] P. P. Rajeevan, K. Sivakumar, K. Gopakumar, C. Patel and H. Abu-Rub, "A Nine-Level Inverter Topology for Medium-Voltage Induction Motor Drive With Open-End Stator Winding," in IEEE Transactions on Industrial Electronics, vol. 60, no. 9, pp. 3627-3636, Sept. 2013.
- [66] B. A. Welcho, "A double-ended inverter-system for the combined propulsion and energy management functions in hybrid vehicles with energy storage", 31st Annual Conference of IEEE Industrial Electronics Society, 2005. IECON 2005
- [67] J. Kim; J. Jung; K. Nam, "Dual inverter control strategy for high speed operation of EV Induction motors," IEEE Trans on Ind. Electron. vol. 51, no. 2, pages 312-330, April 2004
- [68] E.G Shivakumar, V.T Somasekhar, Krushna K Mohapatro, K Gopakumar, L Umanand "A multi-level space phasor based PWM strategy for an open end winding induction motor drive using two inverters with different DC link voltage" Proceedings of 4th IEEE International Conference on Power Electronics and Drive Systems, volume 1, Page(s): 169 - 175 2001

- [69] J Ewanchuk, John Salmon, Chris Chapelsky “ A method for supply voltage boosting in an open ended induction machine using a dual inverter system with a floating capacitor bridge” submitted and accepted for publication, IEEE Trans on Energy Conversion
- [70] Mu shin Kwak; Seung-ki sul “Control of an open winding machine in a grid connected distributed generation system” IEEE Trans on Industry Applications, vol 44, no. 4,pages 1259-1267 July/August 2008,
- [71] M. Amin, "North American electricity infrastructure: System security quality reliability availability and efficiency: Challenges and their societal impacts", Continuing Crises in National Transmission Infrastructure: Impacts and Options for Modernization.
- [72] Gyugyi, L.; , "Power electronics in electric utilities: static VAR compensators ," Proceedings of the IEEE , vol.76, no.4, pp.483-494, Apr 1988
- [73] Urbanek, J.; Piwko, R.J.; Larsen, E.V.; Damsky, B.L.; Furumasu, B.C.; Mittlestadt, W.; Eden, J.D.; , "Thyristor controlled series compensation prototype installation at the Slatt 500 kV substation," Power Delivery, IEEE Transactions on , vol.8, no.3, pp.1460-1469, Jul 1993
- [74] Gyugyi, L.; Schauder, C.D.; Sen, K.K.; , "Static synchronous series compensator: a solid-state approach to the series compensation of transmission lines," Power Delivery, IEEE Transactions on , vol.12, no.1, pp.406-417, Jan 1997
- [75] S. Yang, Y. Liu, X. Wang, D. Gunasekaran, U. Karki and F. Z. Peng, "Modulation and Control of Transformerless UPFC," in IEEE Transactions on Power Electronics, vol. 31, no. 2, pp. 1050-1063, Feb. 2016.
- [76] C. A. Silva, L. A. Cordova, P. Lezana and L. Empringham, "Implementation and Control of a Hybrid Multilevel Converter With Floating DC Links for Current Waveform Improvement," in IEEE Transactions on Industrial Electronics, vol. 58, no. 6, pp. 2304-2312, June 2011.
- [77] Malinowski, M.; Gopakumar, K.; Rodriguez, J.; Pérez, M.A.; , "A Survey on Cascaded Multilevel Inverters," Industrial Electronics, IEEE Transactions on , vol.57, no.7, pp.2197-2206, July 2010
- [78] A. Nabae, I. Takahashi, and H. Akagi, “A new neutral-point clamped PWM inverter,” IEEE Trans. Ind. Applicat., vol. IA-17, pp. 518–523, Sept./Oct. 1981.
- [79] T. Meynard, H. Foch, P. Thomas, J. Courault, R. Jakob, and M. Nahrstaedt, “Multicell converters: Basic concepts and industry applications,” IEEE Trans. Ind. Electron., vol. 49, no. 5, pp. 955–964, Oct. 2002.
- [80] P. Hammond, “A new approach to enhance power quality for medium voltage ac drives,” IEEE Trans. Ind. Appl., vol. 33, no. 1, pp. 202–208, Jan./Feb. 1997.
- [81] H. Akagi, "Classification, Terminology, and Application of the Modular Multilevel Cascade Converter (MMCC)," in IEEE Transactions on Power Electronics, vol. 26, no. 11, pp. 3119-3130, Nov. 2011.
- [82] J. Dixon, A. A. Breton, F. E. Rios, J. Rodriguez, J. Pontt, and M. A. Perez, “High-power machine drive, using non redundant 27-level inverters and active front end rectifiers,” IEEE Trans. Power Electron., vol. 22, no. 6, pp. 2527–2533, Nov. 2007.

- [83] Tolbert, L.A.; Fang Zheng Peng; Cunyngham, T.; Chiasson, J.N.; , "Charge balance control schemes for cascade multilevel converter in hybrid electric vehicles," *Industrial Electronics, IEEE Transactions on* , vol.49, no.5, pp. 1058- 1064, Oct 2002
- [84] M. Veenstra and A. Rufer, "Control of a hybrid asymmetric multilevel inverter for competitive medium-voltage industrial drives", *IEEE Trans. Ind. Appl.*, vol. 41, no. 2, pp. 655-664, Mar./Apr. 2005.
- [85] P. Steimer and M. Manjrekar, "Practical medium voltage converter topologies for high power applications", *Conf. Rec. IEEE IAS Annu. Meeting*, pp. 1723-1730.
- [86] T. Gopalathnam, M. Manjrekar and P. Steimer, "Investigations on a unified controller for a practical hybrid multilevel power converter", *Proc. IEEE APEC*, pp. 1024-1030.
- [87] Wiik, J.A.; Wijaya, F.D.; Shimada, R., "Characteristics of the Magnetic Energy Recovery Switch (MERS) as a Series FACTS Controller," in *Power Delivery, IEEE Transactions on* , vol.24, no.2, pp.828-836, April 2009
- [88] Danang Wijaya, F.; Kusumawan, S.A.; Prabowo, H., "Reducing induction motor starting current using magnetic energy recovery switch (MERS)," in *Information Technology and Electrical Engineering (ICITEE), 2014 6th International Conference on* , vol., no., pp.1-6, 7-8 Oct. 2014
- [89] T. Isobe; J. A. Wiik; F.D. Wijaya; K. Inoue; K. Usuki; T. Kitahara; R. Shimada, "Improved Performance of Induction Motor Using Magnetic Energy Recovery Switch" *Power Conversion Conference - Nagoya, 2007*. pp. 919-924, 2007.
- [90] S. Leng, R. Ul Haque, N. Perera, A. Knight, J. Salmon, "Voltage Control of Grid Connected Induction Motors using Floating Capacitor H-bridge Converters", *7th IET international conference on Power Electronics, Machines and Drives, Manchester, UK, April, 2014*.
- [91] S. Leng, R. Ul Haque, N. Perera, A. Knight, J. Salmon, "Soft Start of Induction Motors using Floating Capacitor H-bridge Converters", *7th IET international conference on Power Electronics, Machines and Drives, , Manchester, UK, April, 2014*.
- [92] J.A. Kay; R.H. Paes; J.G. Seggewiss; R.G. Ellis, *Methods for the control of large medium-voltage motors: application considerations and guidelines, IEEE Transactions on Industry Applications*, Volume: 36, Issue: 6, pp. 1688-1696, 2000.
- [93] *IEEE guide for the presentation of thermal limit curves for squirrel cage induction machines, IEEE Standard 620-1996, August 1*
- [94] S. L. Capitaneanu; B. de Fornel; M. Fadel; J. Faucher; A. Almeida, "Graphical and Algebraic Synthesis for PWM Methods", *EPE Journal Vol. 11 No.3 – August, 2001*.
- [95] B. Wu, *High-Power Converters and AC Drives*, chapter 7, March, 2006 Wiley-IEEE Press.
- [96] S. L. Capitaneanu; B. de Fornel; M. Fadel; J. Faucher; A. Almeida, "Graphical and Algebraic Synthesis for PWM Methods", *EPE Journal Vol. 11 No.3 – August, 2001*.

- [97] Y. He, Y. Wang, Y. Feng, and Z. Wang, "Parameter identification of an induction machine at standstill using the vector constructing method," *IEEE Trans. Power Electron.*, vol. 27, no. 2, pp. 905–915, Feb. 2012.
- [99] J.C. Gomez; M.M. Morcos; C.A. Reineri; G.N. Campetelli; Behavior of induction motor due to voltage sags and short interruptions, *IEEE Transactions on Power Delivery*, Volume: 17, Issue: 2, pp. 434-440, 2002.
- [100] E. W. Gunther and H. Mehta, "A survey of distribution system power quality—Preliminary results," *IEEE Trans. Power Delivery*, vol. 10, pp. 322–329, Jan. 1995
- [101] F. Carlson, "Before and during voltage sags: the relationship between the voltages and the tripping level for line-operated machines," *IEEE Industry Applications Magazine*, Mar/Apr 2005.
- [102] Hector G. Sarmiento, and Eduardo Estrada, "A Voltage Sag Study in an industry with Adjustable Speed Drives", *IEEE Industry Applications Magazine*, January/February 1996, Page(s): 16-19.
- [103] Holtz, J.; Lotzkat, W.; Stadtfeld, S., "Controlled AC drives with ride-through capability at power interruption," in *Industry Applications*, *IEEE Transactions on* , vol.30, no.5, pp.1275-1283, Sep/Oct 1994
- [104] P. Angers; F. Levesque; Voltage dip immunity of PWM drives with ride-through capabilities, *International Conference on Electrical Machines (ICEM)*, pp. 1-5, 2010.
- [105] Po-Tai Cheng; Chian-Chung Huang; Chun-Chiang Pan; Bhattacharya, S., "Design and implementation of a series voltage sag compensator under practical utility conditions," in *Industry Applications*, *IEEE Transactions on* , vol.39, no.3, pp.844-853, May-June 200
- [106] Yu-Hsing Chen; Chang-Yi Lin; Jhao-Ming Chen; Po-Tai Cheng, "An Inrush Mitigation Technique of Load Transformers for the Series Voltage Sag Compensator," in *Power Electronics*, *IEEE Transactions on* , vol.25, no.8, p2211-2221, Aug. 2010
- [107] Fatu, M.; Blaabjerg, F.; Boldea, I., "Grid to Standalone Transition Motion-Sensorless Dual-Inverter Control of PMSG With Asymmetrical Grid Voltage Sags and Harmonics Filtering," in *Power Electronics*, *IEEE Transactions on* , vol.29, no.7, pp.3463-3472, July 2014
- [108] Miret, J.; Camacho, A.; Castilla, M.; García de Vicuña, J.L.; de la Hoz, J., "Reactive current injection protocol for low-power rating distributed generation sources under voltage sags," in *Power Electronics*, *IET* , vol.8, no.6, pp.879-886, 6 2015
- [109] Parkhideh, B.; Bhattacharya, S., "Vector-Controlled Voltage-Source-Converter-Based Transmission Under Grid Disturbances," in *Power Electronics*, *IEEE Transactions on* , vol.28, no.2, pp.661-672, Feb. 2013
- [110] Shaohua Li; Xiuli Wang; Zhiqing Yao; Tai Li; Zhong Peng, "Circulating Current Suppressing Strategy for MMC-HVDC Based on Nonideal Proportional Resonant Controllers Under Unbalanced Grid Conditions," in *Power Electronics*, *IEEE Transactions on* , vol.30, no.1, pp.387-397, Jan. 2015

- [111] Gazafrudi, S.M.M.; Tabakhpour Langerudy, A.; Fuchs, E.F.; Al-Haddad, K., "Power Quality Issues in Railway Electrification: A Comprehensive Perspective," in *Industrial Electronics, IEEE Transactions on* , vol.62, no.5, pp.3081-3090, May 2015
- [112] Sierra, R.; Alcalá, J.; Cardenas, V.; Perez-Ramirez, J.; Rivera, A., "Evaluating the performance of the BTB converter under unbalanced voltage sags," in *Electrical Engineering, Computing Science and Automatic Control (CCE), 2012 9th International Conference on* , vol., no., pp.1-6, 26-28 Sept. 2012
- [113] Castilla, M.; Miret, J.; Camacho, A.; Garcia de Vicuna, L.; Matas, J., "Modeling and Design of Voltage Support Control Schemes for Three-Phase Inverters Operating Under Unbalanced Grid Conditions," in *Power Electronics, IEEE Transactions on* , vol.29, no.11, pp.6139-6150, Nov. 2014
- [114] Xiaoqiang Guo; Wenzhao Liu; Xue Zhang; Xiaofeng Sun; Zhigang Lu; Guerrero, J.M., "Flexible Control Strategy for Grid-Connected Inverter Under Unbalanced Grid Faults Without PLL," in *Power Electronics, IEEE Transactions on* , vol.30, no.4, pp.1773-1778, April 2015
- [115] Muteba, M.C.; Jimoh, A.A.; Nicolae, D.V.; Ogunjuyigbe, A.S.O., "Performance evaluation of a three-phase induction machine with auxiliary winding fed by a leading reactive current," *Power and Energy Systems (AfricaPES) Sept.* pp.-8-10 2008.
- [116] Malik, N.; Sadarangani, C.; Cosic, A.; Lindmark, M., "Induction Machine at Unity Power Factor with Rotating Power Electronic Converter," *Power Electronics, Electrical Drives, Automation and Motion (SPEEDAM), June,* pp. 401-408, 2012.
- [117] A. Ukil; R. Bloch; A. Andenna, " Estimation of Induction Motor Operating Power Factor From Measured Current and Manufacturer Data", *IEEE Transactions on Energy Conversion*, vol.26, no.2, pp.669-706, 2011.
- [118] A.H. Bonnett, "An overview of how AC induction motor performance has been affected by the October 24, 1997 implementation of the Energy Policy Act of 1992", *Industry Applications, IEEE Transactions on*, vol.36, no.1, pp.242-256, 2000.
- [119] Linders, John R., "Effects of Power Supply Variations on AC Motor Characteristics," *Industry Applications, IEEE Transactions on* , vol.IA-8, no.4, pp.383,400, July 1972
- [120] *Rotating Electric Machines Part 2-1: Standard Methods for Determining Losses and Efficiency from Tests, IEC 60034-2-1, 2007.*
- [121] *Standard Test Procedure for Polyphase Induction Motors and Generators. IEEE Standard 112-2004.*
- [122] T. A. Jankowski; F. C. Prenger; D. D. Hill; S. R. O'Bryan; K. K. Sheth; E. B. Brookbank; D. F. A. Hunt; Y. A. Orrego, "Development and Validation of a Thermal Model for Electric Induction Motors", *Industry Electronics, IEEE Transactions on* volume 57, issue 12, pp . 4043-4054, 2010.
- [123] C. G. Nistor, "Analysis of noise and heating for three-phase induction motor fed by inverter" *Optimization of Electrical and Electronic Equipment (OPTIM), 2014 International Conference on*, pp. 389-396, 2014.

- [124] H. Li; R.S. Curiac, "Designing More Efficient Large Industrial Induction Motors by Utilizing the Advantages of Adjustable-Speed Drives" *Industrial Applications*, IEEE Transaction on. vol. 46, no.5, pp. 1805–1809, 2010.
- [125] A. H. Bonnett, "Reliability Comparison Between Standard and Energy Efficient Motors" *Industrial Applications*, IEEE Transaction on. vol. 33, no.1, pp. 135–142, 1997.
- [126] Boglietti, A.; Ferraris, P.; Lazzari, M.; Pastorelli, M., "Influence of the inverter characteristics on the iron losses in PWM inverter-fed induction motors," *Industry Applications*, IEEE Transactions on , vol.32, no.5, pp.1190,1194, Sep/Oct 1996
- [127] Swamy, M.; Shirabe, K.; Kang, J., "Power Loss, System Efficiency, and Leakage Current Comparison between Si IGBT VFD and SiC FET VFD With Various Filtering Options," *Industry Applications*, IEEE Transactions on , vol.PP, no.99, pp.1,1
- [128] Kirschen, D.S.; Novotny, D.W.; Lipo, T.A., "Optimal Efficiency Control of an Induction Motor Drive," in *Energy Conversion*, IEEE Transactions on , vol.EC-2, no.1, pp.70-76, March 1987
- [129] D. S. Kirschen , D. W. Novotny and W. Suwanwisoot , "Minimizing Induction Motor Losses by Excitation Control in Variable Frequency Drives" , IEEE Trans. on Ind. Appl. , vol. IA-20 , no. 5 , pp.1244 -1250 , 1984
- [130] V. Climente-Alarcon; J. A. Antonino-Daviu; E. G. Strangas; M. Riera-Guasp. " Rotor-Bar Breakage Mechanism and Prognosis in an Induction Motor," *Industry Electronics*, IEEE Transactions on volume 62, issue 3 ,pp . 1814-1825, 2015.
- [131] S. Jothibasu; M. K. Mishra, " An Improved Direct AC–AC Converter for Voltage Sag Mitigation," *Industry Electronics*, IEEE Transactions on volume 62, issue 1 ,pp . 21-29, 2015.
- [132] F. Blaabjerg; J.K. Pedersen; S. Rise; H.-H. Hansen; A.M.Trzynadlowski, Can Soft-Starters Help Save Energy? *IEEE Industry Applications Magazine*, vol. 3, no. 5, pp.56-66, 1997.
- [133] F. Abrahamsen, Energy Optimal Control of Induction Motor Drives, Ph.D. dissertation, Dept. Energy Technol., Aalborg University, Aalborg,Denmark, 2000
- [134] A. M. Bazzi and P. T. Krein, "Review of methods for real-time loss minimization in induction machines," *IEEE Trans. Ind. Appl.*, vol. 46, no. 6, pp. 2319–2328, Nov./Dec. 2010.
- [135] S. Lim and K. Nam, "Loss-minimising control scheme for induction motors," *IEE Proc. Electr. Power Appl.*, vol. 151, no. 4, pp. 385–397, Jul. 2004
- [136] F. J. Nola, "Power factor control system for AC induction motor," U.S.Patent 4 052 648, Oct. 4, 1977.
- [137] T. W. Jian, N. L. Schmitz and D. W. Novotny, "Characteristic Induction Motor Slip Values for Variable Voltage Part Load Performance Optimization," in *IEEE Power Engineering Review*, vol. PER-3, no. 1, pp. 26-27, Jan. 1983.
- [138] A. M. Hava, R. J. Kerkman and T. A. Lipo, "Simple analytical and graphical methods for carrier-based PWM-VSI drives," in *IEEE Transactions on Power Electronics*, vol. 14, no. 1, pp. 49-61, Jan 1999.

Appendices

Appendix A

Triangle Intersection Implementation of SVPWM

Generally, there are two widely utilized PWM implementation techniques: the direct digital gate pulse programming technique and the triangle-intersection technique. For the direct method, the gate signal on-state times are calculated from the space-vector voltage equation and directly programmed. For the triangle intersection technique, the time lengths of the inverter states are an end result of the comparison between the triangular carrier wave and the modulation waves. In this thesis, the latter is chosen for its relatively easier implementation.

In practice, carrier-based PWM methods provide a linear utilization of dc voltage within a limited range. For isolated neutral-type loads such as induction motor, the freedom to add a zero-sequence signal to the modulation waves leads to higher dc voltage utilization percentage. Examples of high-performance zero-sequence signal injection methods are: third-harmonic injection PWM (THIPWM) and the triangle intersection implementation of SVPWM method [138]. By far, the latter one is possibly the earliest and simplest zero sequence injection PWM method developed. In addition, it has been shown that the latter one has a slightly higher linearity range than the former one. Therefore, triangle intersection implementation of SVPWM is chosen for the proposed single-phase floating H-bridges for its easier implantation and wider linear range and reduced carrier frequency harmonic distortion characteristics. Fig. A-1 shows block diagram for triangle intersection implementation of SVPWM.

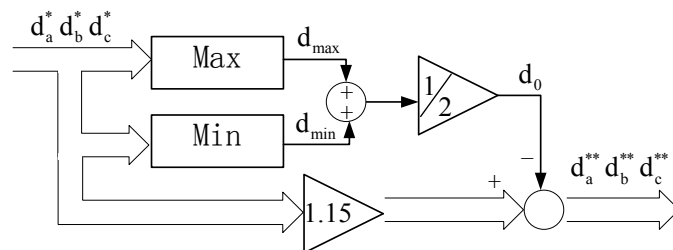


Fig. A-1. Triangle intersection implementation of SVPWM

From Fig. A-1, it can be seen that this method takes the instantaneous average of the maximum and minimum of the original sinusoidal modulation waves d_a^* , d_b^* , d_c^* so that a zero-sequence signal can be obtained as:

$$d_0 = \frac{\max(d_a^*, d_b^*, d_c^*) + \min(d_a^*, d_b^*, d_c^*)}{2} \dots\dots\dots A-1$$

Fig. A-2 shows the relationship between the original modulation signal and the corresponding zero-sequence signal.

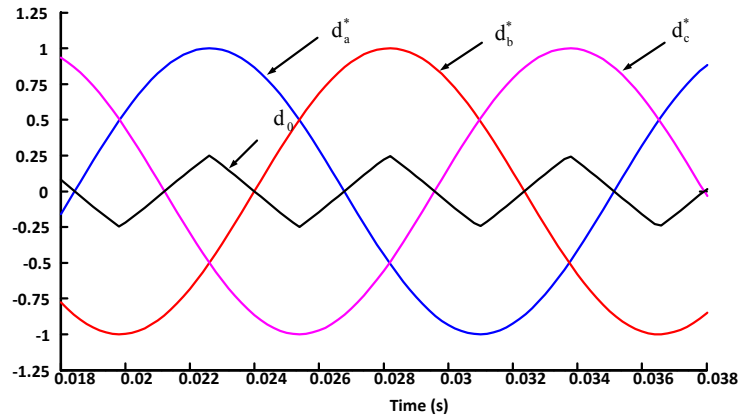


Fig. A-2. Original modulation signal and zero-sequence signal

The introduction of the zero-sequence signal enables the modulation index to be increased by 15 percent before the over modulation region is reached. Therefore, the original sinusoidal modulation waves are scaled up by a factor of 1.15. Subtracting d_0 from each of the individual modulation waves, the modified modulation waves d_a^{**} , d_b^{**} , d_c^{**} can be obtained in Eqn. A-2 and zero-sequence signal injection for phase A modulation wave as an example is presented in Fig. A-3.

$$\begin{aligned} d_a^{**} &= 1.15 \cdot d_a^* - d_0 \\ d_b^{**} &= 1.15 \cdot d_b^* - d_0 \dots\dots\dots A-2 \\ d_c^{**} &= 1.15 \cdot d_c^* - d_0 \end{aligned}$$

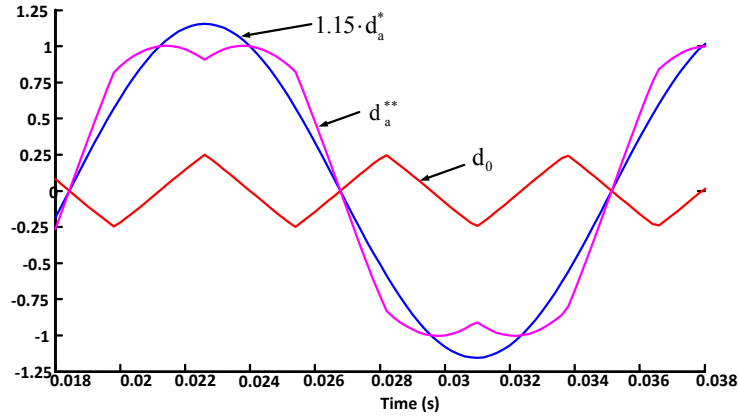


Fig. A-3. Zero-sequence signal injection for phase A

It has been proved that adding d_0 represents injection of 3rd harmonic and its multiples and this method is equivalent to the traditional SVPWM.

Level-shifted multicarrier modulation scheme is chosen in this thesis for its ability to generate superior five-level line to line PWM voltages. This technique involves two triangular carriers, both having the same frequency and amplitude. The triangular carriers are vertically disposed such that the bands they occupy are contiguous. In-phase disposition (IPD), where both carriers are in phase is chosen since it provides the best harmonic profile and simulated waveforms for level-shifted multicarrier modulation technique are presented in Fig. A-4.

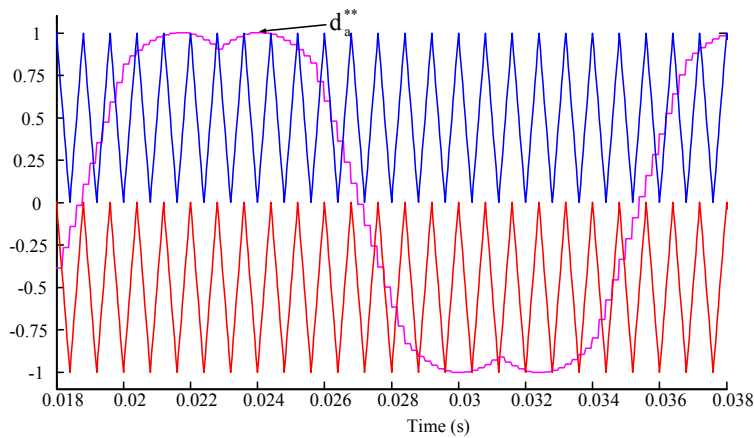


Fig. A-4. Simulated waveforms for level-shifted multicarrier modulation technique

Appendix B

Modified PWM Scheme

The carrier based modulation schemes for multi-level converter can be classified into two categories: a) Level shifted and b) phase shifted modulation. Both modulation schemes can be utilized in the proposed H-bridge converter. In the level shifted PWM scheme, the triangle carriers are vertically disposed and all having the same frequency and amplitude. But the previously described scheme has the disadvantage of keeping one leg on or off during half of the cycle of the modulating signal, and thus PWM switching frequency is less than the four times of the carrier frequency. So modified phase shifted switching scheme is proposed. In the phase shifted multi carrier modulation, the triangular carriers have the same frequency and amplitude with a phase shift between adjacent carrier waves. In the proposed scheme, for one modulating signal, two phase shifted carrier signals are used. The carriers are phase shifted by $\pi/2$ radians or 90° . For positive cycle one carrier and for negative cycle of the modulating signal the phase shifted carrier is used, Fig. B-1.

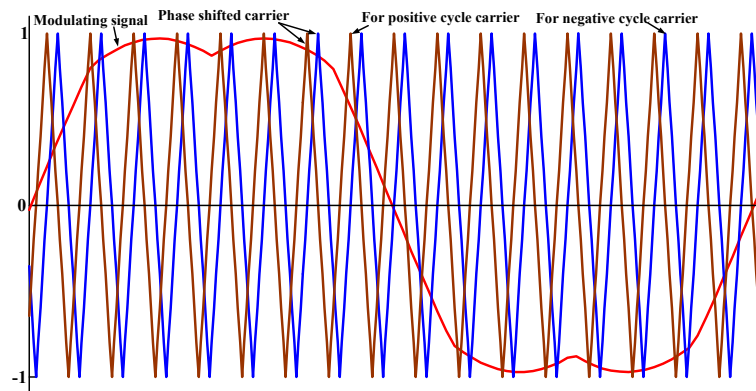


Fig. B-1. Simulated waveforms for phase shifted multicarrier modulation technique

The modulating signal is a three-phase sinusoidal wave with third harmonic injected as described in appendix A. The gate signals are generated by comparing the modulating wave with the carrier waves. The principle of the phase shift modulation for one leg of the converter is shown in Fig. B-1.

The output voltages of each H-bridge along with motor line to line voltages are presented in Fig. B-2. The simulated output voltages are 120° apart from each other, Fig. B-2 (a). The resultant perfect five level wave-shapes seen by the motor is shown in Fig. B-2(b).

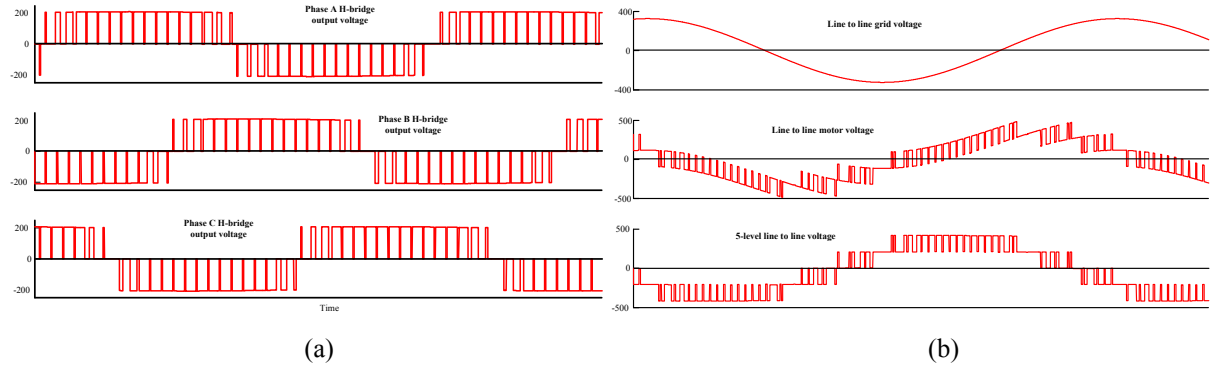


Fig. B-2. a) Output voltage of three phase H bridge; b) resultant five level line to line voltage observed by the motor

Appendix C

Conservative DC Voltage Prediction before Motor Start

It has been shown previously, chapter 3, under the worst case scenario condition (no load, induction motor power factor angle $\phi_m = 90^\circ$) the injected ac voltage increases linearly with motor terminal voltage so as capacitor dc voltage level. The average dc capacitor voltage of the proposed floating capacitor H-bridge converters can be calculated from Eqn. 3-1 and 3-5:

$$V_{dc}^{avg} = \frac{\sqrt{2}(V_m^{p.u} + 1)V_g}{m_a} = \frac{\sqrt{2}\left(\frac{V_m^* + V_g}{V_g}\right)V_g}{m_a} \dots\dots\dots C-1$$

$$= \frac{\sqrt{2}(V_m^* + V_g)}{m_a} \dots\dots\dots C-2$$

From Eqn. C-1 it can be seen, average dc capacitor voltage is directly related motor reference voltage and grid voltage and also higher modulation index results lower dc capacitor voltage. If the predicted DC voltage level exceeds the voltage rating of dc capacitor, the controller will automatically block the PWM enable signal, preventing the motor from starting in the first place. The blockade on the PWM enable signal will not be lifted until a correct motor line voltage reference value is entered by the user or the grid voltage level has been reduced to the correct level or the combination of the above mentioned two. This feature greatly improves the safety and reliability of the proposed system.

Appendix D

dSpace Implementation

The dSpace systems used for motor control combine a data acquisition system with an independent processing system to implement digital control. The system is an embedded or self-contained system. The PCI board installed in the computers is its own entity. None of the processing for a system implemented on the board is done by the host PC. So, software is required to create the model and downloaded to the board for the system to function. The basic block diagram for the system is shown in Fig. D-1. The Real-Time Interface (RTI) I/O blocks can be inserted into a Simulink block diagram to connect the function model with the I/O interfaces and to configure all I/O graphically. In this setup, the desired input signal (i.e., voltage) from the ControlDesk (user-interface) is sent to the dSPACE I/O box and H-bridge via DS 1104 R&D Controller card. The system can also measure and transfer the resulting data (i.e., current, voltage) back to the dSPACE software in real time and thus control the switching signal and eventually the motor voltage.

In this part, key model developments are described.

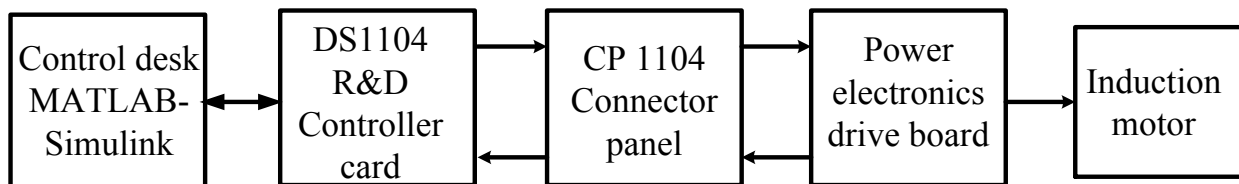


Fig. D-1. Basic system block diagram

Voltage and Current Measurement

Acquisition of the sensor voltage in the system is completed using the ADC blocks in the dSpace library under Simulink in Matlab. To configure the software so that it can get this signal into the controller the right channel number need to be selected. Next, it is important to the “scaling” that occurs in acquiring the signal. The physical input signal range is -10V to $+10\text{V}$. dSPACE always scales this by a factor of 0.1 (multiplies by this number) to place the value on a range of -1V to $+1\text{V}$. This scaling typically needs to be corrected for due to the need to map the meaning of volts to voltage and currents in amperes. This mapping depends on sensor characteristics, and is generally adjusted in Simulink blocks when the sensor signal is processed

before it is used by the main part of the controller. In the DS1104 controls ADC unit featuring two different types of A/D converters: One A/D converter (ADC1) multiplexed to four channels

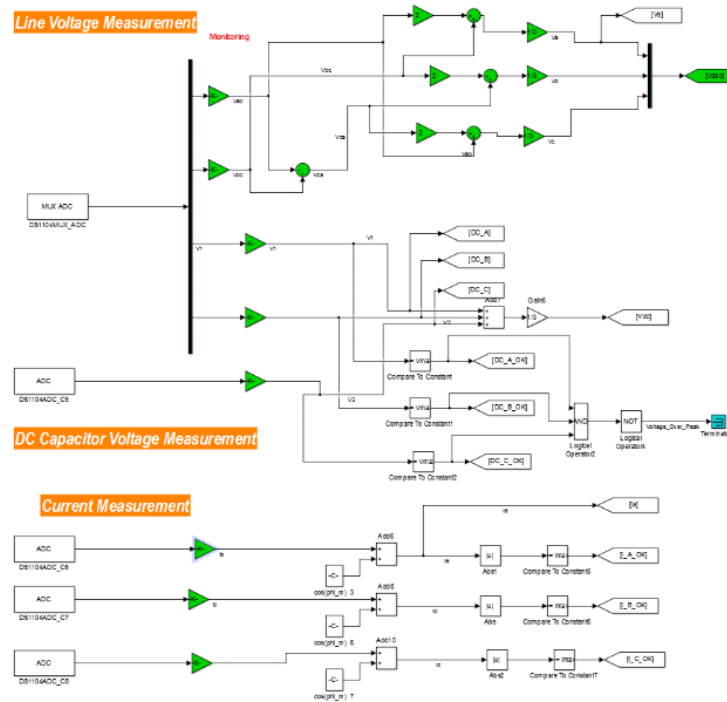


Fig. D-2. Voltage and current measurement implementation in MATLAB/Simulink

(signals ADCH1 ... ADCH4), and Four parallel A/D converters (ADC2 ... ADC5) with one channel each. In the control, the voltages are measured with multiplex A/D converter and currents are measured with parallel A/D converters, Fig. D-2. The gain block is used to translate the sensor signal to accurate values and thus rms block in Simulink is used to measure the rms value of the current and voltage.

Motor Reference voltage generation

The motor reference voltage generation is an important feature of the controller during soft start. The current set limit is defined by the user and depends on motor load condition. If the motor current sensed by the sensor reached the threshold value, a hold signal is generate and keep the motor voltage at that voltage level. During starting motor voltage is ramped up by a predefined ramp rate. During steady state operation motor reference voltage can be modified and ramp up or down with a predefined rate, Fig. D-3.

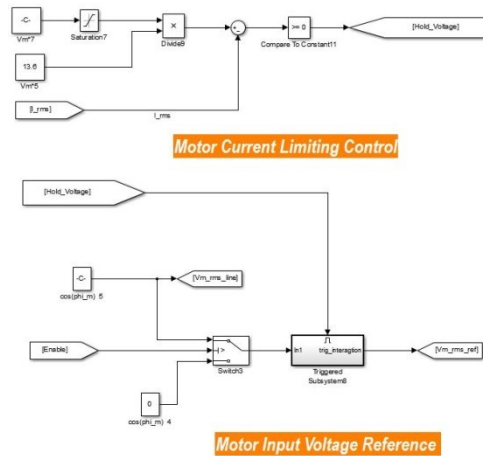


Fig. D-3. Reference voltage generation block

α -angle generation

The controller generate α angle using the Eqn. 2-3. The angle is passed through the lag compensator to smooth the value and limiter/ saturate block is used to limit the angle in between 0 to pi radians. Inverse park transformation is used to generate the modulating signals for the bridge. The reference signal for the inverse park transformation is achieved by the PLL block used in the grid side voltage measurement.

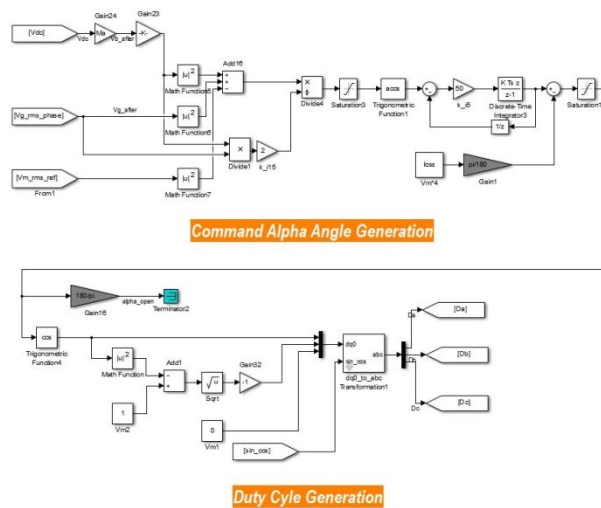


Fig. D-4. α -angle generation in MATLAB/simulink

PWM generation

The generated modulating signal is transformed to third harmonic injected modulated signal by the method defined in appendix A. The signal is then level shifted. The PWM block in dSpace library is used to generate the gate signals to H-bridge, Fig. D-5. The library has two different PWM blocks. 3-phase PWM generation and four single phase PWM generation blocks. The controller needs to use both the PWM block as it requires total twelve output signal with six original signal with the other six as inverted. The inverted signals are generated using hardware with NOT logic.

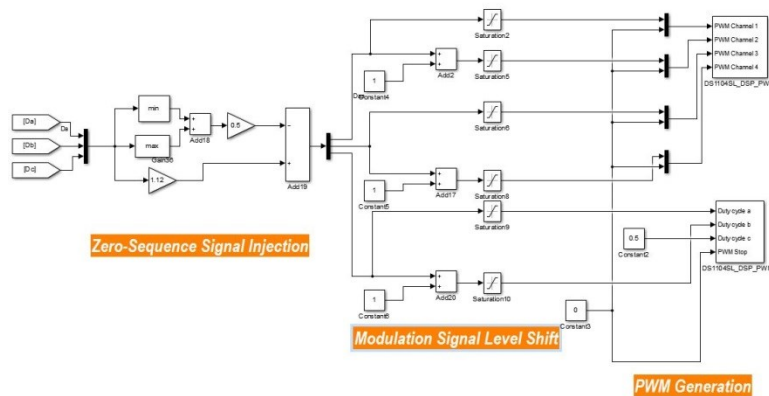


Fig. E-5. PWM generation in MATLAB/simulink

Appendix E

Control Interface

The control algorithms are implemented on a dSPACE CLP1104 platform. The real-time hardware based on PowerPC machinery and set of I/O interfaces make the DS1104 R&D Controller Board a perfect solution for developing smaller control applications in various fields. It is fully programmable from the Simulink block diagram environment and all I/O can be configured graphically. This is a rapid and easy way to implement and test new control functions in a real environment. The following figure, Fig. E-1, shows the real time connections between the system and its controller. Analog-to-digital converters (ADC) read the information of the sensors from system and require digital-to-analog converters (DAC) to apply the control commands. The program is developed in Matlab Simulink environment and thus builds the program to run in real time environment in Control Desk. The overall structure of a real-time program can be simplified into three main sections: Initialization, real-time task or tasks, and the background.

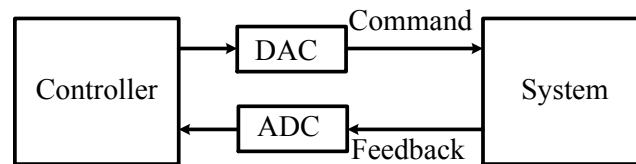


Fig. E-1: Real-time control structure

The initialization section is executed only once at the start of execution. In this part functions are defined for initialization of the system to run once. The next part of the program is the real-time part, the task; what is executed periodically based on the sample time. This part is the core of the control program. In this section, inputs are read (e.g., from an ADC), control signals are computed and output signal are wrote (e.g., with a DAC). Depending on control application there may be multiple tasks in the model. Finally, the last section is the background; this is code executed in the “idle” time between the end of computation of a step and the start of the next step.

The system operation procedure for the H-bridge motor drive system is explained in this section. Fig. E-2 shows the overview of the user interface.

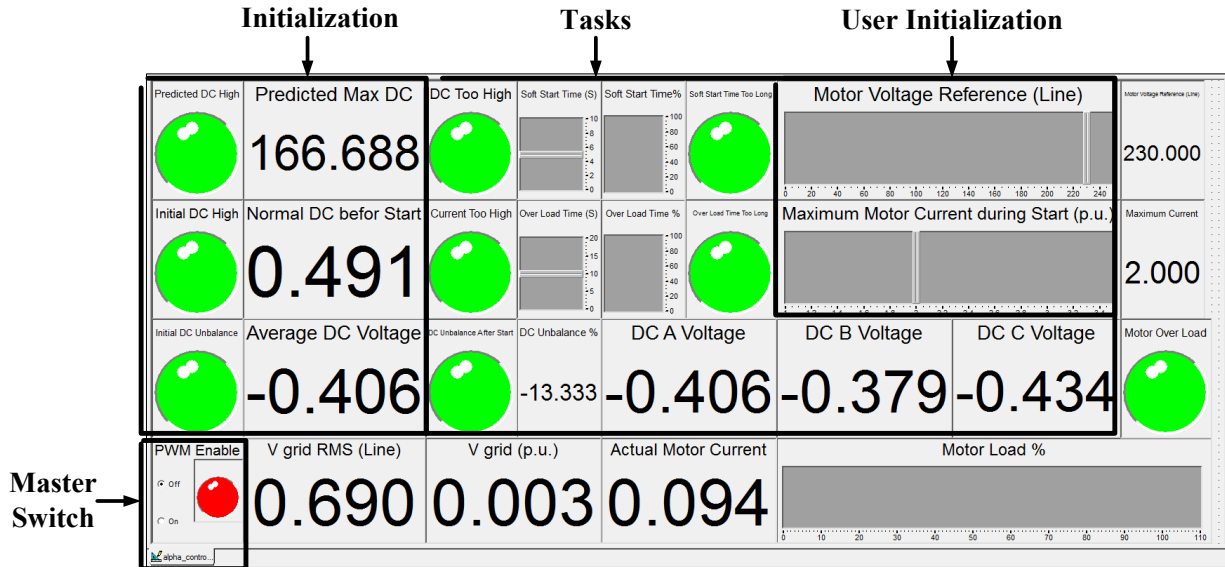


Fig. E-2. User interface of Control desk

The user interface can be divided into several sections: initialization, user initialization, Tasks, and master switch. The initialization part is basically routine safety check before run the motor. In this part, the program checks initial average capacitor dc voltage, capacitor voltage unbalance between the phases and finally predicts maximum capacitor voltage for worst case scenario. The program compare values with preset value defined as maximum capacitor dc voltage or % of unbalance between the phases. If the values surpass the preset value, the indicator light will turn red and master switch will be disabled. In the user initialization part, user can set reference motor voltage and maximum per unit current during starting. Motor reference voltage is useful when running the motor in variable voltage operation, otherwise it is recommended to keep the reference voltage as rated motor voltage indicated in nameplate data. If there is no error signal from the initialization state, the master switch will be enable and turning it on can operate the motor. But the part named as tasks is working throughout the program runtime. If dc voltage or motor current go to high (limit set by the program), or unbalance between the dc voltage occurs, the pwm pulses generated by the controller are disable. The program also checks motor starting time and over loading time. If time requires starting the motor exceeds the preset value or motor is over loaded for a long time (set by the user) the controller will disable pwm pulses.